University of Alberta

Library Release Form

Name of Author: Amy Louise Hurford

Title of Thesis: Wolf movement within and beyond the territory boundary

Degree: Master of Science

Year this Degree Granted: 2005

_____

Signature

Department of Biological Sciences
University of Alberta
Edmonton, Alberta
Canada, T6G 2E9

University of Alberta

WOLF MOVEMENT WITHIN AND BEYOND THE TERRITORY BOUNDARY

by

Amy Louise Hurford

A thesis submitted to the Faculty of Graduate Studies and Research
in partial fulfillment of the requirements for the degree of
Master of Science

in

Environmental Biology and Ecology

Department of Biological Sciences
Edmonton, Alberta
Fall 2005

University of Alberta

Faculty of Graduate Studies and Research

The undersigned certify that they have read, and recommend to the Faculty of Graduate Studies and Research for acceptance, a thesis entitled **Wolf movement within and beyond the territory boundary** submitted by **Amy Louise Hurford** in partial fulfillment of the requirements for the degree of **Master of Science in Environmental Biology and Ecology**.

Dr. Mark Lewis (Supervisor)

Dr. Evelyn H. Merrill

Dr. Stanley A. Boutin

Dr. Fangliang He

Date:

ABSTRACT

Wolf (*Canis lupus*) movements are either beyond or within the territory boundary. Rare dispersal movements beyond the territory boundary occur to colonize new territories. Within their territories wolves raise pups and hunt. I analyze data from GPS collars on wolves and develop mathematical models for movement both within and beyond the territory boundary. I derive an integrodifference model to investigate the effects of reproduction, pair formation and dispersal on colonization rates. For within territory movements, I develop a statistical model to determine the effect of GPS measurement error on measured distributions of turning angles and directional biases. I test for a directional bias with respect to past kills, the territory boundary and elevation gradients for within territory movements. Together these models show the role of pair formation, GPS measurement error and ecological features in determining movement patterns and population spread.

ACKNOWLEDGEMENTS

I gratefully acknowledge financial support for this thesis provided by Mathematics Industry Technology and Complex Systems (MITACS), Alberta Sports Parks Wildlife and Recreation Foundation (ASPWRF), and the Department of Biological Sciences at the University of Alberta. I gratefully acknowledge Dr. Mark Lewis, Mark Hebblewhite, Dr. Evelyn Merrill, the Ya Ha Tinda Elk and Wolf project (see www.ualberta.ca\~mh12 for a list of funding agencies that support this project) and Alberta Cooperative Conservation Research Unit (ACCRU) whose support allowed me to work at Ya Ha Tinda ranch during the winter of 2004. A special thanks to Rick Smith (Ya Ha Tinda Ranch manager) for accommodating scientific research at Ya Ha Tinda and for his kind assistance on many occasions.

This thesis has been greatly improved by insightful ideas and helpful suggestions from Dr. Mark A. Lewis. I thank Mark for his supervision, mathematical expertise, patience, and encouragement. Thanks to my committee members Drs. Evelyn Merrill, Stan Boutin and Fangliang He for helpful suggestions that have improved this thesis. Thanks to Mark Hebblewhite for his field expertise and enjoyable collaboration. Thanks to all the members of the Lewis lab for your encouragement and support. Several key ideas in this thesis were inspired by helpful lab discussions. I thank Caroline Bampfylde, Christina Cobbold, Tomas de Camino-Beck, Raluca Eftimie, Chris Jerde, Marty Krkosek, JungMin Lee, Frithjof Lutscher, Hannah McKenzie, Peter Molnar, Bill Nelson, Erik Noonburg, AnneMarie Pielaat, Alex Potapov, and Marjorie Wonham.

Thanks to my parents, Robyn and Malcolm, and my sister Tracy, for your kindness and support. Thanks to Shawn Leroux for reading and editing numerous thesis drafts. Thanks to Shawn also for welcoming me home from long days of thesis writing with encouragement, kindness and may well cooked meals. Thanks to all my friends who made my time in Edmonton so memorable. Thanks to Cam Stevens, Layla Neufeld, and Shawn Leroux for reading part of my thesis between beach volleyball games and afterwards at Muddy Waters. Lastly, thanks to my intramural buddies - I'll always remember that we made a winning team!

Table of Contents

List of Figures

List of Tables

Chapter 1

Introduction

Wolf (*Canis lupus*) behaviour and movements have been studied at length by biologists around the world. Wolf hunting and pup-rearing movements are confined to a relatively fixed home range that is defended from intruders with little overlap between neighbouring wolf packs (Mech and Boitani, 2003). The area occupied is considered a territory and wolf territories have been documented to be as large as 1645 km^2 (Ballard et al., 1987). However, when dispersing to search for a mate or new pack, wolves will move beyond the boundary of their territories. Wolf dispersal is defined as the movement between the time a wolf permanently leaves its natal home range and the time the wolf establishes or joins a new pack (Boyd-Heger, 97). Wolf dispersal distances are known to range between tens of kilometers (Boyd-Heger, 97) and greater than 800 km (Ballard et al., 1983; Fritts, 1983; Boyd and Pletscher, 1999). Therefore, on the basis of spatial extent, wolf movements can be divided into two groups; 1) long distance dispersal movements; likely associated with finding a mate or a new pack, and 2) shorter movements; likely associated with hunting, territory defense and pup rearing.

Models of animal movement both, beyond and within the territory boundary, can be classified as are either phenomenological or mechanistic. Phenomenological models focus on accurately describing observed patterns. Worton (1987) reviewed phenomenological home range models. Two examples of phenomenological home range models are Minimum Convex Polygons (MCPs, Mohr 1947; Kie et al. 1996) and kernel density estimators (Worton, ????; Kie et al., 1996). Mechanistic models focus on identifying processes that cause observed patterns. Adams (2001) reviewed mechanistic home range models. Of mechanistic models, diffusion models (e.g. correlated random walks) are particularly appropriate for modelling animal movement where autocorrelation exists between successive animal locations (Kareiva and Shigesada, 1983).

Modelling dispersing populations

Diffusion is a "phenomenon by which the particle group as a whole spreads according to the irregular motion of each particle" (Okubo and Levin, 2001). In the context of animal populations, diffusion models predict the spread of invading populations given the dispersal distances of individuals. Several past studies use diffusion equations to model invading mammal populations (Skellam, 1951; Caughley, 1970; Clarke, 1971; Lubina and Levin, 1988).

Integrodifference equations (Kot et al., 1996) are a recent advance on the diffusion modelling framework that allows for discrete yearly reproduction and dispersal as well as non-diffusive motion. They have been used to model invasions of house finches (*Carpodacus mexicanus*, Veit and Lewis 1996), boll weevil (*Anthonomus grandis*, Legaspi et al. 1998), a boll weevil parasitoid (*Catolaccus grandis*, Legaspi et al. 1998), and plants (Clark, 1998; Neubert and Caswell, 2000). In Chapter 2, I derive an integrodifference model that combines dispersal, pair formation, and reproduction to study wolf recolonization to the Greater Yellowstone Ecosystem (GYE). I hypothesize that wolf spread is influenced by a reduced probability of finding mates at low densities and quantify the effect of pair formation, reproduction, and dispersal parameters on recolonization rates.

An Allee effect is "a positive relationship between a component of individual fitness and population density or number" (Stephens et al., 1999; Boukal and Berec, 2002). Since a reduced probability of finding mates at low densities is a mechanism that may cause an Allee effect, the contributions of Chapter 2 to Allee effect theory are discussed. In particular, past studies have not made the distinction between Allee effect mechanisms that reduce the probability of establishing new breeding units (i.e., pair formation) and mechanisms that decrease the per capita growth rate of established breeding units (i.e., cooperative hunting). I derive a mechanistic model where a reduced probability of finding mates at low densities influences the probability of establishing new breeding units. The model I derive predicts wolf recolonization to the GYE at a rate consistent with the observed rate of recolonization.

Modelling within territory movements

Wolf movements within a territory are influenced by many factors. Much of a wolf's time is spent hunting and hunting movements are most likely influenced by prey density and ecological features (Nelson and Mech, 1986; Fuller, 1989; Hebblewhite, 2005). The age of wolf pups also influences wolf hunting movements. In North America, wolf pups are born in early spring. When canid pups are young and not yet able to travel long distances, pack hunting movements are followed by return movements to the den (Siniff and Jessen, 1969). At five to ten weeks old (Mech, 1988) pups are old enough to be moved and pack members bring

food back to the pups at rendezvous sites. Pups are periodically moved to new rendezvous sites until they are four to ten months old when they are able to travel with the rest of the pack (Mech, 1991).

Another factor that influences wolf movement within a territory is territory defense. Wolves advertise the boundary of their territory through scent marking (Peters and Mech, 1975; Rothman and Mech, 1979) and interspecific aggression (Mech, 1970; Murie, 1985). Wolves scent mark the boundary of their territory at least every three weeks (Peters and Mech, 1975). Other factors that influence wolf movement within a territory are snow depth (Nelson and Mech, 1986; Fuller, 1989; Hebblewhite, 2005) and distance to roads (Whittington et al., 2004, 2005).

Data collection on space use within a territory has been greatly advanced by technological innovations that allow Global Positioning System (GPS) collar units to be fixed to animals. Despite their widespread use, atmospheric refraction of GPS signals, multipathing, and poor satellite geometry impact the accuracy of GPS measurements (Johnson and Barton, 2004). For my thesis, GPS collars were deployed on five wolves to record each wolf's location every 15 minutes. Data from four of these collars was used to compare the direction of recorded wolf movement to the direction of ecological features in order to identify directional movement biases.

Several studies report that GPS measurement error can bias the results of movement (Johnson et al., 2002; Jerde and Visscher, 2005) and habitat selection (Frair et al., 2004) models. It is likely that GPS measurement error could influence my ability to detect directional biases. Therefore, Chapter 3 investigates the effect of GPS measurement error on the measured distribution of turning angles (the difference in direction for three successive locations, Turchin 1998) and directional biases (the difference in direction between the animal's next move and the direction of a bias point, i.e., the den, Siniff and Jessen 1969). The effect of GPS measurement error on the measured distributions of turning angles and directional biases was determined using numerical simulations and a statistical model. Furthermore, using numerical simulations, I determine the step length above which the actual direction of movement can be detected in the presence of GPS measurement error.

In Chapter 4, I study the patterns of space use within a territory for four wolves in southeastern Banff National Park (BNP) and adjacent areas outside BNP. Past studies have shown that prey (MacDonald, 1980; Moorcroft and Lewis, 2005) and forage (Ward and Saltz, 1994) density influence animal movement. Responses to scent marks influence the way that canids use space (Moorcroft et al., 1999). I hypothesize that wolf movement is more likely, 1) towards locations of recent past hunting success, 2) towards the territory boundary, and 3) in the direction of flat terrain. I use statistical tests to identify movement bias in the direction of each of the aforementioned ecological features and find that wolves move parallel to their

territory boundary.

Chapter 2

A spatially explicit model for the Allee effect: Why do wolves recolonize so slowly in Greater Yellowstone?

Introduction

Biological invasion theory predicts that populations with high reproductive rates and long distance dispersal will spread quickly (Fisher, 1937). In the Greater Yellowstone Ecosystem (GYE, Montana and Wyoming, USA) the reintroduced gray wolf population (*Canis lupus*) increased by 65% percent between 1996 and 1997 (Smith, 1998). Wolves can also disperse distances greater than 800 km (Ballard et al., 1983; Fritts, 1983; Boyd and Pletscher, 1999). Yet wolves do not recolonize as quickly as biological invasion theory predicts. Assuming logistic population growth and a Gaussian distribution of dispersal distances, the Fisher model (1937) predicts a recolonization rate of 93.9 km/year by wolves to the GYE (see Appendix A). The observed GYE recolonization rate between 1997 and 2002 is an order of magnitude lower, only 9.78 km/year (Tab. (2.3)). This slower than predicted spread suggests a possible Allee effect (Lewis and Kareiva, 1993; Kot et al., 1996; Veit and Lewis, 1996; Wang et al., 2002). A reduced probability of finding mates at low densities is a frequently hypothesized mechanism that can cause an Allee effect (Boukal and Berec 2002, Bessa-Gomes et al. 2004; and references therein). The objective of this chapter, is to determine the effect

of a reduced probability of finding mates at low densities on the spread rate of a sexually reproducing, invading, population.

Recent work defines a *component* Allee effect as "a positive relationship between a component of individual fitness and population density or number" (Stephens et al., 1999; Boukal and Berec, 2002) and a *demographic* Allee effect as a positive relationship between total fitness and population density or number (Stephens et al., 1999). Many mechanisms have been identified that may give rise to an Allee effect in a component of fitness (Dennis, ????; Courchamp et al., 1999; Stephens and Sutherland, 1999; Moller and Legendre, 2001). In canids, Allee effects may arise when hunting is cooperative, as shown for African wild dog *Lycaon pictus* (see Courchamp et al. 2000). However, this is unlikely for wolves if small packs are able to secure more prey per capita than large packs (Schmidt and Mech 1997, but see Vucetich et al. 2004). I suggest the most likely source of an Allee effect in wolves is a reduced probability of finding mates at low densities during the dispersal phase.

An excellent review of approaches used to model Allee effects is found in Boukal and Berec (2002). Many studies have investigated the effect of a reduced probability of finding mates at low densities on population dynamics (Engen et al. 2003; Bessa-Gomes et al. 2004; Berec and Boukal 2004; and numerous others) and some have investigated the effect of a reduced probability of finding mates at low densities on population spread rate (e.g. Veit and Lewis 1996; Wang et al. 2002).

A distinct difference between my model and other studies is that I model the population growth as two separate processes; 1) establishment of new breeding units and 2) net annual change in breeding group size/density through immigration, emigration, births and deaths. I model a reduced probability of finding mates at low densities as influencing only the probability of establishing new breeding units. Even when broken into these two separate processes, a decreased success in finding a mate at low densities should still be considered an Allee effect, since a positive relationship exists between mate density and the probability of finding a mate. This distinction between establishment and subsequent growth yields a biologically realistic model which can be parameterized and validated with empirical data.

To model pair formation it is necessary to understand how organisms search for mates. Because little is known regarding where wolves or other mammals search for mates with respect to the beginning and end of their dispersal paths, I consider the extreme possibilities (searching for the mates at the very beginning and very end). I determine the spread rates predicted by the extreme searching strategies and use these as the upper and lower estimates for the predicted spread rate. The model is validated by comparing the predicted range of spread rates for the parameterized model to an empirical estimate of the recolonization rate for wolves in the GYE. This analysis demonstrates that an Allee effect generated by dispersal and pair

formation is sufficient to explain the rate of recolonization of wolves to the GYE.

Model derivation

Lewis et. al., (in press) delineate three stages to an invasion process: initial establishment from a beachead, early radial expansion, and the established spread of the population (Fig. (2.1)). This established spread stage occurs when the geographic radius covered by the population is large compared to the length scale for local dispersal. At this point in the invasion, a local view of the front shows it to be approximately planar, with the front moving in direction **u** (Fig. (2.1)). Here the two-dimensional population model can be simplified to a one-dimensional model describing progression of the invasion in direction **u**. However, the process for doing this is subtle. It requires that the two-dimensional dispersal kernel is replaced by its one-dimensional marginal distribution. That is the dispersal kernel integrated over direction **v** (Fig. (2.1)). In the case of radially symmetric two-dimensional dispersal, the marginal distribution is the same in each direction **v** (see also the Parameter estimation section). The one-dimensional model has the advantage of being analytically tractable compared to two-dimensional model. The approach taken in this thesis is to apply the one-dimensional modelling approach to all stages of the invasion, while recognizing that, in the early stages of the invasion it only provides an approximate model.

I model local population density $N(x)$ as the sum of the density of individuals in new packs and the density of existing packs after reproduction,

$$\underbrace{N_{t+1}(x)}_{\substack{\text{local density in year} \\ t+1}} = \underbrace{f(N_t(x))}_{\substack{\text{local density after} \\ \text{reproduction by} \\ \text{existing breeding} \\ \text{units}}} + \underbrace{D_t(x),}_{\substack{\text{local density from} \\ \text{formation of new} \\ \text{breeding units}}} \tag{2.1}$$

where t indicates the year and locations in space are denoted as x. In Eq. (2.1), $N_{t+1}(x)$ is the sum of the density due to reproduction by existing breeding units and the density due to the formation of new breeding units. The distinction between new and existing breeding units is that new breeding units were formed less than 1 year ago (see Tabs. (2.1) and (2.2) for definitions and units of all variables and parameters).

The model derivation makes several simplifying assumptions:

A1. Space is homogeneous on the scale for which the model is parameterized.

A2. There is a critical density N_c, below which the population grows geometrically (at rate r) and no dispersers are produced. Once local density has reached N_c it never drops below that level.

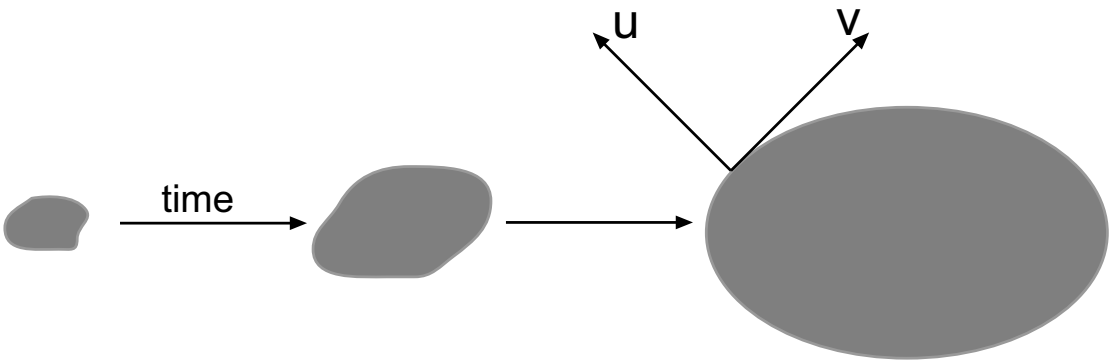

Figure 2.1: Invaded regions are shown in grey. As time progress the figure shows a "beachhead" (left most polygon) that becomes more ecliptically shaped. The rightmost polygon shows an established population. The speed of the planar front **v** advancing in the direction **u** is calculated using the marginal distribution two-dimensional dispersal kernel. This figure is based on Lewis et. al., (in press).

Table 2.1: Table of variables

Variable	Definition	Units
x	location in space after dispersal	km
y	location in space prior to dispersal	km
t	time	years
N_t	density	wolves/km
D_t	density of individuals in new packs	wolves/km
x_t	spatial extent of the disperser producing population	km

A3. When local density exceeds N_c, dispersers are produced at density $G_t(y)$ with a 1:1 sex ratio, where y denotes locations in space prior to dispersal. The distribution of dispersal distances is denoted by the pdf k which is unbiased in either direction (symmetric) and identical for male and female dispersers.

A4. Only dispersers can form pairs (new breeding units), and the establishment of new breeding units depends on the density of dispersers, the distance at which dispersers can detect each other ϕ, and the probability that dispersers that encounter will pair, ψ.

A5. Only dispersers that form pairs can reproduce. Failure to find a mate results in mortality before the next breeding season.

I derive two sub-models for D_t where dispersers search for mates and form pairs, 1) prior to dispersal and 2) following dispersal.

Pair formation prior to dispersal

Let $G_t(y)$ denote the density of dispersers produced at y as a function of local density. I assume an equal sex ratio at any point in space such that the density of a single sex of disperser produced at y is $H_t(y) = G_t(y)/2$. For a female located at y, the expected number of male dispersers she can detect (and vice versa) is denoted by $I_t(y)$ and is given by the formula,

$$I_t(y) = \frac{1}{2}\int_{y-\phi}^{y+\phi} G_t(\xi)\ d\xi, \tag{2.2}$$

where ϕ is the detection distance in km. I approximate I_t by the mid-point rule such that $I_t \approx \phi G_t$. Using the Law of Mass Action, the density of opposite sex encounters is $E_t(y) = H_t(y)I_t(y) \approx \phi G_t^2(y)/2$. Dispersers that encounter each other will pair with probability ψ, such that the density of pairs is ψE_t. Dispersal of pairs occurs via a redistribution kernel $k(x-y)$ yielding J_t, the density of pairs after dispersal,

$$\begin{aligned} J_t(x) &= \int_{\Omega_t} \psi E_t(y) k(x-y) dy, \\ &= \psi\frac{\phi}{2}\int_{\Omega_t} {G_t}^2(y)\ k(x-y)\ dy, \end{aligned} \tag{2.3}$$

where Ω_t is the region over which the density of pairs formed prior to dispersal is non-zero and x is an individual's final location after dispersal. Therefore, the density of individuals in new packs, D_t, when pair

formation occurs prior to dispersal is,

$$\begin{aligned} D_t(x) &= \sigma J_t(x), \\ &= \sigma\psi\frac{\phi}{2}\int_{\Omega_t} {G_t}^2(y)\ k(x-y)\ dy, \end{aligned} \tag{2.4}$$

where σ is the density of wolves in a newly formed pack when the pack is 1 year old.

Pair formation following dispersal

I derive an alternative sub-model for D_t where dispersers disperse first and then pair. The density of either sex of dispersers after dispersal, but prior to pair formation is,

$$H_t(x) = \frac{1}{2}\int_{\Omega_t} G_t(y)k(x-y)\ dy. \tag{2.5}$$

In this case, the number of male dispersers $I_t(x)$ that can be detected by a female disperser located at x is,

$$\begin{aligned} I_t(x) &= \frac{1}{2}\int_{x-\phi}^{x+\phi}\int_{\Omega_t} G_t(y)k(\xi-y)dy\ d\xi, \\ &\approx \phi\int_{\Omega_t} G_t(y)k(x-y)dy. \end{aligned} \tag{2.6}$$

The density of encounters is $E_t = H_t I_t$. Opposite sex encounters result in pair formation with probability ψ; hence, the density of pairs is,

$$\begin{aligned} J_t(x) &= \psi E_t(x) = \psi H_t(x) I_t(x), \\ &= \psi\frac{\phi}{2}\left(\int_{\Omega_t} G_t(y)k(x-y)dy\right)^2. \end{aligned} \tag{2.7}$$

The different pair formation strategies give rise to different densities of new breeding units. Fig. (2.2) compares the density of pairs for the pair formation prior to dispersal (Eq. (2.3)) and pair formation following dispersal (Eq. (2.7)) strategies. Given Eq. (2.7), the density of individuals in newly formed packs is,

$$\begin{aligned} D_t(x) &= \sigma J_t(x), \\ &= \sigma\psi\frac{\phi}{2}\left(\int_{\Omega_t} G_t(y)k(x-y)dy\right)^2. \end{aligned} \tag{2.8}$$

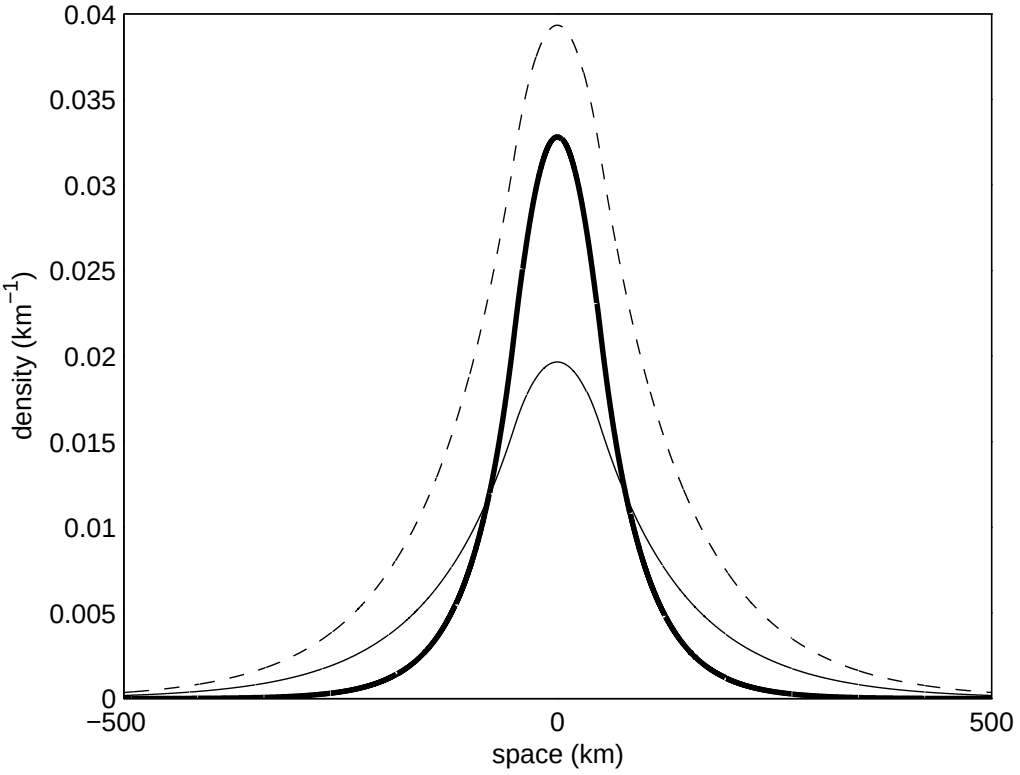

Figure 2.2: Given an initial distribution of dispersers (dashed) I calculate the density of successful dispersers for 1) pair formation prior to dispersal (fine line, Eq. (2.3)) and 2) pair formation following dispersal (bold line, Eq. (2.7)). In the figure, the proportion of total dispersers that are successful (ρ) is the same for both pair formation strategies. Parameter values are: $\alpha = 0.01$, $\phi = 20$ (pair formation prior), $\phi = 84.83$ (pair formation following dispersal), $\psi = 1$, $\gamma = 0.1$ and $x_t = 50$.

General model

I substitute these forms of D_t into Eq. (2.1). The general model for pair formation prior to dispersal is,

$$N_{t+1}(x) = f(N_t(x)) + \sigma\psi\frac{\phi}{2}\int_{\Omega_t} {G_t}^2(y)\ k(x-y)dy, \tag{2.9}$$

and the general model for pair formation following dispersal model is,

$$N_{t+1}(x) = f(N_t(x)) + \sigma\psi\frac{\phi}{2}\left(\int_{\Omega_t} G_t(y)\ k(x-y)\ dy\right)^2. \tag{2.10}$$

The differences between Eqs. (2.9) and (2.10) are a result of dispersal occurring prior to the application of the Law of Mass Action in the pair formation prior to dispersal sub-model (Eqs. (2.2)-(2.3)) and after dispersal in the pair formation following dispersal sub-model (Eqs. (2.5)-(2.7)).

Functional forms

Here, I specify the functional forms of $f(N_t)$, G_t, and $k(x-y)$ that I used for the analysis. I defined disperser production G_t as a piecewise function where a density of γ dispersers/km is produced when local population density exceeds a critical threshold density N_c. Formally,

$$G_t(y) = \begin{cases} \gamma & \text{if } \ N_t(y) \geq N_c, \\ 0 & \text{otherwise.} \end{cases} \tag{2.11}$$

Given this definition of $G_t(y)$, the region Ω_t over which dispersers are produced is the region over which $N_t(y)$ exceeds N_c. I use a geometric population growth function,

$$f(N_t(x)) = rN_t(x) \qquad \text{for} \qquad f(N_t(x)) \leq N_e, \tag{2.12}$$

where N_e is a critical threshold below which population growth is geometric with a reproduction ratio $r > 1$. For simplicity I let $N_e = N_c$. I assume that once local density exceeds the critical threshold N_c it will always remain above the N_c threshold. I do not define a form of the growth function for $f(N_t) > N_c$ as disperser production is constant for $N_t \geq N_c$.

I let $k(x-y)$ be a Laplace kernel,

$$k(x-y) = \frac{\alpha}{2}\exp(-\alpha|x-y|)\ dy. \tag{2.13}$$

It was not possible to choose a dispersal kernel based on fit to the data, since I do not have data on wolf dispersal distances in the GYE. I choose the Laplace kernel for $k(x-y)$ since it can be understood mechanistically as arising from a one-dimensional random walk where wolves 'settle' out from the population at a constant rate to start new packs (Neubert et al., 1995). Substituting the functional forms of $f(N_t)$, G_t, and $k(x-y)$ into the equation for pair formation prior to dispersal (Eq. (2.9)) yields,

$$N_{t+1}(x) = rN_t(x) + \sigma\psi\phi\gamma^2\frac{\alpha}{4}\int_{\Omega_t}\exp(-\alpha|x-y|)dy, \tag{2.14}$$

and into the equation for pair formation following dispersal (Eq. (2.10)) yields,

$$N_{t+1}(x) = rN_t(x) + \sigma\psi\phi\gamma^2\frac{\alpha}{8}\int_{\Omega_t}\exp(-2\alpha|x-y|)dy. \tag{2.15}$$

Parameter Estimation: GYE wolves

I estimated model parameters from demographic, dispersal, and pair formation data from the GYE wolf population. All data used to parameterize models are provided as data tables in Appendix B. Wolves were released into YNP following a period of confinement in reacclimation pens. I omitted data from the first year after packs were released from reacclimation pens as forced confinement influenced the probability that wolves would disperse upon release (Fritts et al., 2001).

Disperser production and critical population size (γ and N_c) were estimated using data on pack sizes and the number of dispersers produced as provided in annual reports for the YNP Wolf Project[1] (Phillips and Smith, 1997; Smith, 1998; Smith et al., 1999, 2000, 2001; Smith and Guernsey, 2002; Smith et al., 2003) and Rocky Mountain Wolf Recovery Project[2] . However, these progress reports do not record when no wolves dispersed from a pack. To correct for this, I augmented the disperser production data by adding observations of no dispersers in the cases where all pack members were accounted for through mortality or survival in the pack. To convert pack sizes and number of dispersers produced to densities, I divided these values by the mean territory diameter ($T_D = 2\sqrt{A_T/\pi}$, where $A_T = 545.6$ km^2 (Carroll et al., 2003) is the mean pack territory area). I used a maximum likelihood fit of Eq. (2.11) to the density data to estimate

[1] available on-line at http://www.nps.gov/yell/nature/animals/wolf/wolfup.html
[2] available online at http://westerngraywolf.fws.gov/annualreports.htm

Table 2.2: Table of parameters

Parameter	Definition	Estimate	Units
N_c	critical threshold density that must be exceed for disperser production	0.25	wolves / km
γ	density of dispersers produced when pack density exceeds N_c	0.09	wolves / km
α	Laplace coefficient	0.02	per km
r	geometric growth rate for packs $>$ l year old	1.33	unitless
σ	the density of wolves in newly fomed breeding units at the end of the first year	0.21	wolves / km / pair
$\psi\phi$	the probability that given two dispersers of the opposite sex meet, they form a pair (ψ) multiplied by the radius at which one disperser can detect another (ϕ)	$20.7^{\star}, 39.2^{\star\star}$	km
T_D	average territory diameter	26.4	km

* pair formation prior to dispersal
** pair formation following dispersal

the parameters γ and N_c.

Data on individual dispersal distances for GYE wolves were unavailable, but Smith et al. (2000) report the mean dispersal distance for GYE wolves from 1995-1999 as $\bar{u} = 76.7$ km. I find that the mean dispersal distance $\bar{u} = 76.7$ km, (Smith et al., 2000) can be equated with the mean of the two-dimensional dispersal kernel with constant settling rate (Eq. (2.16)). The Laplace kernel (Eq. (2.13)) can be understood mechanistically as arising from a one-dimensional random walk with diffusion coefficient D where wolves "settle" out from the population at a constant rate a to start new packs (Neubert et al., 1995). When the wolves are given enough time to settle, the distribution of settled wolves is given by Eq. (2.13) with $\alpha = \sqrt{a/D}$. Alternatively a two-dimensional random walk with constant settling rate yields,

$$k(\mathbf{x} - \mathbf{y}) = \frac{\alpha^2}{2\pi} K_0(\alpha|\mathbf{x} - \mathbf{y}|), \tag{2.16}$$

where K_0 is a zeroth order modified Bessel function of the first kind and $\mathbf{x}$ and $\mathbf{y}$ are the two-dimensional locations in space before and after dispersal (Broadbent and Kendall, 1953). The marginal distribution of this radially symmetric dispersal kernel is the Laplace kernel (Eq. (2.13)). Lewis et al. (in press) show that, for an advancing "planar" invasion front, a one-dimensional model incorporating the marginal distribution of the two-dimensional dispersal kernel is the appropriate model. Now consider an expanding population where the invaded region lies between $\pm x_t$ (see Fig. (2.3B)). I equate the mean of Eq. (2.16) with the reported mean dispersal distance for wolves in the GYE (Smith et al., 2000), such that $\bar{u} = \pi/(2\alpha)$. Therefore, I calculate the Laplace coefficient as $\alpha = \pi/(2\bar{u})$ where $\bar{u} = 76.7$.

As $\psi\phi$ occur as a product in this model (Eqs. (2.14) and (2.15)) it is not necessary to estimate the values of ψ and ϕ separately. During the first four years of recolonization to the GYE the proportion of dispersers that found mates was 0.47 (Smith et al., 2000). I estimate the product $\psi\phi$ so that for each model (Eqs. (2.14) and (2.15)) the proportion of dispersers that find mates in the first four years is 0.47.

I calculate ρ, the proportion of dispersers that find mates in the first τ years, for both the pair formation prior to and following dispersal models (Eqs. (2.14) and (2.15)). I calculate the total number of successful dispersers in any year as twice the integral of J_t over the entire region, where J_t is given by Eqs. (2.3) and (2.7). The total number of dispersers produced in any year for both models is the integral of $G_t(y)$ evaluated on the interval $\Omega_t = (-x_t, x_t)$. Therefore, ρ the mean proportion of dispersers that successfully find mates each year for the first τ years of this model is,

$$\rho = \frac{1}{\tau} \sum_{t=1}^{\tau} \frac{2 \int_{-\infty}^{\infty} J_t(x) dx}{\int_{\Omega_t} G_t(y) dy}. \tag{2.17}$$

For the pair formation prior to dispersal model, J_t is given by Eq. (2.3) such that,

$$\rho = \frac{1}{\tau}\sum_{t=1}^{\tau}\frac{\psi\phi\int_{-\infty}^{\infty}\int_{-x_t}^{x_t}G_t^2(y)k(x-y)\ dy\ dx}{\int_{-x_t}^{x_t}G_t(y)dy,} \tag{2.18}$$

and,

$$\psi\phi = \rho\tau\sum_{t=1}^{\tau}\frac{\int_{-x_t}^{x_t}G_t(y)dy}{\int_{-\infty}^{\infty}\int_{-x_t}^{x_t}{G_t}^2(y)k(x-y)dy\ dx}. \tag{2.19}$$

Substituting G_t (Eq. (2.11)) and $k(x-y)$ (Eq. (2.13)) into Eq. (2.19), I calculate $\psi\phi$ for the pair formation prior to dispersal model as,

$$\psi\phi = \rho\tau\sum_{t=1}^{\tau}\frac{\int_{-x_t}^{x_t}\gamma dy}{\int_{-\infty}^{\infty}\int_{-x_t}^{x_t}\frac{\alpha\gamma^2}{2}\exp(-\alpha|x-y|)dy\ dx}. \tag{2.20}$$

In Appendix A, I show that for the pair formation prior to dispersal model Eq. 2.20 is equal to $\psi\phi = \rho\tau/\gamma$. For the pair formation following dispersal model, where J_t is given by Eq. (2.7),

$$\psi\phi = \rho\tau\sum_{t=1}^{\tau}\frac{\int_{-x_t}^{x_t}G_t(y)dy}{\int_{-\infty}^{\infty}\left(\int_{\Omega_t}G_t(y)k(x-y)dy\right)^2 dx}. \tag{2.21}$$

Substituting G_t (Eq. (2.11)) and $k(x-y)$ (Eq. (2.13)), $\psi\phi$ for the pair formation after dispersal model yields,

$$\begin{aligned}\psi\phi &= \rho\tau\sum_{t=1}^{\tau}\frac{\int_{-x_t}^{x_t}\gamma dy}{\int_{-\infty}^{\infty}\left(\int_{-x_t}^{x_t}\frac{\alpha\gamma}{2}\exp(-\alpha|x-y|)dy\right)^2 dx},\\ &= \frac{4\alpha\rho\tau}{\gamma}\sum_{t=1}^{\tau}\frac{x_t}{\exp(-2\alpha x_t)(3+2\alpha x_t+\exp(2\alpha x_t)(4\alpha x_t-3))}.\end{aligned} \tag{2.22}$$

Hence, only the density of new breeding units formed varies between the two models (Fig. (2.2)). The proportion of dispersers that find mates is the same for both the pair formation prior and pair formation following dispersal models.

I estimate σ using data on wolf pack sizes in the GYE for the first three years following the formation of a new pack. The parameter σ is the density of wolves in a newly formed pack when the pack is 1 year old (where a pack is defined as 1 year old on the first April after pair formation). I convert all pack sizes to densities by dividing by the average territory diameter T_D. I calculate σ as the mean density of individuals in newly formed packs at the first April following pair formation. To find the reproductive ratio r I divided the total density of wolves at time $t+1$ by the total density of wolves at time t. I performed this calculation

for $t = 1$ and $t = 2$ and estimated r as the mean of the results. Since r is the reproductive ratio of packs at low densities which were established for at least 1 year, I included only packs that are 1-3 years old with a density of less than or equal to N_c. I excluded packs that were influenced by human intervention (other than legal control actions).

Model validation: Finding the observed rate of spread

I calculate the spread rate for the model (Eqs. (2.14) and (2.15)) in the next section. I validate the model by comparing the predicted spread rate (Eq. (2.24)) to the observed rate of recolonization by wolves to the GYE. I used maps of wolf territory locations from YNP Wolf Project annual reports from 1997-2002 to estimate the empirical rate of wolf recolonization in the GYE (km/year). I determine the area occupied by disperser producing packs at the start of each year by estimating the 100% minimum convex polygon (MCP, Mohr 1947; Kie et al. 1996) of all territories above the critical threshold for disperser production using the Animal Movements extension (Hooge and Eichenlaug 1997) in ArcView 3.2 (see Fig. (2.4)). For simplicity, the area encompassed by the 100% MCP is assumed circular, with a radius x_t equal to the extent of the disperser producing population at time t. The linear spread rate c (km/year) is the slope of the linear regression of x_t versus time. To be consistent, the linear regression does not include the range radius of the population in 1996 as this is less than 1 year after wolves were released from reacclimation pens.

Analysis and results

I analyzed a general model (Eq. (2.23)) of which the models (Eqs. (2.14) and (2.15)) are special cases. I analyzed the model for two initial conditions. Given initial condition 1 (shown in Fig. (2.3A) and defined in Eq. (A.12)), the region in space occupied by the disperser producing population Ω_t is $(-\infty, x_t]$. Evaluating Eqs. (2.14) and (2.15) in the region $x > x_t$ yields,

$$N_{t+1}(x) = rN_t(x) + A\exp(-w\alpha(x - x_t)), \tag{2.23}$$

where w and A are: $w = 1$, $A = \sigma\psi\phi\gamma^2/4$ (pair formation prior to dispersal) and $w = 2$, $A = \sigma\psi\phi\gamma^2/8$ (pair formation following dispersal). In Appendix A, I show using proof of induction the spread rate for Eq. (2.23) is,

$$c = \frac{1}{w\alpha}\log\left(r + \frac{A}{N_c}\right) \tag{2.24}$$

When parameterized Eq. (2.24) predicts a spread rate of 15.26 km/year for the pair formation prior to dispersal model and 7.59 km/year for the pair formation following dispersal model (Tabs. (2.2)-(2.3)). To estimate the actual rate that wolves introduced to YNP have recolonized the GYE, I calculated the area occupied by wolf packs of density larger than N_c from 1997-2002 (Fig. (2.4)). The area occupied by wolf packs of density greater than N_c increased from 6,542 km^2 in 1997 to a maximum of 29,093 km^2 in 2002. Assuming an approximately circular area, I calculated range radii of packs with density exceeding the critical threshold as 45.6 km in 1997 increasing to 96.2 km in 2002. The linear regression of radii versus time was significant, Radii $= 25.02 + 9.78 \times$ (years since reintroduction), $F_{1,4} = 142.62$, $p = 0.0003$, $R^2 = 0.97$ (Fig. (2.5)). The slope of the linear regression (9.78 km/year) is the mean spread rate, with $SE(c) = 3.43$, resulting in a 95% confidence interval of $7.51 - 12.05$ km/year.

Discussion

These results provide a link between a mechanism that can cause a component Allee effect and population spread rate. To understand population level dynamics at the leading edge of the invasion front, I derived a model (Eqs. (2.14) and (2.15)) with biologically meaningful parameters that describes population density when the probability of finding a mate decreases with decreasing density of potential mates. I parameterized Eq. (2.24) and showed a reduced probability of finding mates at low densities may slow wolf recolonization in the GYE (Tab. (2.3)). The model predicted a spread rate of between 7.59 and 15.26 km/year, which is an order magnitude lower than the spread rate predicted by the Fisher model (see Appendix A). The close agreement between the range of spread rates predicted by the model and the observed GYE wolf recolonization rate of 9.78 km/year suggests that a reduced probability of finding mates at low densities may be causing an Allee effect in GYE wolves.

One advantage of modelling a reduced probability of finding mates at low densities as a mathematical model rather than a simulation model is that model outputs (in this case spread rate) can be expressed as explicit functions of model parameters. Eq. (2.24) quantifies the effect of a reduced probability of finding mates at low densities on population spread rate. This equation (Eq. (2.24)) also provides a useful rule of thumb: if all individuals search for mates at the beginning of their dispersal path the population will spread twice as fast when compared to a population where all individuals search for mates at the end of their dispersal path. This rule of thumb holds for GYE wolves and all populations where A/N_c is much greater than r (see Eq. (2.24)).

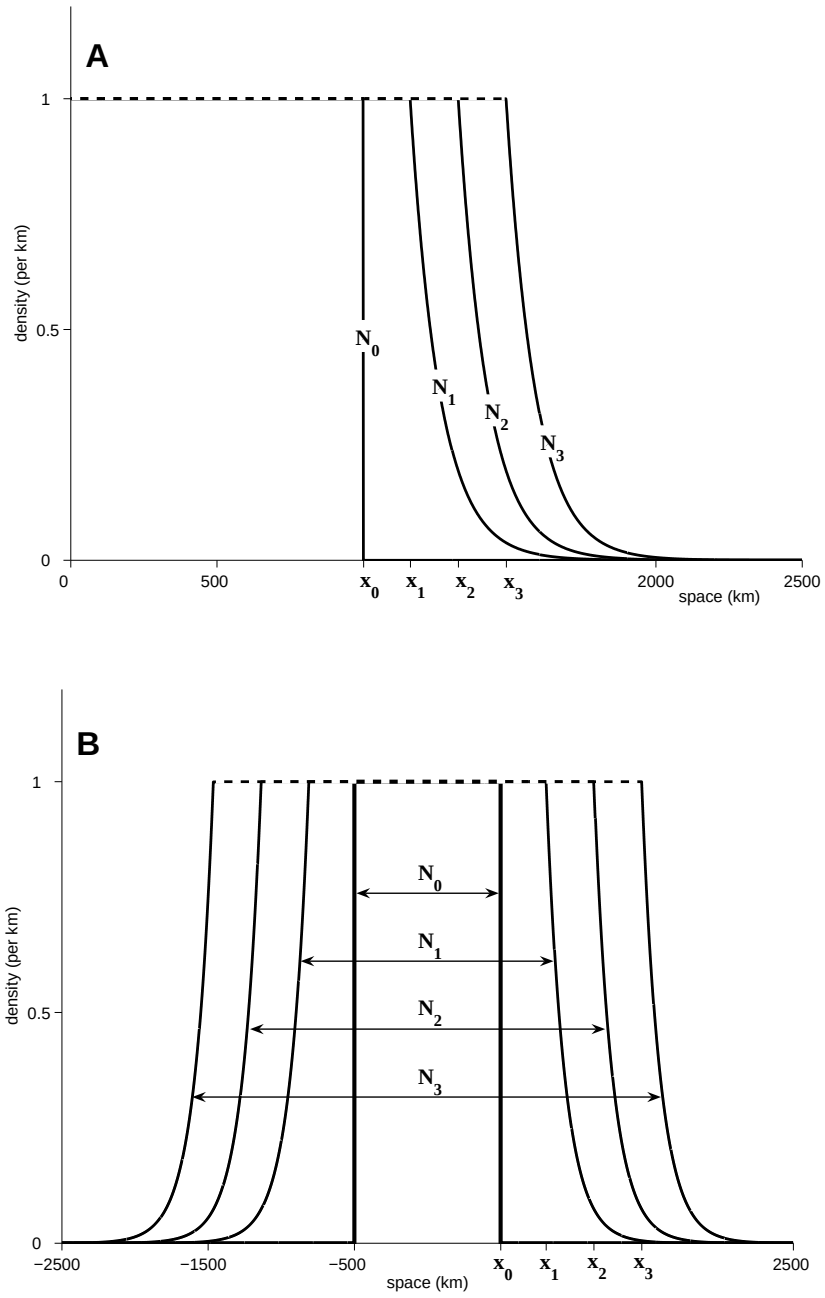

Figure 2.3: Two different initial population densities are shown. A) For initial condition 1, a population has invaded the left side of the domain. Formally, initial condition 1 is defined as $N_0(x) \geq N_c$ for $-\infty < x < x_0$ and $N_0(x) = 0$ otherwise. Example solutions to Eq. (2.14) show the population spreading to the right. The parameters are: $\alpha = 0.01$, $r = 1$, $A = 25$, and $N_c = 1$. The extent population with density greater than N_c is $x_0 = 1001, x_1 = 1161, x_2 = 1342, x_3 = 1523$. B) For initial condition 2, a population has invaded the center of the domain. Formally, initial condition 2 is $N_0(x) \geq N_c$ for $-x_0 \leq x \leq x_0$ and $N_0(x) = 0$, otherwise. Example solutions to Eq. (2.15) show the population spreading in both directions. The parameters are: $\alpha = 0.04, r = 1.135, A = 12.5, N_c = 1$. The extent of the population with density greater than N_c is: $x_0 = 500, x_1 = 811, x_2 = 1137, x_3 = 1464$. In both A and B the dotted line indicates that this analysis focuses on modelling the population dynamics at low densities.

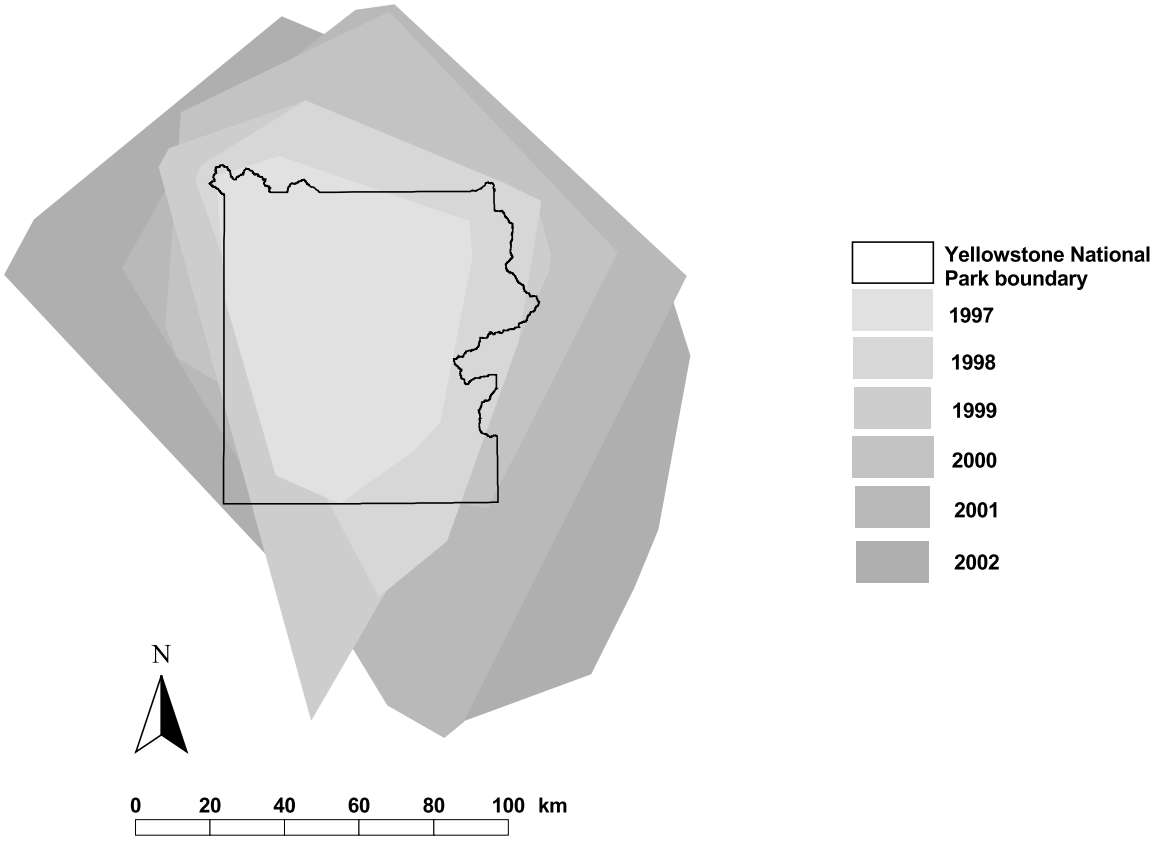

Figure 2.4: For each year, the area occupied by all wolf packs of density N_c or greater is calculated as a Minimum Convex Polygon (MCP) and shown in grey scale. The Yellowstone National Park shape file (black line) was provided by Spatial Analysis Center at Yellowstone National Park.

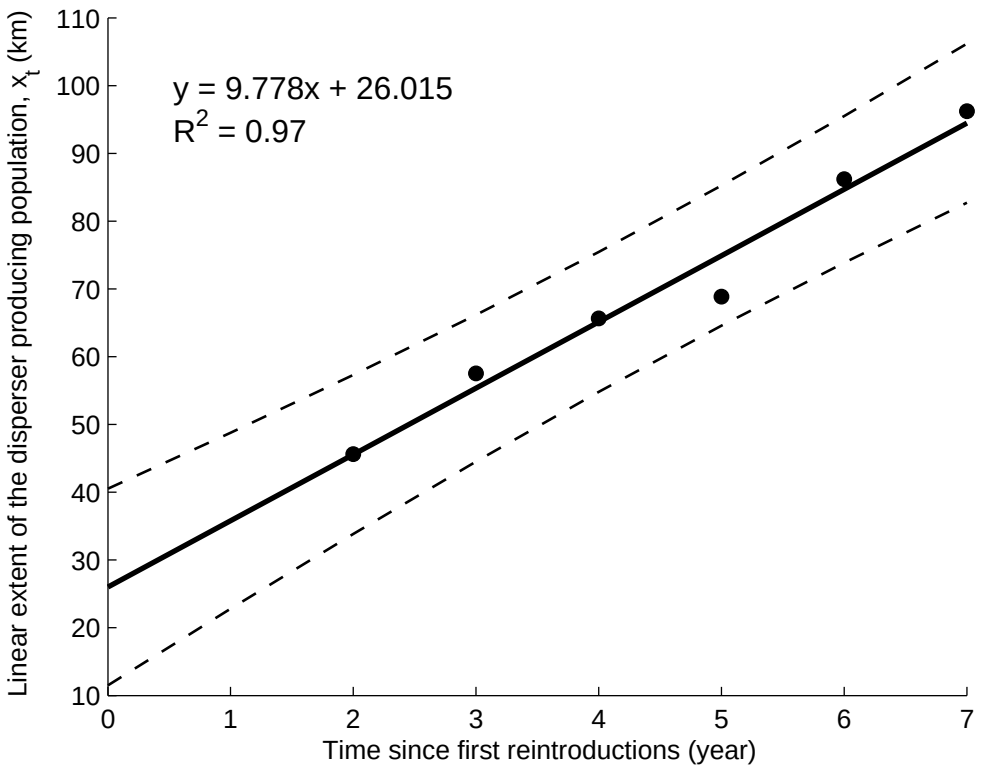

Figure 2.5: The MCP area recolonized is assumed circular with radius equal to x_t the linear extent of recolonization by packs with density N_c or greater (dots). The population spread rate is equal to the slope of the linear regression. The 95% confidence interval for the linear regression are shown as dotted lines.

Table 2.3: The predictions of two models compared to the observed spread rate for wolves recolonizing the GYE

Model	Spread rate (km/year)
Pair formation prior to dispersal	15.26
Observed spread rate (95% CI upper limit)	12.05
Observed spread rate	9.78
Pair formation following dispersal	7.59
Observed spread rate (95% CI lower limit)	7.51

Separating the two processes that lead to population growth (breeding unit establishment and subsequent growth following the establishment of breeding groups) may result in different model outcomes (e.g. unconditional extinction, unconditional survival, or extinction-survival scenarios (Boukal and Berec, 2002)) which may, in turn, suggest different strategies to best control the abundance of target species.

These results invite two main areas of future research. First, note that while Eq. (2.24) precisely describes the relationship between model parameters and spread rate, it is only valid when the population is spreading (e.g. spread rate is greater than zero). In this chapter, I have not determined the full range of model outcomes. This may be especially relevant to wolf populations that were heavily exploited where the population range may retact. Second, while a reduced probabilty of finding mates at low densities is sufficient to explain the observed rate of recolonization other mechanisms may also sufficiently explain this observation. For example, other mechanisms such as sex biased dispersal (as occurs in some large mammals and birds, Pusey 1987) or dispersal triggered by food shortages, aggression, or inbreeding avoidance (**?**). Future work is needed to derive models where the effect of these mechanisms on population spread rate is determined.

This study provides three meaningful results; 1) the derivation of a spatially-explicit model for a reduced probability of finding mates at low densities, 2) a reduced probability of finding mates at low densities may cause an Allee effect for GYE wolves, and 3) a formula for the population spread rate that is a function of demographic, dispersal and pair formation parameters (Eq. (2.24)). While other studies have investigated Allee effects caused by a reduced probability of finding mates at low densities (see Introduction), the utility of this work is in the additional realism garnered from separating breeding group establishment and population size/density changes following establishment through immigration, emigration, births and deaths.

Chapter 3

GPS measurement error gives rise to spurious 180 degree turns and strong directional biases

Introduction

Global Positioning System (GPS) collar data are frequently used in ecological studies of mammal movement. In these studies, GPS collars record the spatial location of an animal at fixed intervals by using satellite technology to pinpoint the animal's locations to varying accuracy. Despite widespread use, there are several sources of error that influence the accuracy of measured GPS locations, such as, canopy cover (Rempel et al., 1995; Moen et al., 1997; D'eon et al., 2002; Di Orio et al., 2003), elevation (Moen et al., 1997; Dussault et al., 2001; D'eon et al., 2002), the type of collar (Di Orio et al., 2003), and the number (Moen et al., 1997; Dussault et al., 2001) and geometry (Dussault et al., 2001; D'eon and Delparte, 2005) of satellites used to determine the fix locations. Furthermore, most commercially available GPS units receive signals from the Navigation System with Timing and Ranging (NAVSTAR) satellites (Johnson and Barton, 2004) and signals from these satellites are degraded by selective availability (a pseudo-random noise code, Hofmann-Wellenhof et al. 2001, p 15-16). Each of the aforementioned sources of GPS error can substantially bias the parameterization of movement (Johnson et al., 2002; Jerde and Visscher, 2005) and habitat selection (Frair et al., 2004) models. In this chapter, I determined 1) the effect of GPS measurement error on the measured distribution of turning angles and directional biases and 2) the minimum distance that must be

moved between GPS locations such that the true direction of movement can be detected in the presence of measurement error.

Distributions of turning angles are frequently used to parameterize movement models, where turning angle is the difference in direction for three successive locations (Fig. (3.1)). Measured distribution of turning angles for wolves (*Canis lupus*) where locations were recorded every 15 minutes are shown in Fig. (3.2). Fig. (3.2) shows a high frequency of direction reversals (180 degree turns) for short step lengths (the distance between successive locations). While large error in measured turning angles can occur at short step lengths (Jerde and Visscher, 2005), no previous studies have determined the effect of GPS error on the distribution of measured turning angles.

I defined an animal's directional bias as the difference in angle between the direction of the animal's move and the direction of the bias point (Fig. (3.1)). For a set of measured movement directions, many observations of near zero difference indicates a strong directional bias. The bias point is a location in space that the animal is thought to move with respect to (i.e., the den). Measuring the difference between the direction of movement and the direction of the bias point allows researchers to determine if the animal moves preferentially in the direction of the hypothesized bias point (e.g., Siniff and Jessen 1969).

If the distance between successive locations is large and GPS measurement error is independent of step length, this error will play a proportionally smaller role in the error of the measured turning angles (Jerde and Visscher, 2005). A secondary objective of this chapter was to determine a step length cutoff, where, for move lengths less than the step length cutoff it is impossible to resolve the true direction of movement. For every measured turning angle two step lengths can be calculated, 1) between the first and second location L_t, and 2) between the second and third location (L_{t+1}, Fig. (3.1)). The magnitude of both step lengths influences the ability to detect the true turning angle or direction of movement in the presence of GPS error (Jerde and Visscher, 2005). While it would be possible to determine the step length cutoff curve for each pair of measured step lengths, the implications of such a result would be cumbersome and challenging to implement. A simpler approach is to determine a step length cutoff that both moves must exceed and remove all locations from the GPS data that do not exceed the cutoff.

For any given study, the step length cutoff is influenced by the type of data used. I determined the step length cutoff for, 1) measured distributions of turning angles which are used to parameterize individual based movement models and random and correlated random walk models (Kareiva and Shigesada, 1983; Turchin, 1998) and 2) measured differences between the direction of an animal's movement and the direction of a bias point (e.g. the den site, Siniff and Jessen 1969). For brevity, I refer to these models as 1) turning angle, and 2) directional bias. In the following sections, I determined the distributions of measured

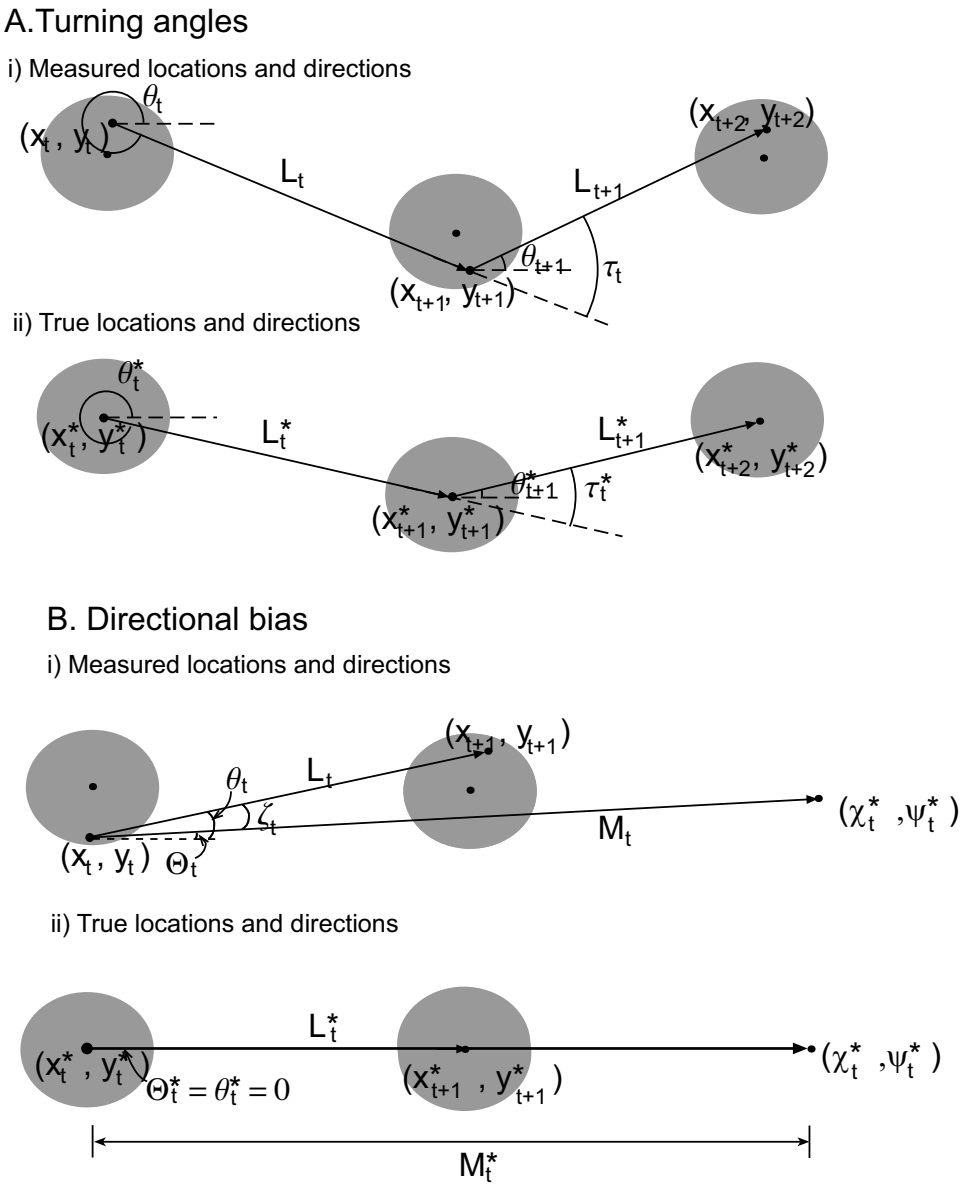

Figure 3.1: The grey circles are used to denote a distribution of measurement error about the animal's true location which is shown as a dot labelled as (x_i^*, y_i^*). True angles are measured with respect to the true locations at the center of the GPS error distributions, whereas measured angles are calculated with respect to measured locations drawn from the GPS measurement error distribution. A.i) shows the measured turning angle τ_t calculated as the difference between the measured directions θ_{t+1} and θ_t. A.ii) shows the true turning angle τ_t^* calculated as the difference between the true directions of movement, $\theta_{t+1}^* - \theta_t^*$. B.i) shows the measured directional bias ζ_t which is the difference between $\Theta_t - \theta_t$. B.ii) shows the true directional bias ζ_t^* calculated as $\Theta_t^* - \theta_t^*$

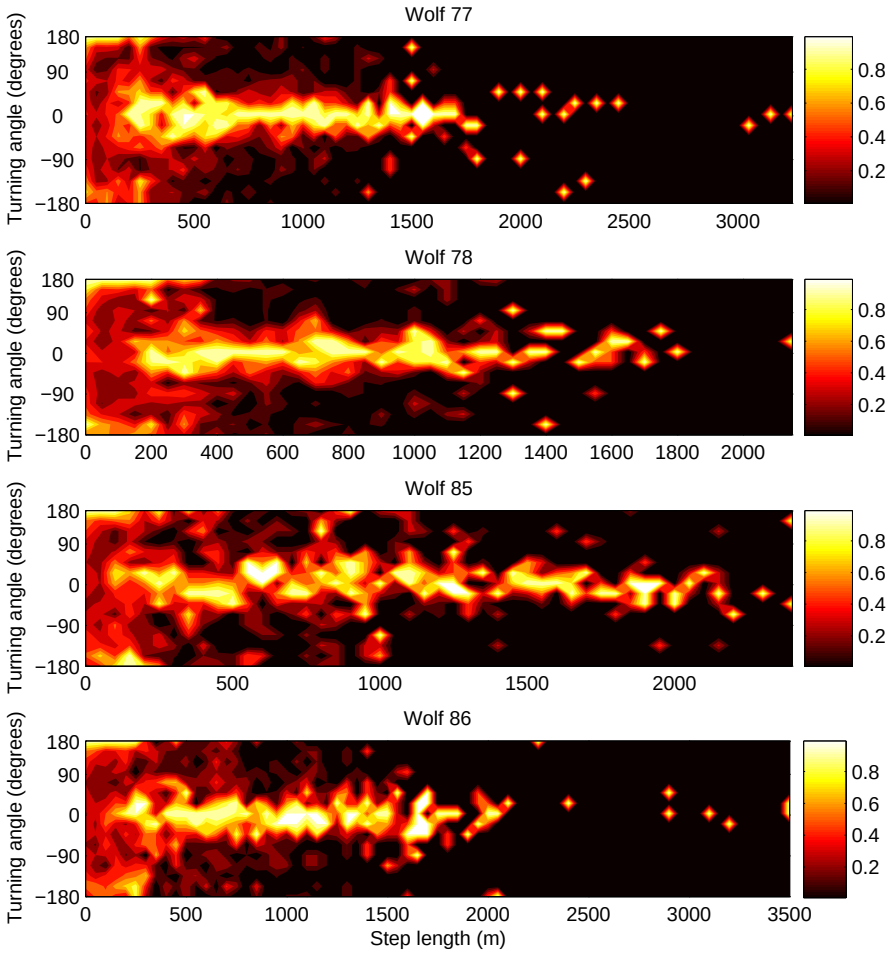

Figure 3.2: GPS data from four wolves where the distribution of turning angles is shown as a function of step length. A high frequency of 180 degree turns are shown in yellow/white for step lengths of < 400 m. The figure was generated by discretizing wolf turning angles into 10 m increments of step length. The sum of the angle frequencies for each step length bin is 1.

turning angles and directional biases in the presence of measurement error using numerical simulations and mathematical analysis. I used numerical simulations, for both types of data and determined the cutoff step length above which the true direction of movement is detected using standard hypothesis testing procedures.

Numerical simulations

Turning angles

I used a numerical simulation to determine the distribution of measured step lengths in the presence of GPS error. The * notation is used to denote true locations, directions, and turning angles. The absence of * indicates a measured location, direction, or turning angle. The numerical simulation consisted of the following steps:

1. I defined a distribution k of GPS measurement error.
2. I defined the animal's true location (x_t^*, y_t^*) for three successive time steps $(t = 1, 2, 3)$ and calculated the true turning angle τ_1^*.
3. I choose one measured location (x_t, y_t) from the GPS measurement error distribution k, centered at each of the three true true locations and calculated the turning angle τ_1 between the three measured locations.
4. I repeated step 3 100 times and used the V test (Zar 1998, p 618-620, see Appendix A) to test if the distribution of turning angles was unimodal with a mean equal to the true turning angle.
5. I repeated steps 2-4 for different true step lengths L^*.
6. I found the minimum distance between the true locations L_{cut}^* that must exist so that the true turning angle is detected.

All directions were measured with respect to horizontal in the anticlockwise direction (see Fig. (3.1)). I defined the GPS error distribution as,

$$k(r) = \frac{1}{2\pi b^2} \exp(-br) \qquad \text{for } 0 \leq r < \infty, \tag{3.1}$$

where r is the distance of the between the measured and true locations and b is a coefficient describing the steepness of the exponential function. An exponential rather than a Gaussian distribution is used to

model GPS error because this fits GPS data from a stationary collar better (H. McKenzie, pers. comm.). The inverse cumulative method (Haefner ????, p 217-218) was used to select measured locations from the distribution of GPS measurement error as described in Appendix A. Moen et al. (1997) expect that 95% of GPS locations fall within 12-31 m of the collar's true location. Assuming that 95% of GPS locations fall with 31 m of the collar's true location, I estimated $b = 6.5$. After having determined the measured locations $(x_1, y_1), (x_2, y_2)$, and (x_3, y_3), the directions of movement on the first and second moves were calculated as,

$$\theta_t = \begin{cases} \tan^{-1} \frac{y_{t+1}-y_t}{x_{t+1}-x_t} & \text{for } x_{t+1} > x_t \text{ and } y_{t+1} \geq y_t, \\ 180 + \tan^{-1} \frac{y_{t+1}-y_t}{x_{t+1}-x_t} & \text{for } x_{t+1} < x_t, \\ 360 + \tan^{-1} \frac{y_{t+1}-y_t}{x_{t+1}-x_t} & \text{for } x_{t+1} > x_t \text{ and } y_{t+1} < y_t. \end{cases} \tag{3.2}$$

Furthermore, the measured turning angle was calculated as,

$$\tau_t = \theta_{t+1} - \theta_t. \tag{3.3}$$

The V test (see Appendix A) was performed to test if the 100 τ_1 values generated by Eq. (3.3) were unimodal distribution with mean equal to the true turning angle τ_1^*. The true cutoff step length, L_{cut}^*, was the value of L^* where the null hypothesis is rejected for all $L^* \geq L_{cut}^*$. The effect of the GPS error coefficient b and the true turning angle τ_1^* on the step length cutoff L_{cut}^* was also determined.

However, L_{cut}^* is the *true* step length cutoff and in the presence of GPS measurement error, short true step lengths will be measured as much larger than they actually are (Jerde and Visscher, 2005). Therefore, step lengths measured to be greater than L_{cut}^* may actually be less than L_{cut}^*. From the GPS data it is only possible to determine the measured step length cutoff. Therefore, I determined the measured step length where it was 95% certain that the true step length was greater than L_{cut}^* using a numerical simulation.

I performed a simulation for true step lengths of $1, 2, ..., 99, 100$ m. For each true step length, I found three measured locations and calculated the two measured step lengths. I repeated this process 10000 times for each true step length and binned each measured step length at 5 m intervals. I calculated the proportion of true step lengths less than L_{cut}^* for each bin. The measured step length cutoff was the bin that contained less than 5% true step lengths less than L_{cut}^*.

Directional bias

Numerical simulations to determine the effect of GPS measurement error on the measured distribution of directional biases were identical to the turning angle simulation except that the difference between the direction of the bias point and the direction of the next move was calculated rather than the turning angle (Fig. (3.1)). The GPS measurement error distribution was Eq. (3.1). Two measured locations were drawn from a distribution of GPS measurement error using the procedure described in Appendix A. The direction between the first and second measured locations was calculated using Eq. (3.2). I let the true location of the bias point be (χ_t^*, ψ_t^*) and there was no measurement error around this point such that the measured and true locations of the bias point were identical. I let the direction from the true first location to the bias point be $\Theta_1^* = \pi$. The direction from the first measured location to the bias point was calculated as,

$$\Theta_t = \begin{cases} \tan^{-1} \frac{\psi_t^* - y_t}{\chi_t^* - x_t} & \text{for } \chi_t^* > x_t \text{ and } \psi_t^* \geq y_t, \\ 180 + \tan^{-1} \frac{\psi_t^* - y_t}{\chi_t^* - x_t} & \text{for } \chi_t^* < x_t, \\ 360 + \tan^{-1} \frac{\psi_t^* - y_t}{\chi_t^* - x_t} & \text{for } \chi_t^* > x_t \text{ and } \psi^* < y_t, \end{cases} \tag{3.4}$$

The difference between the direction of the bias point and the direction of the next move was,

$$\zeta_t = \Theta_t - \theta_t, \tag{3.5}$$

I calculated the V statistic (as shown in Appendix A) to test if the distribution of 100 ζ_1 values generated by Eq. (3.5) were drawn from a unimodal distribution with a mean $\zeta_1^* = \pi$ (since, $\theta_1^* = 0$). The effect of the GPS error coefficient b and the distance between the true location and the bias point, M_1^* on the the true step length cutoff were also determined.

As for the turning angle simulation, I used a numerical simulation to determine the relationship between *measured* and *true* step lengths. I ran a simulation for true step lengths of $1, 2, ..., 99, 100$ m. For each true step length, I found two measured locations and calculated the measured step length. I repeated this process 10000 times for each step length. Each measured step length was binned at 5 m intervals. I calculated the proportion of true step lengths less than L_{cut}^* for each bin. The measured step length cutoff L_{cut} was the bin containing 5% or less true step lengths less than L_{cut}^*.

Analytical approach

I determined the expected distribution of measured turning angles for an animal that does not move for three successive time steps. For analytic tractability, I used a Gaussian distribution to describe the probability density of measured locations (i.e., the distribution of GPS measurement error). I used several change of variables to find the measured distribution of turning angles. The first change of variables was $u_t = x_{t+1} - x_t$, $u_{t+1} = x_{t+2} - x_{t+1}$, $v_t = y_{t+1} - y_t$, and $v_{t+1} = y_{t+2} - y_{t+1}$. These are the x and y displacements for the first and second moves. I used the trigonometric relationship between displacements and angles (i.e., $u_t = L_t \cos\theta_t$) to change from an expression of the x and y displacements for the first and second moves to an expression of the measured directions of the first and second moves. Lastly, I determine the expected measured difference in angle between the directions of the first and second moves. I verified the results of the mathematical analysis by modifying the procedure outlined in the Numerical simulations section so that the distribution of GPS error is equal to a bivariate Gaussian distribution and for the case where the animal does not move between locations ($L^* = 0$).

Similarly, I determined the expected distribution of measured directional biases for an animal located at the bias point that did not move for two successive time steps. With no loss of generality, I let the bias point (χ_t^*, ψ_t^*) be located at $(0, M_t^*)$. I used the change of variables $w_t = -x_t$ and $z_t = M_t^* - y_t$. The final change of variables was to define ζ_t as the difference between the direction of the bias point and the direction of the measured move. All other changes of variables were as described above. Numerical simulations were performed for a bivariate Gaussian distribution of measurement error where the animal was located at the bias point and did not move for two successive time steps to verify the results of the mathematical directional bias analysis. For further details on the mathematical techniques used to determine the measured distribution of turning angles and directional biases see Appendix A.

Results

I found that GPS measurement error gives rise to spurious 180 degree turning angles and strong directional biases. Fig. (3.3) shows the distribution of measured turning angles as a function of step length for true turning angles of $\tau_1^* \in \{-\pi, -3\pi/4, ..., 3\pi/4, \pi\}$. Note that at short step lengths there is a high frequency of 180 degree turns. The step length cutoff (above which the true direction of movement can be detected) is shown as a red line. The step length cutoffs were $0, 0, 4, 12$, and 13 m respectively.

To show that for short step lengths GPS measurement error gives rise to spurious 180 degree turning angles, I mathematically determined that the expected distribution of measured turning angles for an

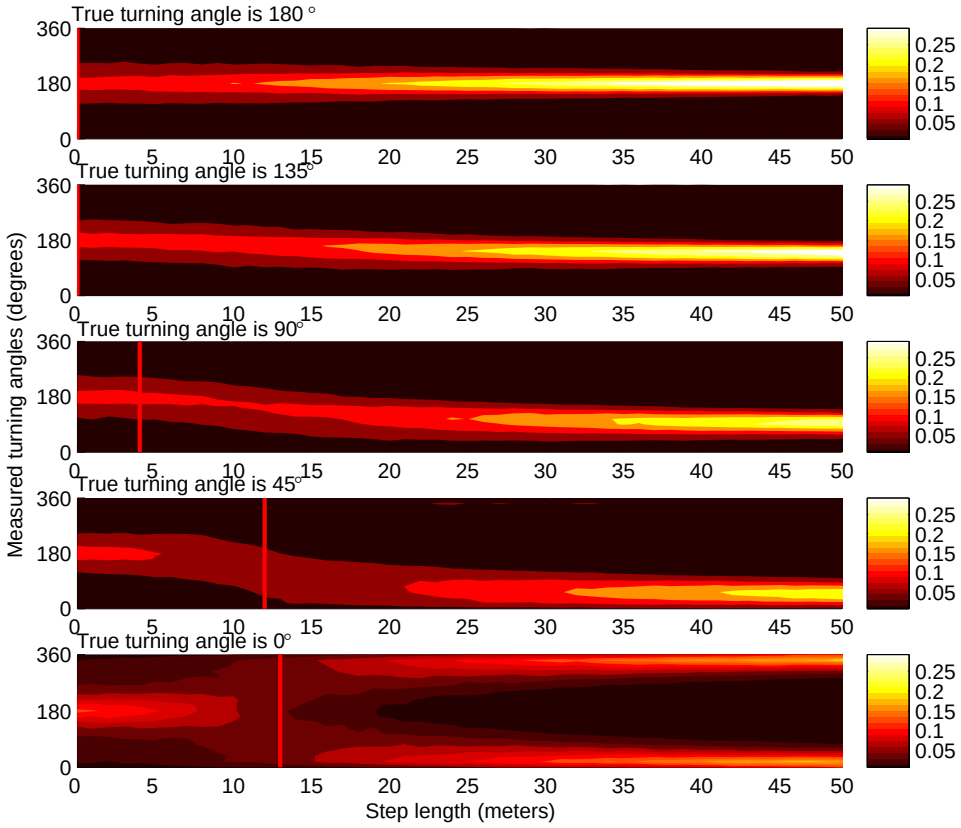

Figure 3.3: Three successive locations each with GPS error were simulated as described in the text. The figure shows the effect of the true turning angle τ_1^* on the true step length cutoff value L_{cut}^* (shown as a red line). The proportion of measured turning angles τ_t are shown as a function of step length. Note that at short step lengths there is a high frequency of measured 180 degree turns irrespective of the true direction of movement. The step length cutoffs shown in the figure from top to bottom are 0,0,4,12,13 m. The parameters for this simulation were $b = 6.5$ and 10000 iterations were performed.

animal that does not move for three successive time steps as,

$$h_{\tau,0}(\tau_t) = \frac{24 - 3\cos\tau_t \left(2\cos\tau_t + \sqrt{4-\cos\tau_t}\left(\pi + 2\tan^{-1}\left(\frac{-\cos\tau_t}{\sqrt{4-\cos^2\tau_t}}\right)\right)\right)}{4\pi\left(\cos^2\tau_t - 4\right)^2}. \tag{3.6}$$

(see Appendix A). This result demonstrates that a stationary animal is most likely to be measured as turning 180 degrees (see Fig. (3.4A)) even though the true turning angle is undefined. I tested Eq. (3.6) against the numerical simulations. The fit of Eq. (3.6) to numerical simulations is shown in Fig. (3.4A). Fig. (3.4A) shows a very close agreement between the numerical simulations and the analytical results.

Similarly, I mathematically determined the expected distribution of measured directional biases for an animal located at the bias point that did not move for two successive time steps. In Appendix A, I showed that the measured distribution of direction biases was,

$$h_{\zeta,0}(\zeta_t) = \frac{16 - 4\cos\zeta_t \left(2\cos\zeta_t - \sqrt{2-\cos^2\zeta_t}\left(\pi + 2\tan^{-1}\left(\frac{\cos\zeta_t}{\sqrt{2-\cos^2\zeta_t}}\right)\right)\right)}{\pi(4\cos^2\zeta_t - 8)^2}. \tag{3.7}$$

Eq. (3.7) has a maximum at $\zeta = 0$ (see Fig. (3.4)). Eq. (3.7) shows a systematic error in measured directional bias when the animal is near the bias point and does not move. Numerical simulations showed a close agreement between the results of the numerical simulation and the analytical results (Fig. (3.4)).

The true step length cutoff varies as a function of the GPS error coefficient b and the true turning angle τ_1^*. Fig. (3.5) shows the effect of b and τ_1^* on the true step length cutoff. The true step length cutoff is a linearly increasing function of b and has a maximum when the true turning angle is zero. Similarly, for directional biases, Fig. (3.6) shows the effect of the GPS error coefficient b and the distance between the true location and the bias point M_1^* on the the true step length cutoff. The step length cutoff was an increasing function of b and a decreasing function of M_1^*.

For $b = 6.5$ and $\tau_1^* = 0$ the step length cutoff was 16.2 m (Fig. (3.5)). However, 16.2 m was the *true* step length cutoff and in the presence of GPS measurement error, short true step lengths will be measured as much larger than they actually are (Jerde and Visscher, 2005). For measured step lengths of between 50-55 m, I found that 95.1% of true step lengths were 16.2 m or greater (Fig. (3.7)). For the directional bias simulations for $b = 6.5$ (implying that 95% of measured locations were within 31 m of the true location) and $M_1^* = 15$ m (i.e., 15 m between the animal's location and the bias point) the true step length cutoff was 15.8 m (Fig. (3.6)). For measured step lengths of between 50-55 m, I found that 95.2% of the true step lengths were 15.8 m or greater (Fig. (3.7)).

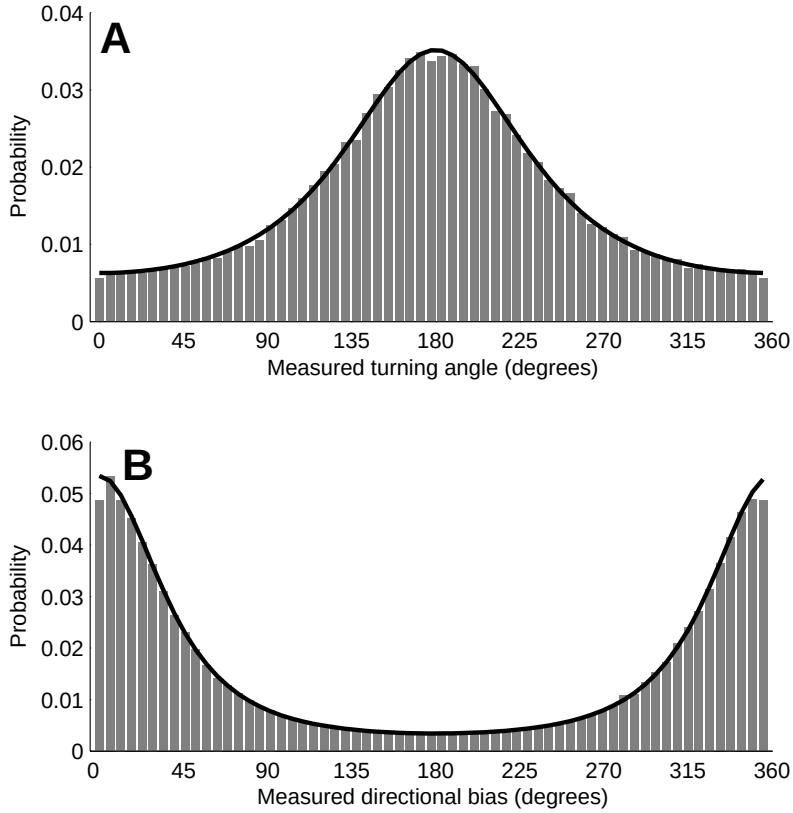

Figure 3.4: A) The grey bars are probability of measured turning angles generated using a numerical simulation. The simulation assumed that the animal did not move for three successive time steps and assumed a Gaussian distribution of GPS measurement error. For each iteration three measured locations were generated and the turning angle calculated. 100000 measured turning angles were calculated. The fit of the analytical solution (Eq. (3.6)) to the simulation data is shown as a black line. B) The grey bars are the probability of measured difference in angle between the direction of the bias point and the direction moved. 100000 iterations were performed and the fit of Eq. (3.7) is shown as a black line. Further details on the simulation procedure can be found in the text.

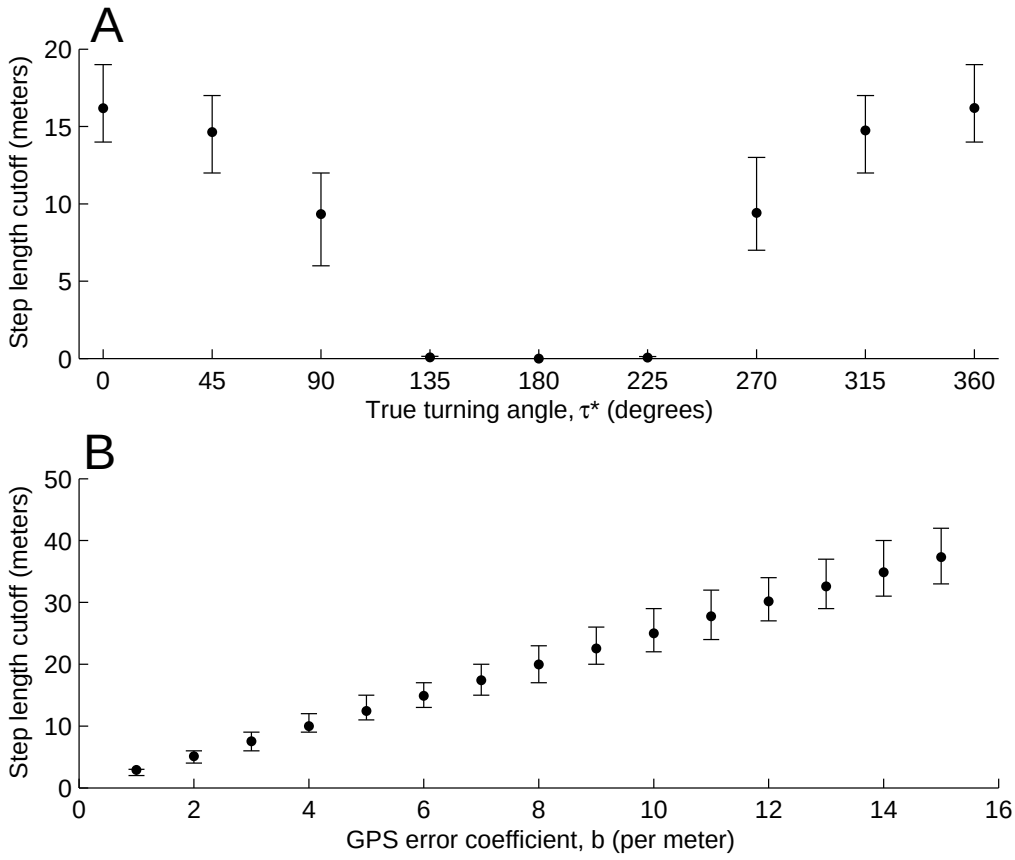

Figure 3.5: The true step length cutoff value determined for different, A) true turning angles τ_1^* for $b = 6.5$ and B) values of the GPS error coefficient b for $\tau_1^* = 0$. The mean L_{cut}^* value is shown as a dot and bootstrapped 95% confidence intervals are shown as vertical bars. 1000 iterations of the code were performed and for each iteration 100 turning angles were generated.

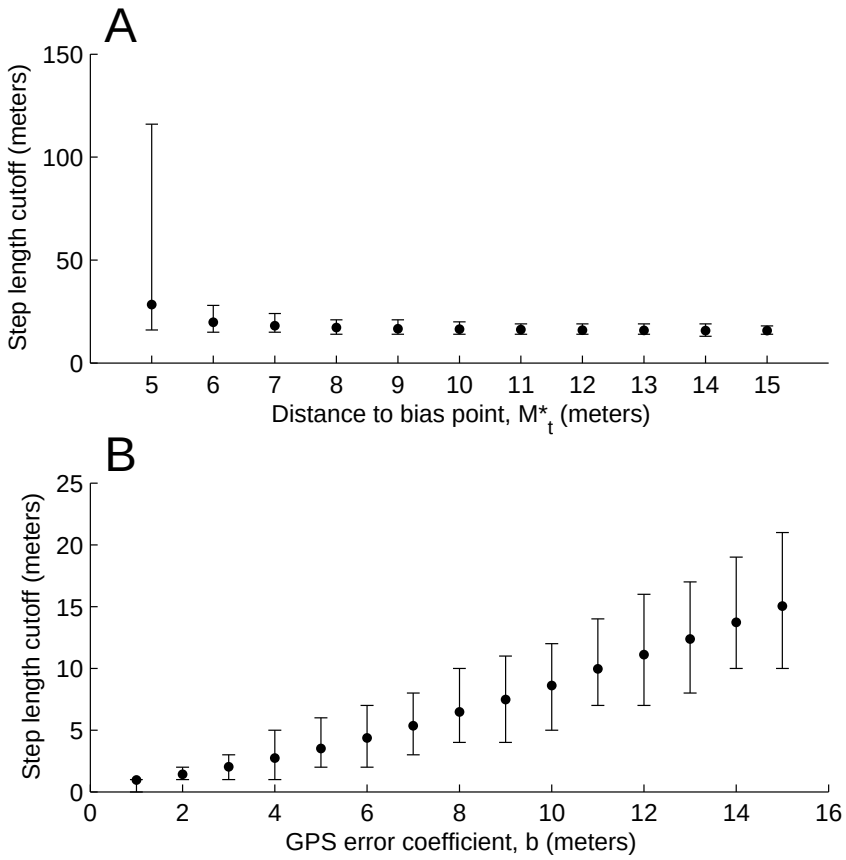

Figure 3.6: The true step length cutoff parameter determined for different, A) distances between the location of the first move and the bias point M_1^* for $b = 6.5$ and B) values of the GPS error coefficient b for $M_1^* = 200$. The mean L_{cut}^* value is shown as a dot and bootstrapped 95% confidence intervals are shown as vertical bars. 1000 iterations of the code were performed and for each iteration 100 directions of movement were generated.

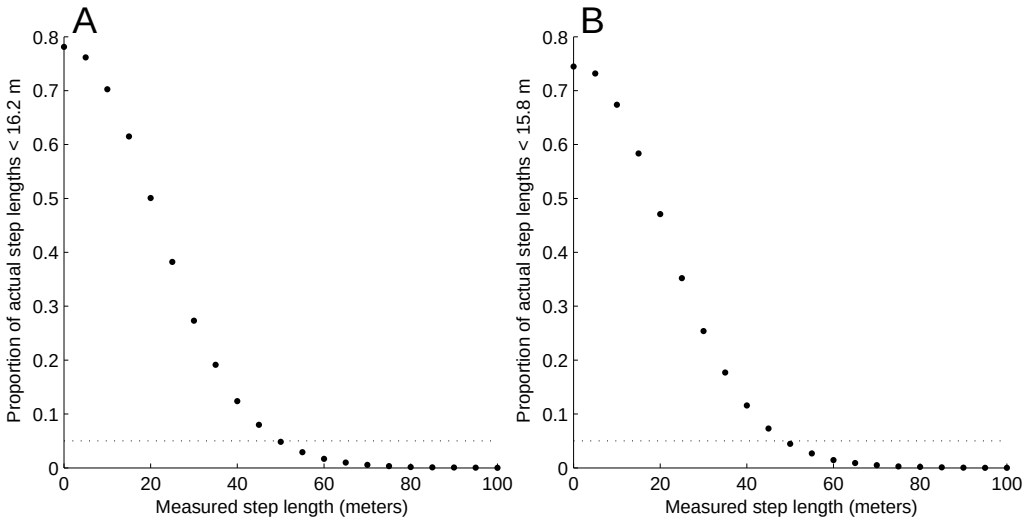

Figure 3.7: The relationship between true and measured step length. A) I performed 10000 iterations where I randomly chose 3 measured locations where the true step length for both moves was the same and between 0 and 100 m. All measured step lengths were binned at 5 m intervals. I calculated the proportion of true step lengths less than 16.2 m for each bin. For a measured step length of 50-55 m the proportion of true step lengths less than 16.2 m was 0.049. An identical procedure was used in B) except that only two measured locations were chosen on each iteration and the proportion of true step lengths less than 15.8 m was calculated. For a measured step length of 50-55 m the proportion of true step lengths less than 15.8 m was 0.048.

Discussion

The close agreement between the results of the numerical simulation and the mathematical analysis (Fig. (3.4)) provides strong evidence to support the conclusion that spurious 180 degree turns and strong directional biases will result from GPS measurement error. These results show that turning angle measurement error is a systematic rather than a random error. Specifically, when the distance between successive GPS locations is small, GPS error will give rise to spurious 180 turns. The measured directional bias is also affected by a systematic error. When the animal is near the bias point and moves only a short distance between GPS locations, the directional bias is most likely measured as zero.

Insight into why spurious 180 degree turns arise from GPS error can be gained by considering a simpler question: why, if an animal does not move for three successive time steps, is it likely that the measured turning angle is 180 degrees? Consider a symmetrical distribution of GPS measurement error in two spatial dimensions with a global maximum at the animal's true location that monotonically decreases away from this point. The most likely direction the animal was measured to have come from is ϕ_{t-1} (see Fig. (3.8B)). Fig. (3.8C) shows ϕ_t the most likely direction the animal was measured to have moved to. If line segments where drawn through the point (x_t, y_t) in the directions of ϕ_{t-1} and ϕ_t both line segments would pass through the maximum of the GPS error distribution. However, ϕ_{t-1} must terminate at the point from which ϕ_t originates because ϕ_{t-1} and ϕ_t are the directions of successive movements. Therefore, $\phi_t - \phi_{t-1}$ the most likely turning angle, must be 180 degrees. A similar argument can be used to explain why an animal located at a bias point that does not move, would be most likely to have a measured directional bias of zero.

The results in this chapter have useful implications for studies analyzing GPS data where turning angles and directional biases are calculated. For example, a knowledge of the distribution of measured turning angles that results from GPS measurement error is especially relevant to studies that identify movement states using measured turning angles and step lengths (e.g., Franke et al. 2004; Morales et al. 2004). Because the turning angle error is systematic spurious 180 degree turns at short step lengths are very likely to be identified as a movement state. Furthermore, studies of an animal's directional bias that fail to consider the effect of GPS measurement error may detect directed movement towards a bias point when no directed movements exists (e.g., Type I statistical error). The results in this chapter, however, do not imply that wolves, for example, do not move with a high frequency of direction reversals for short step lengths. Instead, these results, suggest that biologists should consider GPS measurement error as a possible explanation for high frequency direction reversals when animals move only a short distance between locations. For the wolf data shown in Fig. (3.2) visual inspection suggests that the direction reversals persist for moves up

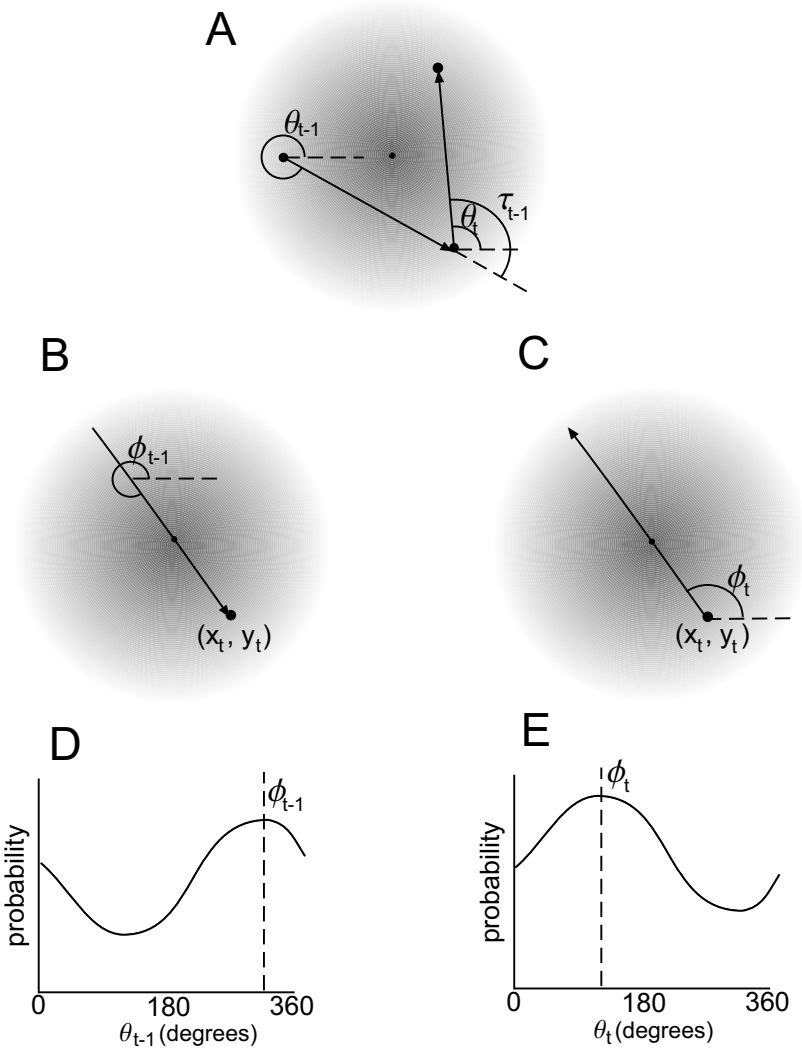

Figure 3.8: For an animal that does not move for three successive time steps, the distribution of GPS error is centered at the same point. The probability density of measured animal locations is shown in grey scale where darker shades represent higher probabilities. A) shows an animal moving in the direction of the arrows with a measured turning angle of τ_t. For an animal measured at (x_t, y_t) the probability the animal was measured to have come **from** the direction θ_{t-1} is the sum of probabilities for all measured locations with a direction of θ_{t-1} between the measured location and (x_t, y_t). D) shows the probability density function for the measured direction the animal came from, θ_{t-1}. The most likely direction the animal came from is ϕ_{t-1} (shown in B). Note that ϕ_{t-1} is the direction of a vector that terminates at (x_t, y_t) and travels through the maximum of the GPS error probability density function. Similarly, E) shows the probability density function for the direction the animal was measured to have moved **to**, θ_t. The most likely direction the animal was measured to have moved to is ϕ_t (shown in C). Turning angles are measured as $\tau_t = \theta_{t+1} - \theta_t$. Therefore, the most likely measured turning angle is $\phi_t - \phi_{t-1} = 180$ as shown in B and C.

to 400 m. For an exponential distribution of GPS error, where 95% of locations are within 31 m of the true location, GPS error can only account for the high frequency of direction reversals for step lengths up to 50-55 m. Therefore, the wolf data in Fig. (3.2) may provide some evidence that a high frequency of direction reversals may be more than a mere consequence of GPS measurement error or that measured locations were less precise than expected.

For studies of turning angles or directional biases, I offer three approaches that could be used to reduce the effect of GPS measurement error; 1) remove all short step lengths and locations near the bias point, 2) answer similar research questions that do not require measuring distributions of angles, or 3) increase the measurement precision. For some animals, study areas, or research questions there may be no reason to expect that turning angles or directional biases would be different at short step lengths than at longer step lengths. In these cases it is recommended that short step lengths be removed prior to the analysis, effectively characterizing movement as either resting (where the animal moves a negligible distance and where the turning angle cannot be determined) and moving (where the step length and turning angle or directional bias can be measured accurately). If removing short step lengths from the data is not an option, researchers should consider whether calculating distributions of angles is necessary to answer the research question. Measured angles are especially sensitive to measurement error because even small location errors can result in large errors in measured angles. Therefore, more data can be retained for questions that concern how animals use space than for questions concerning the angles at which animal's move. This is due to the lesser effect of location measurement error (e.g., suppose the error is equal to a few centimeters) on estimating an animal's true location (e.g., measured within a few centimeters) versus error in estimating the animal's true turning angle (e.g., measured with up to an 180 degree error). Lastly, Johnson and Barton (2004) provide an excellent discussion of factors that influence GPS measurement error. The true direction of movement could be detected at shorter step lengths if the effects of any of the factors discussed were reduced, for example, by using differential correction or by choosing a flat study area.

For studies were removing short step lengths from the data is appropriate, in this chapter, I have determined that for measured step lengths of greater than 50-55 m the true turning angle and directional bias can be determined (for $b = 6.5$). Note that the V test will detect movement in a particular direction, even if that movement is very weak. Using higher step length cutoffs provides greater certainty in the measured distribution of turning angles (Fig. (3.3)). Furthermore, when the difference in magnitude between the true turning angle and 180 degrees is small, it may not be possible to detect the effect of the error. For example, in Fig. (3.3) the step length cutoff is zero when the true turning angle is 135 degrees. A larger sample size is needed for the V test to have sufficient power to detect small differences between 180 degrees

and the true turning angle.

These results suggest a step length cutoff of 50-55 m. A step length cutoff of 50-55 m is not appropriate when; 1) the GPS error coefficient is not 6.5 (Figs. (3.5) and (3.6)), 2) the animal is closer than 15 m from the bias point (Fig. (3.6)), and 3) the number of angles used to test for the bias is much less than the 100 simulated data points used to determine the step length cutoffs for this study. Fortunately, wolves frequently move greater than 55 m when locations are sampled at 30 minute intervals. For animals that move smaller distances a sampling scheme whereby the animal can move greater than 55 m per sampling unit is recommended. For all species, the systematic effects of GPS error may be less likely to cause a bias when the sampling interval of the GPS collar is longer, allowing a longer distance to travelled between fixes.

This work demonstrates that a high frequency of 180 degree turns and strong directional biases may be attributable to GPS measurement error, rather than actual animal movements. Because GPS error gives rise to a systematic bias in measured angles it is very likely that movement models that fail to consider the effect of GPS error could yield biased results, especially if the animal moves short distances between location fixes. I determined a step length cutoff above which the true turning angle or directional bias can be detected. Removing all GPS data observations where the step length does not exceed the recommended cutoff is a simple step that can be taken to prevent GPS measurement error biasing movement model results.

Chapter 4

The e®ect of past kill sites, territory boundary, and terrain on wolf movements

Introduction

Recent advances in Global Positioning System (GPS) technology allow collar units worn by animals to record the animal's location at ¯xed intervals. These technological advances have prompted a complementary advance in modelling animal movements (Turchin, 1998; Manly et al., 2002; Moorcroft and Lewis, 2005). Several recent studies focus on understanding the e®ect of landscape features on animal movements (e.g., Fortin et al. 2005; Fortin 2005; Whittington et al. 2005). In this chapter, I use GPS data and modelling to identify ecological features that in°uence wolf (Canis lupus) movement. In particular, I investigate the e®ects of the location of past kill sites, the territory boundary, and elevation gradients on movement directionality.

Wolf movement ful¯ls two main objectives; hunting and territory defense (Mech and Boitani 2003, p 30)

Figure 4.2: The GPS data for each of the four wolves used in the analysis are shown. Projection: UTM (Universal Trans Mercator), Datum: NAD 1983, zone 11. The bottom left corner of the figure is 534872 Easting and 5678413 Northing and the top right corner is 638251 Easting and 5762115 Northing. The period of data collection and number of fixes are shown in Tab. (4.1). Additional figures of the GPS data collected for each wolf are contained in Appendix C.

Testing for directional biases

I tested the hypotheses that wolves orient their movements with respect to the locations of past kill sites, the territory boundary, and the direction of the steepest downhill slope. I also considered movement biases at several different temporal scales. Chapter 3 showed that a move of 55 m is sufficient to determine the actual direction of movement in the presence of GPS error, if the bias point is at least 15 m from the animal and 95% of GPS locations fall within 30 m of the actual location. Hence, I removed all observations where the wolf did not move at least 55 m. The direction of movement, θ_t, at the next step was calculated as,

$$\theta_t = \begin{cases} \tan^{-1} \frac{y_{t+1}-y_t}{x_{t+1}-x_t} & \text{for } x_{t+1} > x_t \text{ and } y_{t+1} \geq y_t, \\ 180 + \tan^{-1} \frac{y_{t+1}-y_t}{x_{t+1}-x_t} & \text{for } x_{t+1} < x_t, \\ 360 + \tan^{-1} \frac{y_{t+1}-y_t}{x_{t+1}-x_t} & \text{for } x_{t+1} > x_t \text{ and } y_{t+1} < y_t. \end{cases} \tag{4.1}$$

The direction of the bias point,Θ_t, was calculated as,

$$\Theta_t = \begin{cases} \tan^{-1} \frac{\psi_t^*-y_t}{\chi_t^*-x_t} & \text{for } \chi_t^* > x_t \text{ and } \psi_t^* \geq y_t, \\ 180 + \tan^{-1} \frac{\psi_t^*-y_t}{\chi_t^*-x_t} & \text{for } \chi_t^* < x_t, \\ 360 + \tan^{-1} \frac{\psi_t^*-y_t}{\chi_t^*-x_t} & \text{for } \chi_t^* > x_t \text{ and } \psi_t^* < y_t. \end{cases} \tag{4.2}$$

The bias point (χ_t^*, ψ_t^*) is either the location of a past kill site, the nearest point on the territory boundary, or the point one step length away with the lowest elevation. The difference in direction between the direction of the bias point and the direction of the next move is,

$$\zeta_t = \Theta_t - \theta_t. \tag{4.3}$$

(see also Fig. (4.1)).

Sub-sampling procedure

I tested for movement biases at different temporal scales, I subsampled the GPS data by including only pairs of locations where the time between locations is 30, 60 or 120 minutes. I calculated the direction of

movement for the subsampled data as,

$$\phi_t = \begin{cases} \tan^{-1} \frac{y_{t+i}-y_t}{x_{t+i}-x_t} & \text{for } x_{t+i} > x_t \text{ and } y_{t+i} \geq y_t, \\ 180 + \tan^{-1} \frac{y_{t+i}-y_t}{x_{t+i}-x_t} & \text{for } x_{t+i} < x_t, \\ 360 + \tan^{-1} \frac{y_{t+i}-y_t}{x_{t+i}-x_t} & \text{for } x_{t+i} > x_t \text{ and } y_{t+i} < y_t, \end{cases} \tag{4.4}$$

where the difference in time between (x_t, y_t) and (x_{t+1}, y_{t+1}) is 15 minutes and $i \in \{2, 4, 8\}$ (see Fig. (4.1)).

Testing for autocorrelation

I tested for autocorrelation between each successive movement direction as the statistical tests in the following subsections assume independence of the data. Most movement models assume that the direction of successive movements are uncorrelated. However, if movement directions are temporally autocorrelated movement can be modelled as a persistent random walk (Kareiva and Shigesada, 1983; Wu et al., 2000). Temporal autocorrelation in movement directions was tested for using a modified version of Pearson's correlation coefficient (Zar 1998 p 649-651, Fisher 1993, p 151, see Appendix A).

Bias toward locations of past kill sites

Kill sites were located by snow backtracking and ground truthing of Very High Frequency (VHF) radio locations. VHF collared wolves were located using a VHF antennae. Wolf tracks were located in the snow and followed backwards in the snow to locations visited previously by the pack. When kills were encountered, the location, prey species, and estimated kill date (based on state of decomposition and age of wolf tracks) was recorded. When wolves were observed near a kill during aerial telemetry flights the location of the kill was recorded and then verified by travelling to the location of the kill on foot (i.e., ground truthing of VHF locations). Kill site locations were recorded for December 2003 - April 2004. Procedures used for identifying kill sites were as described by **?**. I tested for directed wolf movement for 0-5, 5-10, 10-15, 15-20, 20-25, and 25-30 days following each kill.

Only GPS data collected during the winter (i.e. wolves 77 and 78) were used to test for a movement bias towards the location of past kills because snowtracking was only possible in the winter. For each kill within a wolf's territory during the GPS data collection period, I used GPS data between 0-5 days after the day of the kill and calculated ζ_t where the bias point (χ_t^*, ψ_t^*) is the location of a kill made 0 - 5 days prior. Data from each kill was pooled into one estimate of the directional bias ζ for 0-5 days following a kill. I used the V test (Zar 1998, p618-620, see Appendix A) to test for a directional bias towards kills

made during the past 30 days. The distribution of ζ was similarly calculated for GPS data 5-10, 10-15, 15-20, 20-25, and 25-30 days after the kill.

Bias toward the territory boundary

To test for a bias toward the territory boundary, I defined the territory boundary as a 100% Minimum Convex Polygon (MCP, Mohr 1947; Kie et al. 1996) for all data recovered from the GPS collared wolves. Wolves scent mark at their territory boundary at least every 3 weeks (Peters and Mech, 1975) and it is not necessary that wolves constantly patrol the boundary. I tested for biases that occurred only when wolves were within one-quarter of the radius of a circle equal in area to the 100% MCP territory. The one-quarter distance was chosen arbitrarily, but choices of one-half and one-eighth did not influence the results. The bias point for this analysis is defined as the nearest point on the 100% MCP territory boundary. I hypothesized that wolves will patrol their territory boundary by moving perpendicular to the direction of the nearest point on the territory boundary (χ_t^*, ψ_t^*) (i.e., moving parallel to the boundary). For any point (x_t, y_t) there are two directions that a wolf could move in to patrol along the territory boundary. Therefore, wolves that are patrolling the territory boundary move at a 90 or 270 degree angle with respect to the direction of the nearest point the boundary.

I expected that, ζ_t (the difference in direction between the direction of the nearest point on the territory boundary and the next move) is distributed as a mixture of von Mises distributions. The von Mises distribution is used instead of a normal distribution when the data is circular and has been used to model animal movements in numerous previous studies (i.e., Moorcroft and Lewis 2005). The von Mises distribution has a strength parameter κ, and when $\kappa = 0$ the von Mises distribution is a uniform distribution between 0 and 360 degrees. The von Mises distribution has one other parameter μ which is the mean of the distribution. Because the wolves can patrol the boundary by moving in either of two directions, I hypothesized that ζ was a weighted mixed of two von Mises distributions with means of $\mu_1 = 90$ and $\mu_2 = 270$ degrees. Therefore, the hypothesized distribution of ζ is,

$$BVM(\zeta, q, \kappa_1, \kappa_2) = \frac{q}{2\pi I_0(\kappa_1)} \exp\left(\kappa_1 \cos\left(\zeta - 90\right)\right) + \frac{1-q}{2\pi I_0(\kappa_2)} \exp\left(\kappa_2 \cos\left(\zeta - 270\right)\right). \tag{4.5}$$

The likelihood ratio test was used to test Eq. (4.5) against a uniform alternative as shown in Grimshaw et al. (2001). The logarithmic likelihood for the uniform distribution, LL_0, is the logarithmic likelihood of $BVM(\zeta, 0, 0, 0)$. The logarithmic likelihood for Eq. (4.5), LL_1, is the logarithmic likelihood of $BVM(\zeta, \hat{q}, \hat{\kappa}_1, \hat{\kappa}_2)$ where hats denote maximum likelihood parameter estimates. The likelihood ratio test

statistic is calculated as,

$$\Lambda = 2(LL_1 - LL_0). \tag{4.6}$$

This test statistic follows the standard approximation of the χ^2 distribution (Grimshaw et al., 2001) with 3 degrees of freedom.

Bias towards downhill

I hypothesized that wolves move either toward or perpendicular to the direction of the steepest downhill slope. The former is the hypothesis that wolves move downhill; the latter is the hypothesis that wolves move along contours. I formulated six competing hypotheses where each hypothesis is expressed as a von Mises distribution,

$$VM(\kappa, \zeta) = \frac{1}{2\pi I_0(\kappa)} \exp\left(\kappa \cos(\zeta)\right). \tag{4.7}$$

Each of the six models are shown in Tab. (4.2) where ζ is the distribution of differences between the direction of downhill and the direction of movement. The magnitude of the steepest downhill slope is ϵ_t. To be consistent with Fortin (2005), $\Theta_t^{\perp}$ is defined as the direction perpendicular to the direction of the steepest downhill slope that minimizes the difference between the direction of the last movement and $\Theta_t^{\perp}$. Because all models are not nested, Akaike Information Criteria (AIC, Burnham and Anderson 2002) was used to select the best model among the six alternatives. AIC values are calculated as,

$$AIC_i = -2LL_i + 2k \tag{4.8}$$

(Burnham and Anderson, 2002) where k is the number of model parameters and LL_i is the logarithmic likelihood for model i. The ΔAIC is the lowest AIC value subtracted from all other models. ΔAIC values greater than 10 indicate strong evidence to support the best model (i.e., lowest AIC, Burnham and Anderson 2002). The data used for this analysis was subsampled at 30 minute intervals. For this analysis I do not test for directed movement for the 60 or 120 minute subsampled data. At these sampling frequencies there are large distances between (x_t, y_t) and (x_{t+i}, y_{t+i}) such that the elevations at (x_t, y_t) and (x_{t+i}, y_{t+i}) are likely not representative of the change in elevation between the points.

Results

The autocorrelation statistics in Tab. (4.3) show that the direction of movement from the GPS collars sampling the wolves' locations every 15 minutes are temporally autocorrelated. However, when the data

Table 4.2: Models for movement direction with respect to elevation

Models	Description
$VM(0, \zeta)$	Movement is random with respect to the downhill direction
$VM(\kappa, \zeta)$	Directed downhill movement
$VM(d\epsilon, \zeta)$	Magnitude of preference for downhill depends on the magnitude of the downhill slope
$VM(0, \zeta^{\perp})$	Movement is random with respect to the direction perpendicular to the downhill direction
$VM(\kappa, \zeta^{\perp})$	Directed movement perpendicular to the direction of downhill
$VM(d\epsilon, \zeta^{\perp})$	Magnitude of the preference for movement perpendicular to the downhill direction is proportional to the magnitude of the downhill slope

are subsampled such that there is 30, 60, or 120 minutes intervals between locations the direction of movement was uncorrelated for all wolves except for wolf 77 (subsampled at 60 and 120 minutes) and wolf 78 (subsampled at 120 minutes). Autocorrelated data are excluded from all subsequent analyses.

For bias towards kills made during the past 30 days, wolf 77 was found to move back to past kill sites 0-5, 15-20 and 20-25 days old. However, no movement biases were detected for wolf 78. Fig. (4.3) shows the location of kills and GPS data used for the analysis. For all wolves and all uncorrelated subsampling regimes except wolf 78 (subsampled at 60 minutes) and wolf 86 (subsampled at 60 minutes), I found a significant preference for movement perpendicular to the direction of the nearest point on the territory boundary (Tab. (4.5)). Fig. (4.4) shows all the GPS locations that were less than one-quarter of the territory radius away from the boundary. For slope bias, there was strong evidence for movement preferentially in the direction perpendicular to the direction of the steepest downhill slope for all four wolves (Tab. (4.6)).

Discussion

Wolves move to hunt and defend territory (Mech and Boitani 2003, p 30). Various ecological features such as snow depth (Nelson and Mech, 1986; Fuller, 1989; Hebblewhite, 2005) and distance to roads (Whittington et al., 2004, 2005) influence wolf movement. In this chapter, I found some evidence that wolves return to locations of past kill sites, move perpendicular to the direction of the territory boundary, and move perpendicular to the direction of the steepest downhill slope. Other results showed that the measured direction of wolf movement, when locations are sampled every 15 minutes, are temporally autocorrelated (Tab. (4.3)). When locations are sampled at 30 minute intervals, movement directions are no longer temporally autocorrelated and all analysis were performed using GPS data subsampled at a 30 minute intervals or longer. Wolves 77 and 78 showed autocorrelation at the 60 minute (wolf 77 only) and 120 minute subsampling intervals. GPS data for both these wolves was collected during the winter and temporal autocorrelation in movement directions may be due to constraints imposed by deep snow.

Wolf 77 showed a bias towards kills that were 0-5, 15-20, and 20-25 days old; however, wolf 78 showed no bias. These results are not conclusive and several additional factors may have influenced results. Firstly, the study area in and near BNP is very mountainous and there may be a joint effect of elevation and the location of past kill sites on wolf movement. Secondly, past kill sites are described as points in the model, however, if past kill sites that are sufficiently close may be perceived as an area rather than two distinct points. Thirdly, the location of only a few kill sites was known. These kill sites may not be representative of the distribution of kill sites for the study period. Additionally, an overlap between the west boundary

Table 4.3: Temporal autocorrelation results for movement directions for 4 different temporal subsampling regimes

Wolf		Subsampled at			
		15 mins	30 mins	60 mins	120 mins
77	r_{aa}	-0.0008	-0.0009	-0.05	-0.07
	No. of obs.	4349	2286	1158	584
	Reject H_0?	yes	no	yes	yes
78	r_{aa}	-0.004	0.0001	-0.0007	-0.0081
	No. of obs.	4062	2242	1141	576
	Reject H_0?	yes	no	no	yes
85	r_{aa}	-0.0013	-0.0018	-0.0006	0.0016
	No. of obs.	2241	1236	641	472
	Reject H_0?	yes	no	no	no
86	r_{aa}	-0.0023	-0.0015	-0.009	-0.0013
	No. of obs.	3255	1835	943	708
	Reject H_0?	yes	no	no	no

Table 4.4: Bias towards kill sites from the previous 30 days.

Wolf	Days after kill	Subsampled at			
		30 mins		60 mins	
77	0-5	n = 1968	u = 2.19*	-	-
	5-10	n = 2434	u = -0.10	-	-
	10-15	n = 2324	u = 0.95	-	-
	15-20	n = 2677	u = 1.79*	-	-
	20-25	n = 1797	u = 1.77*	-	-
	25-30	n = 1337	u = 0.72	-	-
78	0-5	n = 1390	u = 1.17	n = 706	u = 1.38
	5-10	n = 1875	u = 0.07	n = 956	u = 0.67
	10-15	n = 2243	u = 0.33	n = 1137	u = 0.95
	15-20	n = 2677	u = 0.53	n = 1359	u = 1.29
	20-25	n = 2674	u = -0.03	n = 1358	u = 1.30
	25-20	n = 2555	u = 0.63	n = 1301	u = 1.28

The u-statistic is calculated for the V test. The number of observations used for the analysis is n. Only uncorrelated movement directions are shown and * denotes a significant result.

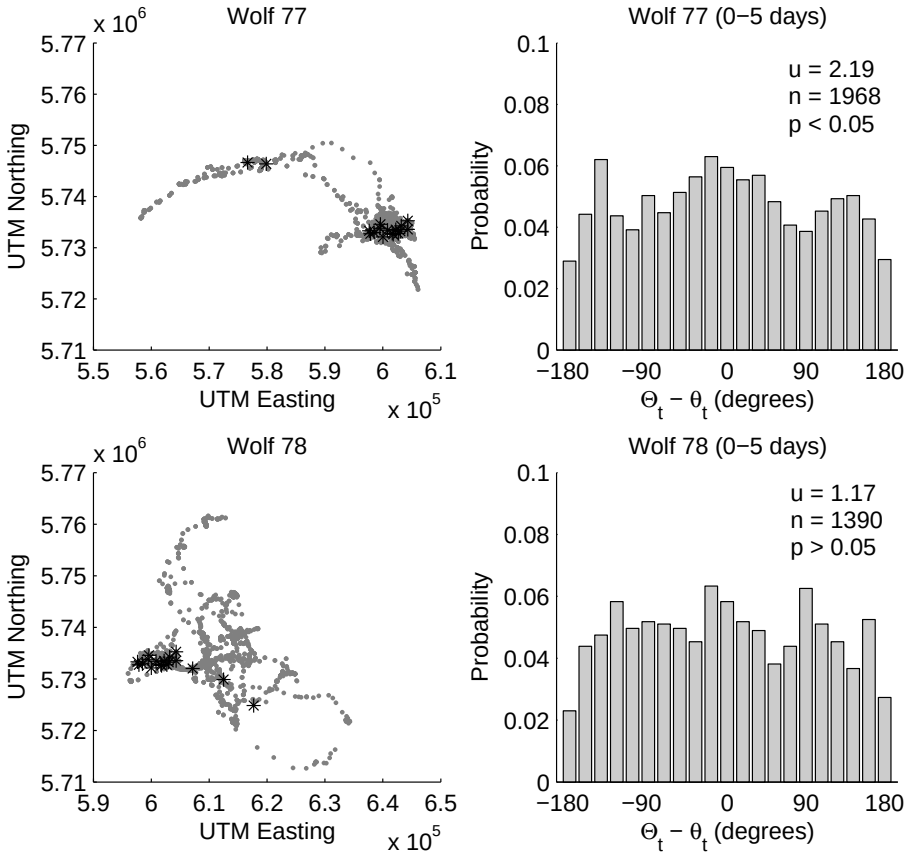

Figure 4.3: The location of kill sites found during GPS data collection period (*) for wolf 77 and 78. The histogram shows the difference between the direction of a kill made 0-5 days ago and the direction in which the wolf moved. Wolf 77 shows a significant bias towards the location of kills made 0-5 days ago where as wolf 78 does not.

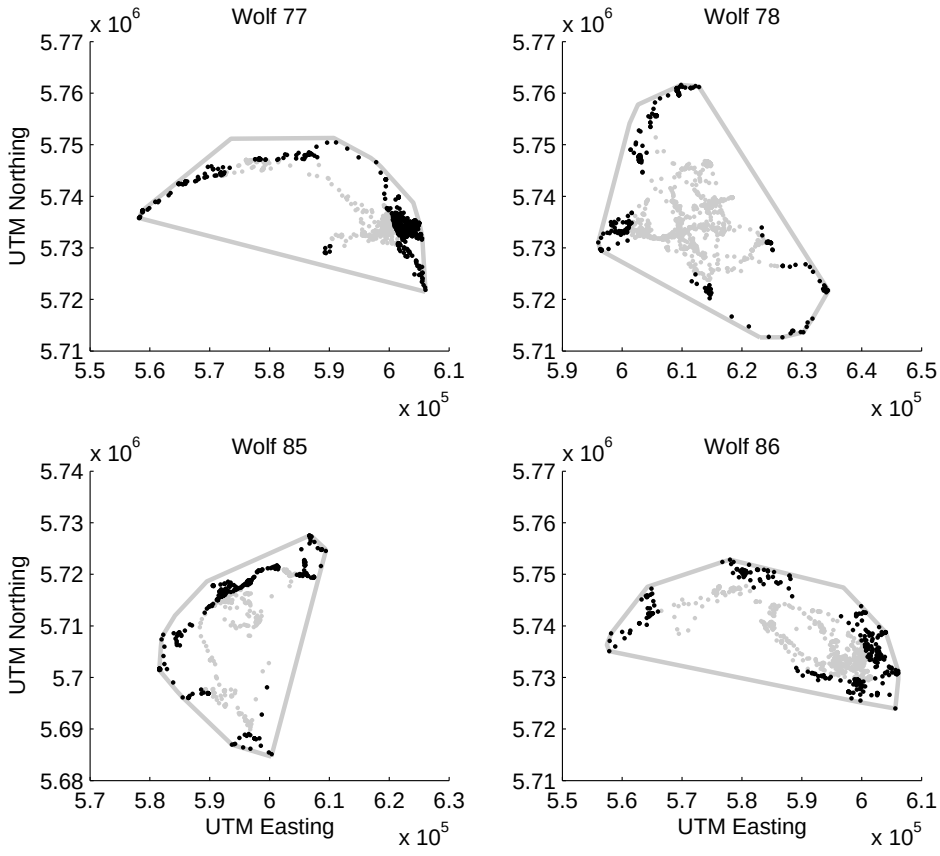

Figure 4.4: For each wolf, I calculated the radius of a circle with the same area as each territory 100% MCP. GPS locations that were less than a quarter of this radius away were classified as near the boundary (black). All other GPS points are shown in grey. The 100% MCP territories are shown as grey lines

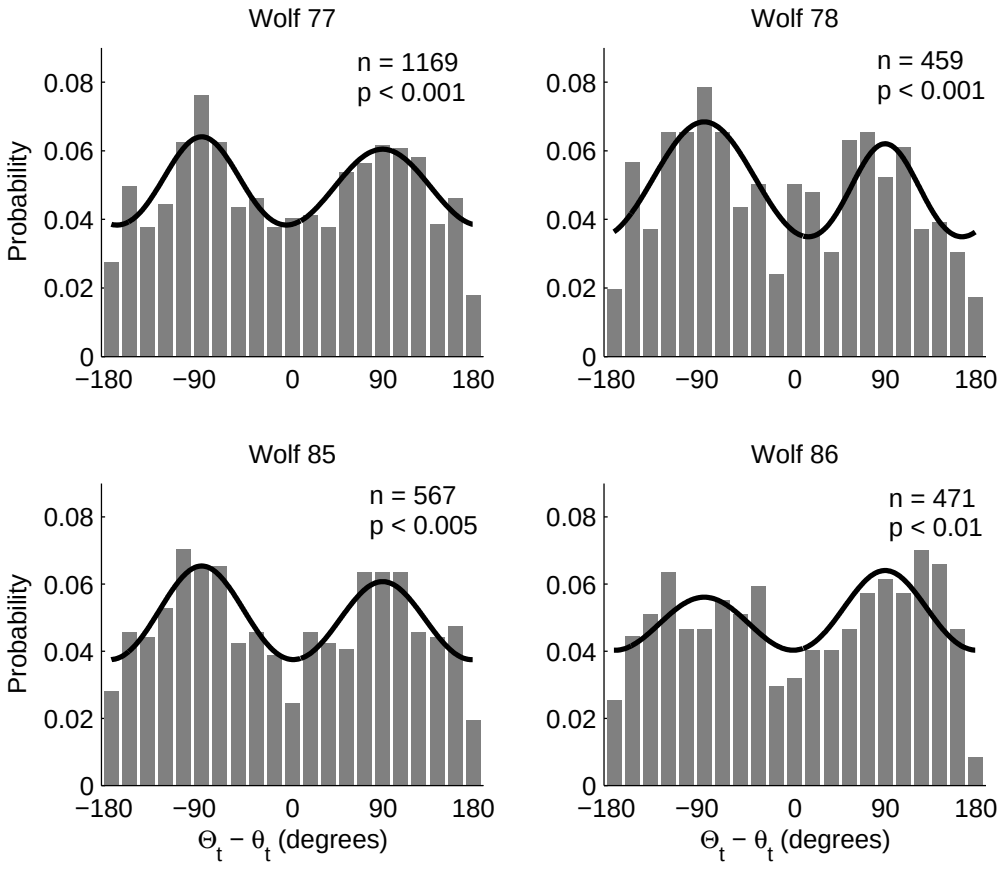

Figure 4.5: The difference between the direction of the next move and the direction of the territory boundary is shown as a histogram for four wolves. p-values are shown for the likelihood ratio test. The maximum likelihood parameter estimates are: wolf 77, $\hat{q} = 0.64, \hat{\kappa}_1 = 0.73, \hat{\kappa}_2 = 1.58$, wolf 78, $\hat{q} = 0.29, \hat{\kappa}_1 = 2.10, \hat{\kappa}_2 = 0.80$, wolf 85, $\hat{q} = 0.50, \hat{\kappa}_1 = 1.05, \hat{\kappa}_2 = 1.17$, and wolf 86, $\hat{q} = 0.44, \hat{\kappa}_1 = 1.20, \hat{\kappa}_2 = 0.74$.

Table 4.5: Bias perpendicular to the nearest point on the territory boundary.

Wolf		Subsampled at		
		30 mins	60 mins	120 mins
77	LL_1	-2130.8	-	-
	Λ	15.0	-	-
	p	< 0.005	-	-
78	LL_1	-832.2	-436.1	-
	Λ	22.7	2.7	-
	p	< 0.001	> 0.25	-
85	LL_1	-1032.5	-526.5	-461.8
	Λ	19.2	20.3	13.8
	p	< 0.001	< 0.001	< 0.005
86	LL_1	-860.8	-435.8	-306.2
	Λ	9.72	3.21	12.6
	p	< 0.01	> 0.25	< 0.01

Autocorrelated subsampling regimes are not shown. LL_1 is the logarithmic likelihood for Eq. (4.5) and Λ is calculated as shown in Eq. (4.6). The p-value for the χ^2 test is shown.

Table 4.6: Movement direction with respect to the direction of the steepest downhill slope

Model	LL	k	AIC	Δ AIC
Wolf 77				
$VM(0,\xi)$	-2216.5	0	4433.0	1782.2
$VM(\kappa,\xi)$	-2216.5	1	4435.0	1784.2
$VM(d\epsilon,\xi)$	-2216.4	1	4434.9	1784.1
$VM(0,\xi^{\perp})$	-2216.5	0	4433.0	1782.2
$VM(\kappa,\xi^{\perp})$	-1324.4	1	2650.8	0
$VM(d\epsilon,\xi^{\perp})$	-2216.5	1	4435.0	1784.2
Wolf 78				
$VM(0,\xi)$	-2648.4	0	5296.8	1925.4
$VM(\kappa,\xi)$	-2648.2	1	5298.4	1927.0
$VM(d\epsilon,\xi)$	-2647.1	1	5296.2	1924.8
$VM(0,\xi^{\perp})$	-2648.4	0	5296.8	1925.4
$VM(\kappa,\xi^{\perp})$	-1684.7	1	3371.4	0
$VM(d\epsilon,\xi^{\perp})$	-2648.4	1	5298.8	1927.4
Wolf 85				
$VM(0,\xi)$	-1841.6	0	3683.2	1688.8
$VM(\kappa,\xi)$	-1841.6	1	3685.2	1690.8
$VM(d\epsilon,\xi)$	-1841.6	1	3685.2	1690.8
$VM(0,\xi^{\perp})$	-1841.6	0	3683.2	1688.8
$VM(\kappa,\xi^{\perp})$	-996.2	1	1994.4	0
$VM(d\epsilon,\xi^{\perp})$	-1841.6	1	3685.2	1690.8
Wolf 86				
$VM(0,\xi)$	1020.0	0	2040.0	929.4
$VM(\kappa,\xi)$	1019.1	1	2040.2	929.6
$VM(d\epsilon,\xi)$	1019.6	1	2041.2	930.6
$VM(0,\xi^{\perp})$	1020.0	0	2040.0	929.4
$VM(\kappa,\xi^{\perp})$	554.3	1	1110.6	0
$VM(d\epsilon,\xi^{\perp})$	1020.2	1	2042.0	931.4

LL is the logarithmic likelihood for each model, k is the number of model parameters and the AIC value is calculated using Eq. (4.8). ΔAIC is calculated by subtracting the lowest AIC value from all other AIC values. A description of models is found in Tab. (4.2). Model parameters are described in the text.

of the wildhorse pack and the east boundary of the Ya Ha Tinda pack territories is evident from the GPS data (Fig. (4.2)). Several kills where located within this region of overlap, and the wolves may have moved differently towards kills made in the proximity of the boundary.

The four wolves showed evidence of boundary patrolling (Tab. (4.5)) at the 30 minute sampling interval. At longer sampling intervals this effect became less evident, suggesting that movement was non-directed or influenced by other factors. This result is reasonable as it is unlikely that more than a few hours are spent marking the boundary. While I found that wolves patrol their territory boundaries, I have not determined what impact this would have on wolf space use, which is a direction for future research.

However, just as elevation and the territory boundary may have influenced the results of the past kill site analysis, past kill sites and elevation may have influenced the territory boundary analysis. If any two of the three factors hypothesized to influence movement are spatially indistinct a mechanism causing the bias cannot be isolated. For some wolves some of the MCP territory boundaries fall along mountain ranges or valleys (e.g. the north and east MCP territory boundary for wolf 77). Yet, wolf 78 shows a strong bias towards the territory boundary and the 100% MCP territory boundary for this wolf appear unassociated with elevation. Therefore, wolf 78 shows evidence of movement parallel to the territory boundary. Wolves 77, 85 and 86 also show evidence of movement parallel to the territory boundary, however, this result may be due in part to the association of the territory boundary with mountain ranges or valleys.

The same GPS data was used to define the territory boundary and test for a bias with respect to the boundary, there are two reasons why using the same data to define the territory boundary would not bias my results. Firstly, the shape of the MCP territory boundary is influenced by only the outer most points. Therefore, there are many combinations of temporally sequenced points that could exist within the same MCP. Secondly, the vertices of the MCP territory were not necessarily visited in order. Therefore, the animal is not required to move from one vertex to the next and will not necessarily travel along the MCP territory boundary.

Lastly, all of the wolves showed very strong evidence in support of movement in the direction perpendicular to the direction of the steepest downhill slope (Tab. (4.6)). For a continuous surface, the gradient in the direction perpendicular to the direction of the steepest downhill slope is zero (Stewart 1999, p 696). Therefore, these results suggest that wolves move along contour lines. Again, the implications of this movement strategy on patterns of space use by wolves is an area of future research.

Future directions

The earliest mechanistic models for animal home ranges assumed that animals moved with a bias towards a central point (Holgate, 1971; Okubo, 1980). More recently, Lewis and Murray (1993) showed that home ranges may also arise due to movement away from the territory boundary. Both mechanisms give rise to finite ranges, but the use of space within these ranges is different. Moorcroft et al. (1999) show that the pattern of space use that arises when the magnitude of the centralizing tendency is dependent on the density of foreign scent marks is more consistent with coyote GPS collar locations than a model with a constant bias towards the home range center.

The results in this chapter identify new movement strategies that are consistent with the measured distributions of directional biases for GPS data recovered from four wolves in the BNP-Ya Ha Tinda region. Zub et al. (2003), in contrast to Peters and Mech (1975), found that wolves scent mark uniformly throughout their territories. Yet, the densities of space use within a wolf territory influences scent mark densities. The expected space use density, given wolf boundary patrolling movements can be determined using the methods shown in **?** and Moorcroft and Lewis (2005). The effect of contouring movements on patterns of space use could also be determined using these methods. Understanding the mechanisms that give rise to the observed pattern of space use is particularly relevant to predator-prey dynamics where differences in predator density can result in shifts in prey distribution which can in turn impact vegetation (Fortin et al., 2005). Furthermore, consideration of predator movements have been notably absent from past studies of predator-prey dynamics (Lima, 2002).

While useful, the numerical methods used in **?** and Moorcroft and Lewis (2005) are computationally intensive. The methods described in this chapter are a preliminary step that can be used to identify the best mechanisms to test in the simulation models of Moorcroft and Lewis (2005). In this chapter I showed that, 1) when wolves are near the territory boundary, they exhibit patrolling movements along the boundary edge, and 2) wolves move along contour lines perpendicular to the direction of downhill. I found some evidence of a wolf returning to the location of a kill made less than 30 days prior, however, further studies are needed to identify the frequency and factors which influence return movements to past kills. This chapter, provides a simple methodology for testing animal movement hypotheses. These hypotheses can be used to understand how wolves use space.

Chapter 5

Concluding Remarks

Wolves (*Canis lupus*) raise pups and hunt within the bounds of their territories. While most of a wolf's life is spent within a territory, wolves will disperse from their natal territories. Wolf movements are primarily for hunting and territory defense within the territory. Wolves disperse beyond the territory boundary to search for mates or a new pack.

Mechanistic models can identify underlying processes that give rise to observed patterns. Furthermore, diffusion models (Okubo and Levin, 2001; Moorcroft and Lewis, 2005) have been used to model mammal dispersal (Skellam, 1951; Caughley, 1970; Clarke, 1971; Lubina and Levin, 1988) and home range movements (Lewis and Murray, 1993; Moorcroft et al., 1999; Moorcroft and Lewis, 2005). The conventional diffusion modelling framework (Fisher, 1937) when parameterized for wolf recolonizing the Greater Yellowstone Ecosystem (GYE, Phillips and Smith 1997; Smith 1998; Smith et al. 1999, 2000, 2001; Smith and Guernsey 2002; Smith et al. 2003) predicted a rate of recolonization an order of magnitude faster than the rate of recolonization calculated from range maps from 1997-2002. Slower than expected spread rates may be caused by Allee effects (Lewis and Kareiva, 1993; Kot et al., 1996; Veit and Lewis, 1996; Wang et al., 2002).

The most likely mechanism causing an Allee effect in wolves is a reduced probability of finding mates at low densities. In Chapter 2, I showed that when the Allee effect is considered, the predicted rate of recolonization is consistent with the observed rate of recolonization for wolves to the GYE. The reduced probability of finding mates at low densities influences only the establishment of new breeding units and not the growth of established breeding units. Most models for the Allee effect do not distinguish between the establishment and subsequent growth of breeding units. Using a proof by induction, I quantified the expected rate of recolonization when wolves have a reduced probability of finding mates at low densities

as a function of reproduction, pair formation and dispersal parameters.

GPS measurement error will bias the results of movement (Johnson et al., 2002; Jerde and Visscher, 2005) and habitat selection (Frair et al., 2004) models if not dealt with properly. In Chapter 3, I showed that GPS measurement error gives rise to a systematic error in measured turning angles and directional biases. For an animal moving a very short distance with an actual turning angle equal to zero degrees, I showed that in the presence of GPS measurement error the animal is most likely to be measured as turning 180 degrees. Similarly, an animal that is near the bias point (e.g., the den) and moves a short distance away is most likely to be measured moving towards the bias point. These results are demonstrated using both numerical simulations and mathematical analysis. In Chapter 3, I also determined that for measured step lengths of 50-55 m, the actual turning angles and directions of movement can be detected in the presence of GPS measurement error when 95% of GPS locations are measured within 31 m of the true location.

GPS collar technology has enabled researchers to record patterns of territory space use by animals. In Chapter 4, this data is used to understand the effect of ecological features on the direction of wolf movements. I showed that when sampled at 30 minute intervals wolves moved parallel to territory boundary. This result suggested that wolves patrolled the boundary and did so for no more than a few hours. I also showed that wolves moved preferentially in the direction perpendicular to the direction of the steepest downhill slope. Because the distance moved between locations was small, this result likely demonstrates that wolves move along contour lines. These new movement behaviours can be incorporated in future mathematical models of movement to understand the effects on wolf space use.

Future directions

The modelling framework in Chapter 2 could be modified to investigate the effect of harvest on the rate of range expansion. Determining the level of survivorship necessary for the population to persist will aid wolf conservation planning and management. For the modelling framework presented in Chapter 2, it is not only the survivorship that influences wolf spread rate, but who is killed - a disperser or a resident. An understanding of the effect of harvesting dispersing and resident wolves on range expansion and retraction could contribute to understanding the effects of wolf livestock depredation and wolf population dynamics.

I showed that removing all GPS observations less than 50-55 m is travelled between locations will remove turning angle and directional biases. However, the true step length cutoffs were much smaller, 16.8 and 15.2 m respectively. Results for numerical simulations determining the relationship between measured and true step lengths are shown in Jerde and Visscher (2005). However, mathematical results similar to those presented in Chapter 3 for turning angles and directional biases would complement these results.

Understanding factors that influence predator movement will aid future work on predator-prey dynamics. Understanding predator prey dynamics in heterogeneous landscapes requires understanding, 1) how predators and prey respond to ecological features such as snow, terrain, and territory boundaries, 2) how predators and prey respond to each others movements (e.g., Hugie and Dill 1994), and 3) how these responses influence space use by both the predator and prey (e.g., Lewis and Murray 1993; Moorcroft et al. 1999; Lewis and Moorcroft 2001). While not simple, advances gained from incorporating predator movement in studies of predator-prey dynamics will be valuable (Lima, 2002).

Results in this thesis demonstrate how mechanistic models can be used to understand observed patterns. I showed that density dependent pair formation for wolves that disperse beyond the territory boundary influences wolf recolonization rates, that spurious 180 degree turns and strong directions biases can arise from GPS measurement error and that wolf movement within a territory is influenced by the territory boundary and elevation gradients.

Bibliography

Adams, E. 2001. Approaches to the study of territory size and shape. Annual Review of Ecology and Systematics, **32**:277–303.

Armstrong, H. and A. Robertson. 2000. Energetics of free-ranging large herbivores: When should costs affect foraging behaviour? Canadian Journal of Zoology-Revue Canadienne De Zoologie, **78**:1604–1615.

Bain, L. and M. Engelhardt. 1997. Introduction to probability and mathematical statistics, 2 ed. Duxbury Press, Belmont, CA.

Ballard, W., R. Farnell, and R. Stephenson. 1983. Long-distance movement by gray wolves, Canis lupus. Can. Field-Nat., **97**:333.

Ballard, W., J. Whitman, and C. Gardner. 1987. Ecology of an exploited wolf population. Wildlife Monographs, **51**.

Berec, L. and D. Boukal. 2004. Implications of mate search, mate choice and divorce rate for population dynamics of sexually reproducing species. Oikos, **104**:122–132.

Bessa-Gomes, C., S. Legendre, and J. Clobert. 2004. Allee effects, mating systems and the extinction risk in populations with two sexes. Ecol. Lett., **7**:802–812.

Boukal, D. and L. Berec. 2002. Single-species models of the Allee effect: Extinction boundaries, sex ratios and mate encounters. J. Theor. Biol., **218**:375–394.

Boyd, D. and D. Pletscher. 1999. Characteristics of dispersal in a colonizing wolf population in the central rocky mountains. J. Wildl. Manage., **63**:1094–1108.

Boyd-Heger, D. 97. Dispersal, Genetic Relationships, and Landscape Use by Colonizing Wolves in the Central Rocky Mountains. Ph.D. thesis, University of Montana.

Broadbent, S. and D. Kendall. 1953. The random walk of Trichostrongylus retoraeformis. Biometrics, **9**:460–466.

Burnham, K. and D. Anderson. 2002. Model selection and multimodel inference: A practical infomation theoretic approach, 2 ed. Springer-Verlag, New York.

Carroll, C., M. Phillips, N. Schumaker, and D. Smith. 2003. Impacts of landscape change on wolf restoration success: Planning a reintroduction program based on static and dynamic spatial models. Conserv. Biol., **17**:536–548.

Caughley, G. 1970. Liberation, dispersal and distribution of Himalayan Thar (Hemitragus-Jemlahicus) in New-Zealand. New Zealand Journal of Science, **13**:220–239.

Clark, J. 1998. Why trees migrate so fast: Confronting theory with dispersal biology and the paleorecord. American Naturalist, **152**:204–224.

Clarke, C. 1971. Liberations and dispersal of red deer in northern South Island districts. New Zealand Journal of Science, **1**:194–207.

Courchamp, F., T. Clutton-Brock, and B. Grenfell. 1999. Inverse density dependence and the Allee effect. TREE, **14**:405–410.

Courchamp, F., T. Clutton-Brock, and B. Grenfell. 2000. Multipack dynamics and the allee effect in the African wild dog, Lycaon pictus. Animal Conservation, **3**:277–285.

Dennis, B. ???? Alee effects: population growth, critical density, and the chance of extinction. Natural Resource Modeling, **3**:481–538.

D'eon, R. and D. Delparte. 2005. Effects of radio-collar position and orientation on gps radio-collar performance, and the implications of pdop in data screening. Journal of Applied Ecology, **42**:383–388.

D'eon, R., R. Serrouya, G. Smith, and C. Kochanny. 2002. Gps radiotelemetry error and bias in mountainous terrain. Wildlife Society Bulletin, **30**:430–439.

Di Orio, A., R. Callas, and R. Schaefer. 2003. Performance of two gps telemetry collars under different habitat conditions. Wildlife Society Bulletin, **31**:372–379.

Dussault, C., R. Courtois, J. Ouellet, and J. Huot. 2001. Influence of satellite geometry and differential correction on gps location accuracy. Wildlife Society Bulletin, **29**:171–179.

Engen, S., R. Lande, and B. Saether. 2003. Demographic stochasticity and allee effects in populations' with two sexes. Ecology, **84**:2378–2386.

Fisher, N. 1993. Statistical Analysis of Circular Data. Cambridge University Press, Cambridge.

Fisher, N. and A. Lee. 1983. A correlation coefficient for circular data. Biometrika, **70**:327332.

Fisher, R. 1937. The wave of advance of advantageous genes. Annals of Eugenics, pages 355–369.

Fortin, D. 2005. Elk winter foraging at fine scale in yellowstone national park. Oecologia.

Fortin, D., H. Beyer, M. Boyce, D. Smith, T. Duchesne, and J. Mao. 2005. Wolves influence elk movements: Behavior shapes a trophic cascade in yellowstone national park. Ecology, **86**:1320–1330.

Frair, J., S. Nielsen, E. Merrill, S. Lele, M. Boyce, R. Munro, G. Stenhouse, and H. Beyer. 2004. Removing GPS collar bias in habitat selection studies. Journal of Applied Ecology, **41**:201–212.

Franke, A., T. Caelli, and R. Hudson. 2004. Analysis of movements and behavior of caribou (rangifer tarandus) using hidden markov models. Ecological Modelling, **173**:259–270.

Fritts, S. 1983. Record dispersal by a wolf from Minnesota. J. of Mammal., **64**:166–167.

Fritts, S., C. Mack, D. Smith, K. Murphy, M. Phillips, M. Jimenez, E. Bangs, J. Fontaine, C. Niemeyer, W. Brewster, and T. Kaminsi. 2001. Large Mammal Restoration: Ecological and Sociological Challenges in the twenty-first century, chapter Outcomes of Hard and Soft Releases of Reintroduced Wovles in Central Idaho and the Greater Yellowstone Area, pages 125–148. Island Press, Washington, D.C., USA.

Fuller, T. 1989. Population dynamics of wolves in north-central minnesota. Wildlife Monograph, **105**.

Grimshaw, S., D. Whiting, and T. Morris. 2001. Likelihood ratio tests for a mixture of two von mises distributions. Biometrics, **57**:260–265.

Haefner, J. ???? Modeling biological systems. Chapman and Hall., USA.

Hebblewhite, M. 2005. Predation by wolves interacts with the north pacific oscillation (npo) on a western north american elk population. Journal of Animal Ecology, **74**:226–233.

Hebblewhite, M. and E. Merrill. 2002. Ya Ha Tinda elk and wolf ecology project progress report 2002.

Hofmann-Wellenhof, B., H. Lichtenegger, and J. Collins. 2001. GPS: Theory and Practice, 5 ed. Springer-Verlag/Wien, Austria.

Holgate, P. 1971. Statistical Ecology: Sampling and Modeling Biological Populations and Population Dynamics, chapter Random walk models for animal behavior, pages 1–12. University Park, PA, Penn State University Press.

Hugie, D. and L. Dill. 1994. Fish and game - a game-theoretic approach to habitat selection by predators and prey. Journal of Fish Biology, **45**:151–169.

Jerde, C. and D. Visscher. 2005. Gps measurement error influences on movement model parameterization. Ecological Applications, **in press**.

Johnson, C. and C. Barton. 2004. Where in the world are my field plots? using gps effectively in enironmental field studies. Front Ecol Environ, **2(9)**:475–482.

Johnson, C., K. Parker, D. Heard, and M. Gillingham. 2002. Movement parameters of ungulates and scale-specific responses to the environment. Journal of Animal Ecology, **71**:225–235.

Kareiva, P. and N. Shigesada. 1983. Analyzing insect movement as a correlated random-walk. Oecologia, **56**:234–238.

Kie, J., J. Baldwin, and C. Evans. 1996. Calhome: a program for estimating animal home ranges. Wildlife Society Bulletin, **24**:342–344.

Kot, M., M. Lewis, and P. van den Driessche. 1996. Dispersal data and the spread of invading organisms. Ecology, **77**:2027–2042.

Legaspi, B., J. Allen, C. Brewster, J. Morales-Ramos, and E. King. 1998. Areawide management of the cotton boll weevil: Use of a spatio-temporal model in augmentative biological control. Ecological Modelling, **110**:151–164.

Lewis, M. and P. Kareiva. 1993. Allee dynamics and the spread of invading organisms. Theor. Popul. Biol., **43**:141–158.

Lewis, M. and P. Moorcroft. 2001. Ess analysis of mechanistic models for territoriality: the value of scent marks in spatial resource partitioning. Journal of Theoretical Biology, **210**:449–461.

Lewis, M. and J. Murray. 1993. Modeling territoriality and wolf deer interactions. Nature, **366**:738–740.

Lewis, M., M. Neubert, H. Caswell, J. Clark, and K. Shea. ???? Conceptual ecology and invasions biology: reciprocal approaches to nature, chapter A guide to calculating discrete-time invasion rates from data.

Lima, S. 2002. Putting predators back into behavioral predator-prey interactions. Trends in Ecology Evolution, **17**:70–75.

Lubina, J. and S. Levin. 1988. The spread of a reinvading species - range expansion in the california sea otter. American Naturalist, **131**:526–543.

MacDonald, D. 1980. The red fox, Vulpes-vulpes, as a predator upon earthworms, Lumbricus-terrestris. Z. Tierpsychol., **52**:171–200.

Manly, B., L. McDonald, D. Thomas, T. McDonald, and W. Erickson. 2002. Resource selection by animals: statistical design and analysis for field studies, 2 ed. Kluwer Academic Publishers, Dordrecht, Netherlands.

Marell, A., J. Ball, and A. Hofgaard. 2002. Foraging and movement paths of female reindeer: Insights from fractal analysis, correlated random walks, and levy flights. Canadian Journal of Zoology-Revue Canadienne De Zoologie, **80**:854–865.

Mech, L. 1970. The wolf: the ecology and behavior of an endangered species. Double Day and Company Inc, NY, USA.

Mech, L. 1988. The artice wolf: living within the pack. Voyageur Press, Stillwater, MN, USA.

Mech, L. 1991. The way of the wolf. Voyageur Press, Stillwater, MN, USA.

Mech, L. and L. Boitani. 2003. Wolves: Behavior, Ecology and Conservation. University of Chicago Press, Chicago, USA.

Moen, R., J. Pastor, and Y. Cohen. 1997. Accuracy of gps telemetry collar locations with differential correction. Journal of Wildlife Management, **61**:530–539.

Mohr, C. 1947. Table of equivalent populations of north american small mammals. American Midland Naturalist, **37**:223–249.

Moller, A. and S. Legendre. 2001. Allee effect, sexual selection and demographic stochasticity. Oikos, **92**:27–34.

Moorcroft, P. and M. Lewis. 2005. Home Range Patterns: Mechanistic Approaches to the Analysis of Animal Movement.

Moorcroft, P., M. Lewis, and R. Crabtree. 1999. Home range analysis using a mechanistic home range model. Ecology, **80**:1656–1665.

Morales, J., D. Haydon, J. Frair, K. Holsiner, and J. Fryxell. 2004. Extracting more out of relocation data: Building movement models as mixtures of random walks. Ecology, **85**:2436–2445.

Murie, A. 1985. The wolves of Mount McKinley. University of Washington Press, Seattle, USA.

Nams, V. 2005. Using animal movement paths to measure response to spatial scale. Oecologia, **143**:179–188.

Nelson, M. and L. Mech. 1986. Relationship between snow depth and gray wolf predation on white-tailed deer. Journal of Wildlife Management, **50**:471–474.

Neubert, M. and H. Caswell. 2000. Demography and dispersal: Calculation and sensitivity analysis of invasion speed for structured populations. Ecology, **81**:1613–1628.

Neubert, M., M. Kot, and M. Lewis. 1995. Dispersal and pattern-formation in a discrete-time predator-prey model. Theor. Popul. Biol., **48**:7–43.

Okubo, A. 1980. Diffusion and ecological problems: mathematical models. Springer-Verlag, New York.

Okubo, A. and S. Levin. 2001. Diffusion and ecological problems, 2 ed. Springer-Verlag, New York, USA.

Peters, R. and L. Mech. 1975. Scent-marking in wolves. American Scientist, **63**:628–637.

Phillips, M. and D. Smith. 1997. Yellowstone Wolf Project: Biennial Report 1995 and 1996. National Park Service, Yellowstone Center for Resources, Yellowstone National Park, Wyoming, YCR-NR-97-4.

Pusey, A. 1987. Sex-biased dispersal and inbreeding avoidance in birds and mammals. Trends in Ecology Evolution, **2**:295–299.

Rempel, R., A. Rodgers, and K. Abraham. 1995. Performance of a gps animal location system under boreal forest canopy. Journal of Wildlife Management, **59**:543–551.

Rothman, R. and L. Mech. 1979. Scent-marking in lone wolves and newly formed pairs. Animal Behaviour, **27**:750–.

Schmidt, P. and L. Mech. 1997. Wolf pack size and food acquisition. Am. Nat., **150**:513–517.

Shigesada, N. and Kawasaki. 1997. Biological Invasions: Theory and Practice. Oxford University Press, Oxford.

Siniff, D. and C. Jessen. 1969. A simulation model of animal movement patterns. Adv. Ecol. Res., **6**:185–219.

Skellam, J. 1951. Random dispersal in theoretical populations. Biometrika, **38**:196–218.

Smith, D. 1998. Yellowstone Wolf Project: Annual Report, 1997. National Park Service, Yellowstone Center for Resources, Yellowstone National Park, Wyoming, YCR-NR-98-2.

Smith, D. and D. Guernsey. 2002. Yellowstone Wolf Project: Annual Report, 2001. National Park Service, Yellowstone Center for Resources, Yellowstone National Park, Wyoming, YCR-NR-2002-04.

Smith, D., K. Murphy, and D. Guernsey. 1999. Yellowstone Wolf Project: Annual Report, 1998. National Park Service, Yellowstone Center for Resources, Yellowstone National Park, Wyoming, YCR-NR-99-1.

Smith, D., K. Murphy, and D. Guernsey. 2000. Yellowstone Wolf Project: Annual Report, 1999. National Park Service, Yellowstone Center for Resources, Yellowstone National Park, Wyoming, YCR-NR-2000-01.

Smith, D., K. Murphy, and D. Guernsey. 2001. Yellowstone Wolf Project: Annual Report, 2000. National Park Service, Yellowstone Center for Resources, Yellowstone National Park, Wyoming, YCR-NR-2001-02.

Smith, D., D. Stahler, and D. Guernsey. 2003. Yellowstone Wolf Project: Annual Report, 2002. National Park Service, Yellowstone Center for Resources, Yellowstone National Park, Wyoming, YCR-NR-2003-04.

Stephens, P. and W. Sutherland. 1999. Consequences of the Allee effect for behaviour, ecology and conservation. TREE, **14**:401–405.

Stephens, P., W. Sutherland, and R. Freckleton. 1999. What is the Allee effect? Oikos, **87**:185–190.

Turchin, P. 1998. Quantitative Analysis of Movement. Sinauer Associates Inc., Sunderland, Ma.

U. S. Fish and Wildlife Service, Nez Perce Tribe, National Park Service, and USDA and Wildlife Services. 2003. Rocky Mountain Wolf Recovery 2002 Annual Report. USFWS, Ecological Services, 100 N Park, Suite 320, Helena MT.

U. S. Fish and Wildlife Service, Nez Perce Tribe, National Park Service, and USDA Wildlife and Services. 2000. Rocky Mountain Wolf Recovery 1999 Annual Report. USFWS, Ecological Services, 100 N Park, Suite 320, Helena MT.

U.S. Fish and Wildlife Service, Nez Perce Tribe, National Park Service, and USDA Wildlife Services. 2001. Rocky Mountain Wolf Recovery 2000 Annual Report. USFWS, Helena, MT.

U.S. Fish and Wildlife Service, Nez Perce Tribe, National Park Service, and USDA Wildlife Services. 2002. Rocky Mountain Wolf Recovery 2001 Annual Report. USFWS, Ecological Services, 100 N Park, Suite 320, Helena MT.

Veit, R. and M. Lewis. 1996. Dispersal, population growth, and the Allee effect: Dynamics of the house finch invasion of eastern North America. Am. Nat., **148**:255–274.

Vucetich, J., R. Peterson, and T. Waite. 2004. Raven scavenging favours group foraging in wolves. Anim. Behav., **67**:1117–1126.

Wang, M., M. Kot, and M. Neubert. 2002. Integrodifference equations, Allee effects, and invasions. J. Math. Biol., **44**:150–168.

Ward, D. and D. Saltz. 1994. Foraging at different spatial scales - dorcas gazelles foraging for lilies in the negev desert. Ecology, **75**:48–58.

Whittington, J., C. St Clair, and G. Mercer. 2004. Path tortuosity and the permeability of roads and trails to wolf movement. Ecology and Society, **9**.

Whittington, J., C. St Clair, and G. Mercer. 2005. Spatial responses of wolves to roads and trails in mountain valleys. Ecological Applications, **15**:543–553.

With, K. 1994. Using fractal analysis to assess how species perceive landscape structure. Landscape Ecology, **9**:25–36.

Worton, B. ???? Kernel methods for estimating the utilization distribution in home range studies. Ecology, **70**:164–168.

Worton, B. 1987. A review of models of home range for animal movement. Ecological Modelling, **38**:277–298.

Wu, H., B. Li, T. Springer, and W. Neill. 2000. Modelling animal movement as a persistent random walk in two dimensions: Expected magnitude of net displacement. Ecological Modelling, **132**:115–124.

Zar, J. 1998. Biostatistical Analysis, 4 ed. Prentice Hall, New Jersey.

Zollner, P. and S. Lima. 1997. Landscape-level perceptual abilities in white-footed mice: Perceptual range and the detection of forested habitat. Oikos, **80**:51–60.

Zub, K., J. Theuerkauf, W. Jedrzejewski, B. Jedrzejewska, K. Schmidt, and R. Kowalczyk. 2003. Wolf pack territory marking in the bialowieza primeval forest (poland). Behaviour, **140**:635–648.

Appendix A

Fisher's model

Fisher's model overestimates the rate of wolf recolonization to the GYE. Fisher's model is,

$$\frac{\partial N}{\partial t} = rN\left(1 - \frac{N}{K}\right) + D\frac{\partial^2 N}{\partial x^2} \tag{A.1}$$

(Fisher, 1937). The diffusion coefficient D is calculated as $D = \bar{u}^2/\pi$ (Shigesada and Kawasaki, 1997) where $\bar{u}$ is the mean dispersal distance ($\bar{u} = 76.7$, Smith et al. 2000). The reproductive rate r is calculated as the slope of a linear regression of $N_{t+1} - N_t$ versus N_t, where N_t is the density of wolves is YNP at time t (see Tab. (B.1)). We assume the area of YNP is 10,000 km^2 and calculate the density of wolves in YNP from 1996–2002. The spread rate is calculated as c = $\sqrt{rD}$, r = 1.18, D = 1872 km^2/year.

Calculating $\psi\phi$

To estimate $\psi\phi$, I derive a relationship between $\psi\phi$ and ρ the proportion of dispersers that find mates. For GYE wolves $\rho = 0.47$ (Smith et al., 2000) for the first four years following the initial introduction ($\tau = 4$). I use this information to calculate the product $\psi\phi$ for the pair formation prior and the pair formation following dispersal models. For the pair formation prior to dispersal model, $\psi\phi$ is given by Eq. (2.20). Eq. (2.20) is,

$$\begin{aligned} \psi\phi &= \rho\tau \sum_{t=1}^{\tau} \frac{\int_{-x_t}^{x_t} \gamma \, dy}{\gamma^2 \int_{-\infty}^{\infty} k(x) \, dx}, \\ &= \rho\tau \sum_{t=1}^{\tau} \frac{\int_{-x_t}^{x_t} dy}{\gamma \int_{-\infty}^{\infty} k(x) \, dx}, \end{aligned} \tag{A.2}$$

where,

$$K(x) = \int_{-x_t}^{x_t} \frac{\alpha}{2} \exp(-\alpha|x-y|)\ dy. \tag{A.3}$$

Making the substitution $u = x - y$,

$$K(x) = \frac{\alpha}{2} \int_{x+x_t}^{x-x_t} \exp(-\alpha|u|)\ du. \tag{A.4}$$

The integral of Eq. (A.4) is,

$$K(x) = \begin{cases} \exp(\alpha x)\sinh(\alpha x_t) & \text{for } x \leq x_t, \\ (1 - \exp(-\alpha x_t)\cosh(\alpha x)) & \text{for } -x_t < x < x_t, \\ \exp(-\alpha x)\sinh(\alpha x_t) & \text{for } x \geq x_t. \end{cases} \tag{A.5}$$

Let,

$$L(x) = \int_{-\infty}^{\infty} K(x)\ dx \tag{A.6}$$

Using the result from Eq. (A.5),

$$\begin{aligned} L(x) &= \left(\int_{-\infty}^{-x_t} \exp(\alpha x)\sinh(\alpha x_t)\ dx + \int_{-x_t}^{x_t} 1 - \exp(-\alpha x_t)\cosh(\alpha x)\ dx \right. \\ &\qquad \left. + \int_{x_t}^{\infty} \exp(-\alpha x)\sinh(\alpha x_t)\ dx \right) \\ &= \frac{1}{\alpha}(2\exp(-\alpha x_t)\sinh(\alpha x_t) + 2\alpha x_t + \exp(-2\alpha x_t) - 1) \\ &= 2x_t \end{aligned} \tag{A.7}$$

Substituting Eq. (A.7) for the denominator of Eq. (A.2) yields,

$$\begin{aligned} \psi\phi &= \rho\tau \sum_{t=1}^{\tau} \frac{\int_{-x_t}^{x_t} dy}{2\gamma x_t}, \\ &= \rho\tau \sum_{t=1}^{\tau} \frac{2x_t}{2\gamma x_t}, \\ &= \frac{\rho\tau}{\gamma} \end{aligned} \tag{A.8}$$

For GYE wolves, $\rho = 0.47$ where $\tau = 4$ (Smith et al., 2000). The parameter γ is estimated using the methods in the Parameter Estimation section of Chapter 2. These values were used to calculate $\psi\phi = 20.7$ for the pair formation prior to dispersal model. For the pair formation following dispersal model, Eq. (2.22)

can be written as,

$$\psi\phi = \rho\tau \sum_{t=1}^{\tau} \frac{\int_{-x_t}^{x_t} \gamma dy}{\int_{-\infty}^{\infty} K^2(x)\ dx} \tag{A.9}$$

where $K(x)$ is given by Eq. (A.3). Using the result from Eq. (A.5) where $L(x)$ is the denominator of Eq. (A.9),

$$\begin{aligned} L(x) &= \gamma^2 \left(\int_{-\infty}^{-x_t} \exp(2\alpha x) \sinh^2(\alpha x_t)\ dx + \int_{-x_t}^{x_t} (1 - \exp(-\alpha x_t)\cosh(\alpha x))^2\ dx \right. \\ &\quad \left. + \int_{x_t}^{\infty} \exp(-2\alpha x) \sinh^2(\alpha x_t)\ dx \right), \\ &= \frac{\gamma^2 \exp(-2\alpha x_t)(3 + 2\alpha x_t + \exp(2\alpha x_t)(4\alpha x_t - 3))}{2\alpha}. \end{aligned} \tag{A.10}$$

Substituting Eq. (A.10) for the denominator of Eq. (A.9) yields,

$$\begin{aligned} \psi\phi &= \rho\tau \sum_{t=1}^{\tau} \frac{\int_{-x_t}^{x_t} \gamma\ dy}{\frac{\gamma^2 \exp(-2\alpha x_t)(3+2\alpha x_t+\exp(2\alpha x_t)(4\alpha x_t-3))}{2\alpha}}, \\ &= \frac{4\tau\alpha\rho}{\gamma} \sum_{t=1}^{\tau} \frac{x_t}{\exp(-2\alpha x_t)(3 + 2\alpha x_t + \exp(2\alpha x_t)(4\alpha x_t - 3))}. \end{aligned} \tag{A.11}$$

To estimate $\psi\phi$ I use the information that $\rho = 0.47$ and $\tau = 4$. The parameters γ and α were estimated as 0.09 and 0.02 in the Parameter Estimation section of Chapter 2. Furthermore, x_1, x_2, x_3, x_4 are equal to 10.4, 45.5, 57.5, and 65.6 respectively, as estimated in the Model Validation section. Therefore, $\psi\phi = 39.2$ for the pair formation following dispersal model.

Finding the spread rate of Eq. (2.23)

Initial condition 1

I find N_{t+1} and the population spread rate c for Eqs. (2.14) and (2.15) for two different initial conditions. Initial condition 1 (Fig. (2.3A)) is defined as,

$$\begin{aligned} N_0(x) &\geq N_c \quad \text{for } -\infty < x \leq x_0, \\ &= 0 \quad \text{otherwise.} \end{aligned} \tag{A.12}$$

Given initial condition 1, the region in space occupied by the disperser producing population Ω_t is $(-\infty, x_t]$. Evaluating Eqs. (2.14) and (2.15) in the region $x > x_t$ yields,

$$N_t(x) = rN_{t-1}(x) + A\exp(-w\alpha(x - x_{t-1})), \tag{A.13}$$

where w and A are: $w = 1$, $A = \sigma\psi\phi\gamma^2/4$ (pair formation prior to dispersal, Eq. (2.14) and $w = 2$, $A = \sigma\psi\phi\gamma^2/8$ (pair formation following dispersal, Eq. (2.15)). I suppose that solutions for Eq. (A.13) have a slope of $\exp(-w\alpha x)$ for $x > x_t$ such that,

$$N_t(x) = B_t\exp(-w\alpha x) \qquad \text{for } x > x_t. \tag{A.14}$$

Substituting Eq. (A.14) into Eq. (A.13) yields,

$$\begin{aligned} N_{t+1}(x) &= rB_t\exp(-w\alpha x) + A\exp(w\alpha x_t)\exp(-w\alpha x), \\ &= B_{t+1}\exp(-w\alpha x), \end{aligned}$$

where,

$$B_{t+1}(x) = rB_t + A\exp(-w\alpha x_t) \qquad \text{for } x > x_t. \tag{A.15}$$

Therefore, I show that if N_t has a slope of $\exp(-w\alpha x)$, N_{t+1} also has a slope of $\exp(-w\alpha x)$. I look for solutions in the region $x > x_0$ by solving Eq. (A.13) for $t = 1$, where $N_0(x)$ is described by initial condition 1,

$$N_1(x) = A\exp(w\alpha x_0)\exp(-w\alpha x) \qquad \text{for } x_0 < x. \tag{A.16}$$

Therefore, $B_1 = A\exp(w\alpha x_0)$ and N_t and N_{t+1} have a slope of $\exp(-w\alpha x)$ for all t.

Solutions to Eq. (A.13) have an exponential slope for $x > x_t$ where $A > 0$ such that,

$$N_t(x) = B_t\exp(-w\alpha x) \qquad \text{for } x > x_t. \tag{A.17}$$

The point at which the population starts the exponential drop is x_t where,

$$N_t(x_t) = N_c. \tag{A.18}$$

I calculate x_t from Eqs. (A.17) and (A.18) to yield,

$$\exp(w\alpha x_t) = \frac{B_t}{N_c}. \tag{A.19}$$

I can substitute Eqs. (A.17) and (A.19) into equation A.13 to find the relationship between B_{t+1} and B_t such that,

$$\begin{aligned} B_{t+1} &= B_t \left(r + \frac{A}{N_c} \right), \\ &= B_1 \left(r + \frac{A}{N_c} \right)^t, \end{aligned} \tag{A.20}$$

where $B_1 = A \exp(w\alpha x_0)$. Substituting Eq. (A.20) into Eq. (A.17), N_t is given by the equation,

$$N_t(x) = \exp(-w\alpha(x - x_0)) \left(r + \frac{A}{N_c} \right)^{t-1} \quad \text{for } x > x_t. \tag{A.21}$$

Eq. (A.21) is graphically depicted in Fig. (2.3A). The extent of the disperser producing population is,

$$x_{t+1} = \frac{1}{w\alpha} \log \left(\exp(\alpha x_0) \frac{A}{N_c} \left(r + \frac{A}{N_c} \right)^{t-1} \right), \tag{A.22}$$

and I find the rate of population spread is given explicitly in terms of the model parameters as,

$$c = x_{t+1} - x_t = \frac{1}{w\alpha} \log \left(r + \frac{A}{N_c} \right). \tag{A.23}$$

Initial condition 2

I show that the spread rate for Eqs. (2.14) and (2.15) is the same for both initial conditions. Initial condition 2 (Fig. (2.3)) is defined as,

$$\begin{aligned} N_0(x) &\geq N_c \quad \text{for } -x_0 \leq x \leq x_0, \\ &= 0 \quad \text{otherwise.} \end{aligned} \tag{A.24}$$

For this initial condition it is not possible to provide a general model for different values of w.

Pair formation prior to dispersal

Evaluating Eq. (2.14) where the limits of integration are dictated by initial condition 2 gives $\Omega_t = [-x_t, x_t]$. Therefore, Eq. (2.9) where $x > x_t$ yields,

$$N_{t+1}(x) = rN_t(x) + 2A\exp(-\alpha x)\sinh(\alpha x_t), \tag{A.25}$$

where $A = \sigma\psi\phi\gamma^2/4$. I consider solutions to Eq. (A.25) of the form $N_t(x) = B_t\exp(-\alpha x)$ for $x > x_t$. Substituting N_t into Eq. (A.25), the relationship between B_{t+1} and B_t is,

$$B_{t+1} = rB_t + 2A\sinh(\alpha x_t). \tag{A.26}$$

I evaluate B_1 as,

$$B_1 = 2A\sinh(\alpha x_0) \quad x > x_0, \tag{A.27}$$

and therefore show that $N_t = B_t\exp(-\alpha x)$ for all t where $x > x_t$. I use Eq. (A.19) ($w = 1$) to calculate the extent of the disperser producing population,

$$\exp(\alpha x_{t+1}) = r\frac{B_t}{N_c} + \frac{2A}{N_c}\sinh(\alpha x_t). \tag{A.28}$$

I substitute $B_t = N_c\exp(\alpha x_t)$ from Eq. (A.19) to yield,

$$x_{t+1} = \frac{1}{\alpha}\log\left(r\exp(\alpha x_t) + \frac{2A}{N_c}\sinh(\alpha x_t)\right). \tag{A.29}$$

Eq. (A.29) can be evaluated through cobwebbing (as shown in Fig. (10) in Kot et al. 1996). The cobwebbing diagram for Eq. (A.29) is shown in Fig. (A.1). The spread rate for this model, $c = x_{t+1} - x_t$, is the vertical distance between the dashed line and the 1:1 line. Note that the spread rate for Eq. (A.29) becomes constant as $t \to \infty$. The spread rate, $c = x_{t+1} - x_t$, becomes constant as $x_t \to \infty$,

$$c = \lim_{x_t\to\infty}\frac{1}{\alpha}\log\left(r\exp(\alpha x_t) + \frac{2A}{N_c}\left(\frac{\exp(\alpha x_t) - \exp(-\alpha x_t)}{2}\right)\right) - x_t. \tag{A.30}$$

Since $\exp(-\alpha x_t) \to 0$ as $x_t \to \infty$,

$$\begin{aligned} c &= \lim_{x_t\to\infty}\frac{1}{\alpha}\log\left(\exp(\alpha x_t)\left(r + \frac{A}{N_c}\right)\right) - x_t, \\ &= \lim_{x_t\to\infty}\frac{1}{\alpha}\log\left(r + \frac{\sigma\psi\phi\gamma^2}{4N_c}\right). \end{aligned} \tag{A.31}$$

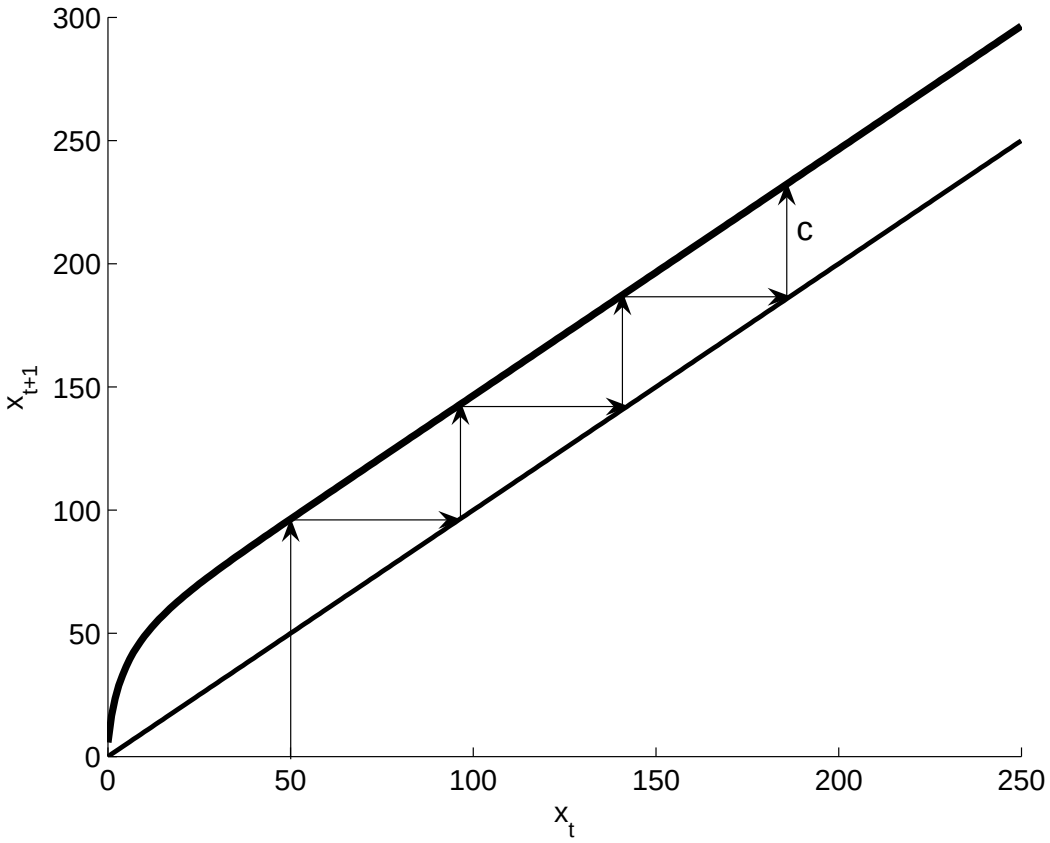

Figure A.1: Finding the extent of the disperser producing population via cobwebbing. Eq. (A.29) (dark line) predicts the spatial extent of the disperser producing population x_{t+1} as a function of x_t for initial condition 2. The 1:1 line is shown as a light line. The vertical distance between the dashed line and the 1:1 line is the spread rate for a given value of x_t. This figures shows an asymptotically constant spread rate because the two curves are parallel for large x_t. The parameter values used to generate this figure are: $r = 1.33$, $\alpha = 0.05$, $A = 1.1$, and $N_c = 0.247$.

Therefore, Eq. (A.31) yields the same result as Eq. (A.23) and the spread rate for Eq. (2.14) is the same for either initial condition.

Pair formation following dispersal

For initial condition 2, I evaluate Eq. (2.15) as,

$$N_{t+1}(x) = rN_t(x) + 2A(\exp(-2\alpha x)(\cosh(2\alpha x_t) - 1), \tag{A.32}$$

for $x < x_t$ where $A = \sigma\psi\phi\gamma^2/8$. I let $N_t = B_t \exp(-2\alpha x)$ and substitute N_t into Eq. (A.32). Therefore, B_{t+1} as a function of B_t is,

$$B_{t+1} = rB_t + 2A(\cosh(2\alpha x_t) - 1). \tag{A.33}$$

I evaluate B_1 as,

$$B_1 = 2A(\cosh(2\alpha x_0) - 1) \qquad \text{where } x > x_0, \tag{A.34}$$

and therefore I show that $N_t = B_t \exp(-2\alpha x)$ holds for all t where $x > x_t$.

I use Eq. (A.19) (where $w = 2$) to find x_{t+1} for Eq. (A.33),

$$\exp(2\alpha x_{t+1}) = r\frac{B_t}{N_c} + \frac{2A}{N_c}(\cosh(2\alpha x_t) - 1). \tag{A.35}$$

I substitute $B_t = N_c \exp(2\alpha x_t)$ from Eq. (A.19) into Eq. (A.35) and calculate the extent of the disperser producing population, x_{t+1} as,

$$x_{t+1} = \frac{1}{2\alpha}\log\left(r\exp(2\alpha x_t) + \frac{2A}{N_c}(\cosh(2\alpha x_t) - 1)\right). \tag{A.36}$$

Eq. (A.36) can be evaluated by cobwebbbing (see Fig. (A.1)). The spread rate, $c = x_{t+1} - x_t$ becomes constant as $x_t \to \infty$, therefore the asymptotic spread rate is,

$$c = \lim_{x_t\to\infty} \frac{1}{2\alpha}\log\left(r\exp(2\alpha x_t) + \frac{2A}{N_c}\left(\frac{\exp(2\alpha x_t) + \exp(-2\alpha x_t)}{2} - 1\right)\right) - x_t. \tag{A.37}$$

Since $\exp(-2\alpha x_t) \to 0$ and $\exp(2\alpha x_t) >> A/N_c$ as $x_t \to \infty$,

$$\begin{aligned} c &= \lim_{x_t\to\infty} \frac{1}{2\alpha}\log\left(\exp(2\alpha x_t)\left(r + \frac{A}{N_c}\right)\right) - x_t, & \text{(A.38)}\\ &= \lim_{x_t\to\infty} \frac{1}{2\alpha}\log\left(r + \frac{\sigma\psi\phi\gamma^2}{8N_c}\right), & \text{(A.39)} \end{aligned}$$

where Eq. (A.38) yields the same results as Eq. (A.23) and therefore the population spread rate for Eq. (2.15) does not depend on the initial condition.

V test

The V test (Zar 1998, p 618-620), also referred to as the Rayleigh test for a specified mean (Fisher 1993, p 151), tests for a unimodal circular distribution with a specified mean, μ. The test statistics were calculated as,

$$V = R\cos(\bar{\vartheta} - \mu), \tag{A.40}$$

where $\bar{\vartheta}$ is the mean direction of movement, R is the resultant length of the measured angles ϑ, and n is the total number of observations. The mean direction $\bar{\vartheta}$ and R the resultant length are calculated as,

$$\begin{aligned} R &= \sqrt{X^2 + Y^2}, & \bar{\vartheta} &= \cos^{-1}\tfrac{X}{R}, \\ X &= \tfrac{\sum_{i=1}^{n}\cos\vartheta_i}{n}, & Y &= \tfrac{\sum_{i=1}^{n}\sin\vartheta_i}{n}, \end{aligned}$$

The u-statistic was used to determine significance. The u-statistic was calculated as,

$$u = V\sqrt{\frac{2}{n}}, \tag{A.41}$$

and the critical u value for $\alpha = 0.05, n = 100$ is $u_{0.05,100} = 1.645$ (Zar (1998), Table B.35).

Numerical procedure for selecting a measured locations from a distribution of GPS measurement error

The distribution of GPS measurement error is k, Eq. (3.1). The three true locations are (x_1^*, y_1^*), (x_2^*, y_2^*) and (x_3^*, y_3^*). The notation * is used to denote actual locations, directions, and turning angles. It resulted in no loss of generality to assume that the first move is in the x-direction so that,

$$(x_1^*, y_1^*) = (0, 0) \qquad (x_2^*, y_2^*) = (L^*, 0),$$

where L^* is the step length for the first move. Since, the step length cutoff is the step length that must be exceeded on both steps in order for the actual turning angle to be detected, the distance moved between

the second and third location is also L^*. I let,

$$(x_3^*, y_3^*) = (L^*(1 + \cos\tau_1^*), L^* \sin\tau_1^*).$$

I determined the distance between the true and measured locations, $r_{i,t}$ (where i is index notation for each iteration of the code), by generating a random GPS error using the inverse cumulative method (Haefner ????, p 217-218). I choose a random number $\rho_{i,t}$ from a uniform distribution between 0 and 1 and calculated the numerical cumulative density function of $K(r) = 2\pi r k(r)$. I determined $r_{i,t}$ as the minimum value of r where $K(r) > \rho_{i,t}$. The locations x_1, x_2, y_1, and y_2 were calculated as,

$$\begin{aligned} x_1 &= x_1^* + r_{i,1}\cos\epsilon_{i,1}, & y_1 &= y_1^* + r_{i,1}\sin\epsilon_{i,1}, \\ x_2 &= x_2^* + r_{i,2}\cos\epsilon_{i,2}, & y_2 &= y_2^* + r_{i,2}\sin\epsilon_{i,2}, \\ x_3 &= x_3^* + r_{i,3}\cos\epsilon_{i,3}, & y_3 &= y_3^* + r_{i,3}\sin\epsilon_{i,3}, \end{aligned} \tag{A.42}$$

A similar procedure was used for the directional bias simulations where only two measured locations were drawn from the distribution of GPS measurement error.

Analytically determining the distributions of measured turning angles and directions

Each measured location is a random variable drawn from a distribution of GPS measurement error. To determine the expected distribution of measured turning angles, I use several change of variables to move from distributions of GPS error in location to distributions of GPS error in angles. For the function $\mathbf{f}(\mathbf{x})$ and the change of variables $\mathbf{x} = \mathbf{w}(\mathbf{y})$, where and D is the range of the transformation,

$$g(y_1, ..., y_n) = \int_D ... \int f(w_1(y_1, ..., y_n), ..., w_n(y_1, ..., y_n))\ |J|\ dy_1 ... dy_n, \tag{A.43}$$

(Bain and Engelhardt 1997 p 206-7) where $\mathbf{x} = (x_1, x_2, ..., x_n)$, $\mathbf{y} = (y_1, y_2, ..., y_n)$ and where $|J|$ is the determinant of the Jacobian matrix,

$$J = \begin{vmatrix} \frac{\partial x_1}{\partial y_1} & \frac{\partial x_1}{\partial y_2} & ... & \frac{\partial x_1}{\partial y_n} \\ \frac{\partial x_2}{\partial y_1} & & & \vdots \\ \vdots & & & \\ \frac{\partial x_n}{\partial y_1} & ... & & \frac{\partial x_n}{\partial y_n}, \end{vmatrix}. \tag{A.44}$$

Turning angles

The turning angle is defined as $\tau_t = \theta_{t+1} - \theta_t$. With no loss of generality, I let $\theta_t^* = 0$ such that $\tau_t^* = \theta_{t+1}^*$. On the first move the animal moves a distance of L_t^*. The restriction that $L_t = L_{t+1}$ (from the Numerical simulation section) is relaxed for greater generality and, therefore, I let the actual distance moved on the second step be L_{t+1}^*. I let the actual locations of the animal be,

$$(x_t^*, y_t^*) = (0, 0), \qquad (x_{t+1}^*, y_{t+1}^*) = (L_t^*, 0),$$
$$(x_{t+2}, y_{t+2}) = (L_t^* + L_{t+1}^* \cos\theta_{t+1}^*, L_{t+1}^* \sin\theta_{t+1}^*).$$

I define a measurement error function f_t that describes the probability density for a measured location (x_t, y_t). Functions in this section are indexed as τ to indicate that these functions are steps in the procedure to calculate the distribution of measured turning angles. In this section a Gaussian distribution of error is used for analytic tractability. I define the GPS error distribution as a bivariate Gaussian distribution with $\sigma_x = \sigma_y$ and covariance $\rho = 0$,

$$f_{\tau,t}(x_t, y_t) = \frac{1}{2\pi\sigma^2} \exp\left(-\frac{(x_t^2 + y_t^2)}{2\sigma^2}\right). \tag{A.45}$$

The probability density function for the measured location at $t + 1$ is,

$$f_{\tau,t+1}(x_{t+1}, y_{t+1}) = \frac{1}{2\pi\sigma^2} \exp\left(-\frac{((x_{t+1} - L_t^*)^2 + y_{t+1}^2)}{2\sigma^2}\right), \tag{A.46}$$

and finally the probability density function at $t + 2$ is,

$$f_{\tau,t+2}(x_{t+2}, y_{t+2}) = \frac{1}{2\pi\sigma^2} \exp\left(-\frac{(x_{t+2} - (L_t^* + L_{t+1}^* \cos\theta_{t+1}^*))^2 + (y_{t+1} - L_{t+1}^* \sin\theta_{t+1}^*)^2}{2\sigma^2}\right). \tag{A.47}$$

The probability of any three successive locations $(x_t, y_t), (x_{t+1}, y_{t+1})$ and (x_{t+2}, y_{t+2}) is,

$$j_\tau = f_{\tau,t}(x_t, y_t) f_{\tau,t+1}(x_{t+1}, y_{t+1}) f_{\tau,t+2}(x_{t+2}, y_{t+2}) \tag{A.48}$$

I use the change of variables,

$$\begin{aligned} u_{t+1} &= x_{t+2} - x_{t+1}, & u_t &= x_{t+1} - x_t, \\ v_{t+1} &= y_{t+2} - y_{t+1}, & v_t &= y_{t+1} - y_t, \end{aligned} \tag{A.49}$$

in Eq. (A.48) such that,

$$g_\tau(u_t, u_{t+1}, v_t, v_{t+1}) = \frac{1}{12\pi^2\sigma^4} \exp\left(-\frac{(u_t - u_{t+1})^2 - u_t u_{t+1} + (v_t + v_{t+1})^2 - v_t v_{t+1} + c_1}{3\sigma^2}\right), \tag{A.50}$$

where,

$$\begin{aligned} c_1 = L_t^*(L_t^* - 2u_t - u_{t+1}) \\ + L_{t+1}^*[L_{t+1}^* - u_{t+1} + (L_t^* - u_t - 2u_{t+1})\cos\mu - (v_t + 2v_{t+1})\sin\mu]. \end{aligned}$$

I change to polar coordinates where,

$$\begin{aligned} u_t &= L_t \cos\theta_t, & v_t &= L_t \sin\theta_t, \\ u_{t+1} &= L_{t+1}\cos\theta_{t+1} & v_{t+1}, &= L_{t+1}\sin\theta_{t+1}, \end{aligned}$$

and make the substitution $\tau_t = \theta_{t+1} - \theta_t$ (as shown in Eq. (A.43)) such that,

$$h_\tau(\tau_t) = \int_0^{2\pi}\int_0^\infty\int_0^\infty \frac{L_t L_{t+1}}{12\pi^2\sigma^4} \exp\left(-\frac{L_t^2 + L_{t+1}^2 + L_t L_{t+1}\cos\tau_t + c_2}{3\sigma^2}\right) dL_t\ dL_{t+1}\ d\theta_t, \tag{A.51}$$

where,

$$\begin{aligned} c_2 = L_t^*(L_t^* - 2L_t\cos\theta_t - L_{t+1}\cos(\tau_t + \theta_t)) \\ + L_{t+1}^*(L_{t+1}^* - L_t\cos(\theta_t - \mu) - 2L_{t+1}\cos(\tau_t + \theta_t - \mu) + L_t^*\cos\mu). \end{aligned}$$

I was not able to solve Eq. (A.51) and instead find solutions for the special case $L_t^* = L_{t+1}^* = 0$ when the animal does not move between locations.

Special case: $L_t^* = L_{t+1}^* = 0$

For the special case $L_t^* = L_{t+1}^* = 0$, $c_2 = 0$ in Eq. (A.51) such that,

$$\begin{aligned} h_{\tau,0}(\tau_t) &= \int_0^{2\pi} \int_0^{\infty} \int_0^{\infty} \frac{L_t L_{t+1}}{12\pi^2\sigma^4} \\ &\qquad \exp\left(-\frac{L_t^2 + L_{t+1}^2 + L_t L_{t+1}\cos\tau_t}{3\sigma^2}\right)\, dL_t\, dL_{t+1}\, d\theta_t, \\ &= \int_0^{\infty} \int_0^{\infty} \frac{L_t L_{t+1}}{6\pi\sigma^4} \\ &\qquad \exp\left(-\frac{L_t^2 + L_{t+1}^2 + L_t L_{t+1}\cos\tau_t}{3\sigma^2}\right)\, dL_t\, dL_{t+1}, \end{aligned} \tag{A.52}$$

Integration on the plane (L_t, L_{t+1}) is performed over the first quadrant. Changing to polar coordinates, $L_t = R\cos\beta$, $L_{t+1} = R\sin\beta$, where $|J| = R$, such that,

$$\begin{aligned} h_{\tau,0}(\tau_t) &= \int_0^{\pi/2} \int_0^{\infty} \frac{R^3\cos\beta\sin\beta}{6\pi\sigma^4} \exp\left(-\frac{R^2(1+\cos\beta\sin\beta\cos\tau_t)}{3\sigma^2}\right) dR\, d\beta, \\ &= \frac{1}{6\pi\sigma^4} \int_0^{\pi/2} \cos\beta\sin\beta \\ &\qquad \int_0^{\infty} R^3 \exp\left(-\frac{R^2(1+\cos\beta\sin\beta\cos\tau_t)}{3\sigma^2}\right) dR\, d\beta. \end{aligned} \tag{A.53}$$

Using another change of variables (e.g. see Eq. (A.43)),

$$\eta = \frac{R^2(1+\cos\beta\sin\beta\cos\tau_t)}{3\sigma^2}, \qquad d\eta = \frac{2R(1+\cos\beta\sin\beta\cos\tau_t)}{3\sigma^2} dR$$

$$\begin{aligned} h_{\tau,0}(\tau_t) &= \frac{1}{6\pi\sigma^2} \int_0^{\pi/2} \cos\beta\sin\beta \left(\frac{3\sigma^2}{1+\cos\beta\sin\beta\cos\tau_t}\right)^2 \\ &\qquad \frac{1}{2}\int_0^{\infty} \eta\exp(-\eta)\, d\eta\, d\beta, \\ &= \frac{3}{4\pi} \int_0^{\pi/2} \frac{\cos\beta\sin\beta}{(1+\cos\beta\sin\beta\cos\tau_t)^2}\, d\beta. \end{aligned}$$

Let,

$$h_{\tau,0}(\tau_t) = \frac{3}{4\pi}\, \frac{dF}{dx}. \tag{A.54}$$

where $x = -\cos\tau_t$ and,

$$\begin{aligned}
\frac{dF_{\tau,0}}{dx} &= \int_0^{\pi/2} \frac{\cos\beta\sin\beta}{(1-x\cos\beta\sin\beta)^2}\, d\beta, && \text{(A.55)}\\
&= \int_0^{\pi/2} \frac{d}{dx}\frac{1}{1-x\cos\beta\sin\beta}\, d\beta,\\
&= \frac{d}{dx}\int_0^{\pi/2} \frac{1}{1-x\cos\beta\sin\beta} d\beta. && \text{(A.56)}
\end{aligned}$$

Therefore, taking the antiderivative yields,

$$F_{\tau,0}(x) = \int_0^{\pi/2} \frac{1}{1-x\cos\beta\sin\beta}\, d\beta. \tag{A.57}$$

I apply the standard change of variables $z = \tan\beta$, such that,

$$\cos\beta\sin\beta = \frac{\cos\beta\sin\beta}{\cos^2\beta+\sin^2\beta} = \frac{\frac{\sin\beta}{\cos\beta}}{1+\left(\frac{\sin\beta}{\cos\beta}\right)^2} = \frac{z}{1+z^2}, \tag{A.58}$$

Substituting Eq. (A.58) into Eq. (A.57) where $d\beta = dz/(1+z^2)$ yields,

$$\begin{aligned}
F_{\tau,0}(x) &= \int_0^{\infty} \frac{1}{1-\frac{xz}{1+z^2}}\frac{dz}{1+z^2}, && \text{(A.59)}\\
&= \int_0^{\infty} \frac{1}{1-\frac{xz}{1+z^2}}\frac{dz}{1+z^2}\\
&= \int_0^{\infty} \frac{dz}{z^2-xz+1} = \int_0^{\infty} \frac{dz}{\left(z-\frac{x}{2}\right)^2+1-\frac{x^2}{4}}\\
&= \int_0^{\infty} \frac{dz}{\left(1-\frac{x^2}{4}\right)\left[\left(\frac{z-\frac{1}{2}x}{\sqrt{1-\frac{x^2}{4}}}\right)^2+1\right]}. && \text{(A.60)}
\end{aligned}$$

Finally, let,

$$\phi = \frac{z-\frac{1}{2}x}{\sqrt{1-\frac{x^2}{4}}}, \qquad dz = \sqrt{1-\frac{x^2}{4}}d\phi,$$

$$
\begin{aligned}
F_{\tau,0}(x) &= \frac{1}{\sqrt{1-\frac{x^2}{4}}} \int_{-\frac{x}{2\sqrt{1-\frac{x^2}{4}}}}^{\infty} \frac{d\phi}{\phi^2+1}. \\
&= \frac{1}{\sqrt{1-\frac{x^2}{4}}} \tan^{-1}\phi \Bigg|_{-\frac{x}{2\sqrt{1-\frac{x^2}{4}}}}^{\infty} \qquad \text{(A.61)} \\
&= \frac{\pi + 2\tan^{-1}\left(\frac{x}{\sqrt{4-x^2}}\right)}{\sqrt{4-x^2}}.
\end{aligned}
$$

$$
\begin{aligned}
\frac{dF_{\tau,0}}{dx} &= \frac{2\left(\frac{x^2}{(4-x^2)^{3/2}} + \frac{1}{\sqrt{4-x^2}}\right)}{\sqrt{4-x^2}\left(1+\frac{x^2}{4-x^2}\right)} + \frac{x\left(\pi + 2\tan^{-1}\left(\frac{x}{\sqrt{4-x^2}}\right)\right)}{(4-x^2)^{3/2}} \qquad \text{(A.62)} \\
&= \frac{8 - x\left(2x - \sqrt{4-x^2}\left(\pi + 2\tan^{-1}\left(\frac{x}{\sqrt{4-x^2}}\right)\right)\right)}{(x^2-4)^2} \qquad \text{(A.63)}
\end{aligned}
$$

Substituting Eq. (A.62) into Eq. (A.54) and re-substituting $x = -\cos\tau_t$,

$$
\begin{aligned}
h_{\tau,0}(\tau_t) &= \frac{3}{4\pi}\frac{dF_{\tau,0}}{dx}, \qquad \text{(A.64)} \\
&= h_{\tau,0}(\tau_t) = \frac{24 - 3\cos\tau_t\left(2\cos\tau_t + \sqrt{4-\cos\tau_t}\left(\pi + 2\tan^{-1}\left(\frac{-\cos\tau_t}{\sqrt{4-\cos^2\tau_t}}\right)\right)\right)}{4\pi\left(\cos^2\tau_t - 4\right)^2}. \qquad \text{(A.65)}
\end{aligned}
$$

Directional bias

The directional bias is defined as $\zeta_t = \Theta_t - \theta_t$. I let $\Theta_t^* = \pi$ such that $\zeta^* = \pi - \theta_t^*$. On the first step the animal moves a distance of L_t^*. The distance between the the actual location of the animal at time t and the bias point is M_t^*. I let the actual locations of the animal and bias point be,

$$
(x_t^*, y_t^*) = (0,0), \qquad (x_{t+1}^*, y_{t+1}^*) = (L_t^*, 0), \qquad (\chi^*, \psi^*) = (0, M_t^*).
$$

The distribution of measurement error for each of the animals actual locations are Eqs. (A.45) and (A.46). There is no measurement error about the bias point. The probability of any pair of locations (x_t, y_t),

(x_{t+1}, y_{t+1}) is $g_\zeta = f_t f_{t+1}$. I use the change of variables,

$$\begin{aligned} u_t &= x_{t+1} - x_t, & v_t &= y_{t+1} - y_t, \\ w_t &= -x_t, & z_t &= M_t^* - y_t, \end{aligned}$$

where w_t and z_t are the x and y displacements. The product of Eqs. (A.45) and (A.46) with the change of variables is,

$$h_{\zeta,0}(\zeta_t) = \frac{1}{4\pi^2\sigma^4} \exp\left(-\frac{w_t^2 + (M_t^* - z_t)^2 - (L_t^* + w_t - u_t)^2 + (M_t^* - z_t + v_t)^2}{2\sigma^2}\right). \tag{A.66}$$

I use another change of variables,

$$\begin{aligned} u_t &= L_t \cos\theta_t & v_t &= L_t \sin\theta_t \\ w_t &= M_t \cos\Theta_t & z_t &= M_t \sin\Theta_t \end{aligned}$$

where $|J| = L_t M_t$ and $\zeta_t = \Theta_t - \theta_t$ such that,

$$h_{\zeta,0}(\zeta_t) = \int_0^{2\pi}\int_0^\infty\int_0^\infty \frac{L_t M_t}{4\pi^2\sigma^4} \exp\left(\frac{L_t^2 + 2M_t^2 - 2L_t M_t \cos\zeta_t + c_3 + c_4}{2\sigma^2}\right)\, dL_t\, dM_t\, d\theta_t, \tag{A.67}$$

where,

$$\begin{aligned} c_3 &= L_t^*(L_t^* - 2L_t\cos\theta_t + 2M_t\cos(\zeta_t + \theta_t)), \\ c_4 &= M_t^*(2M_t^* + 2L_t\sin\theta_t - 4M_t\sin(\zeta_t + \theta_t)), \end{aligned} \tag{A.68}$$

I was not able to solve Eq. (A.67) and instead find solutions for $M_t^* = L_t^* = 0$.

Special case: $M_t^* = L_t^* = 0$

I find analytic solutions for the distribution of the directional biases for the special case where the animal is located at the bias point and does not move between locations such that c_3 and c_4 are equal to zero in Eq. (A.51). Therefore,

$$\begin{aligned} h_{\zeta,0}(\zeta_t) &= \int_0^{2\pi}\int_0^\infty\int_0^\infty \frac{L_t M_t}{4\pi^2\sigma^4} \\ &\qquad \exp\left(-\frac{L_t^2 + M_t^2 - 2L_t M_t\cos\zeta_t}{2\sigma^2}\right)\, dL_t\, dM_t\, d\theta_t, \\ &= \int_0^\infty\int_0^\infty \frac{L_t M_t}{2\pi\sigma^4} \exp\left(-\frac{L_t^2 + M_t^2 - 2L_t M_t\cos\zeta_t}{2\sigma^2}\right)\, dL_t\, dM_t, \end{aligned} \tag{A.69}$$

I consider L_t and M_t as two coordinates and integration on the plane (L_t, M_t) is performed over the first quadrant. Changing to polar coordinates, $L_t = R\cos\beta$, $M_t = R\sin\beta$,where $|J| = R$, such that,

$$h_{\zeta,0}(\zeta_t) = \frac{1}{2\pi\sigma^4}\int_0^{\pi/2}\cos\beta\sin\beta\int_0^{\infty}R^3\exp\left(-\frac{R^2(3-\cos 2\beta-2\cos\zeta_t\sin 2\beta)}{4\sigma^2}\right)dR\ d\beta. \tag{A.70}$$

I make another change,

$$\eta = \frac{R^2(3-\cos 2\beta-2\cos\zeta_t\sin 2\beta)}{4\sigma^2}, \quad d\eta = \frac{R(3-\cos 2\beta-2\cos(\zeta_t)\sin(2\beta))}{2\sigma^2}$$

$$\begin{aligned} h_{\zeta,0}(\zeta_t) &= \frac{1}{\pi}\int_0^{\pi/2}\int_0^{\infty}\frac{4\cos\beta\sin\beta\ \eta\exp(-\eta)\ d\eta}{(3-\cos 2\beta-2\cos\zeta_t\sin 2\beta)^2}\ d\beta. \\ &= \frac{4}{\pi}\int_0^{\pi/2}\frac{\cos\beta\sin\beta}{(3-\cos 2\beta-2\cos\zeta_t\sin 2\beta)^2}\ d\beta. \end{aligned} \tag{A.71}$$

Let,

$$h_{\zeta,0}(\zeta_t) = \frac{4}{\pi}\ \frac{dF_{\zeta,0}}{dx}. \tag{A.72}$$

where $x = 2\cos\zeta_t$ and,

$$\begin{aligned} \frac{dF_{\zeta,0}}{dx} &= \int_0^{\pi/2}\frac{\cos\beta\sin\beta}{(3-\cos 2\beta-x\sin 2\beta)^2}\ d\beta, \\ &= \int_0^{\pi/2}\frac{d}{dx}\frac{1}{2(3-\cos 2\beta-x\sin 2\beta)}\ d\beta, \end{aligned} \tag{A.73}$$

where d/dx can be taken out of the integral because the last integral is convergent for all x between -1 and 1.

$$F_{\zeta,0}(x) = \int_0^{\pi/2}\frac{1}{2(3-\cos 2\beta-x\sin 2\beta)}\ d\beta. \tag{A.74}$$

Using the double angle formula,

$$\begin{aligned} 3-\cos 2\beta-x\sin 2\beta &= 3(\cos^2\beta+\sin^2\beta)-(\cos^2\beta-\sin^2\beta)-2x\cos\beta\sin\beta, \\ &= 2(\cos^2\beta+2\sin^2\beta+x\cos\beta\sin\beta), \end{aligned}$$

Furthermore,

$$2(\cos^2\beta+2\sin^2\beta+x\cos\beta\sin\beta) = \frac{2(2z^2-xz+1)}{1+z^2}, \tag{A.75}$$

where $z = \tan\beta$ and the steps used to find Eq. (A.75) are shown in Eq. (A.58). Substituting Eq. (A.75) into Eq. (A.74) and completing the square and factoring the denominator yields,

$$\begin{aligned} F_{\zeta,0}(x) &= \frac{1}{4}\int_0^\infty \frac{dz}{2z^2 - xz + 1}, \\ &= \frac{1}{8}\int_0^\infty \frac{dz}{\left(\frac{1}{2} - \frac{x^2}{16}\right)\left[\left(\frac{z-\frac{x}{4}}{\sqrt{\frac{1}{2}-\frac{x^2}{16}}}\right)^2 + 1\right]}. \end{aligned} \tag{A.76}$$

Finally, let,

$$\phi = \frac{z - \frac{x}{4}}{\sqrt{\frac{1}{2} - \frac{x^2}{16}}}, \qquad dz = \sqrt{\frac{1}{2} - \frac{x^2}{16}}\, d\phi,$$

$$\begin{aligned} F_{\zeta,0}(x) &= \frac{1}{8\sqrt{\frac{1}{2} - \frac{x^2}{16}}} \int_{-\frac{x}{4\sqrt{\frac{1}{2}-\frac{x^2}{16}}}}^\infty \frac{d\phi}{\phi^2 + 1}, \\ &= \frac{1}{8\sqrt{\frac{1}{2} - \frac{x^2}{16}}} \tan^{-1}\phi \Bigg|_{-\frac{x}{4\sqrt{\frac{1}{2}-\frac{x^2}{16}}}}^\infty, \\ &= \frac{\pi + 2\tan^{-1}\frac{x}{\sqrt{8-x^2}}}{4\sqrt{8-x^2}}. \end{aligned} \tag{A.77}$$

$$\begin{aligned} \frac{dF_{\zeta,0}}{dx} &= \frac{16 - 2x^2 + \pi x\sqrt{8-x^2} + 2x\sqrt{8-x^2}\tan^{-1}\left(\frac{x}{8-x^2}\right)}{4\left(x^2-8\right)^2}, \\ &= \frac{16 - x\left(2x - \pi\sqrt{8-x^2} - 2\sqrt{8-x^2}\tan^{-1}\left(\frac{x}{\sqrt{8-x^2}}\right)\right)}{4(x^2-8)^2}. \end{aligned} \tag{A.78}$$

Substituting Eq. (A.78) into Eq. (A.72) and re-substituting $x = 2\cos\zeta_t$,

$$\begin{aligned} h_{\zeta,0}(\zeta_t) &= \frac{4}{\pi}\frac{dF_{\zeta,0}}{dx} \\ &= \frac{16 - 4\cos\zeta_t\left(2\cos\zeta_t - \sqrt{2-\cos^2\zeta_t}\left(\pi + 2\tan^{-1}\left(\frac{\cos\zeta_t}{\sqrt{2-\cos^2\zeta_t}}\right)\right)\right)}{\pi(4\cos^2\zeta_t - 8)^2}. \end{aligned} \tag{A.79}$$

Testing for correlation between two directions

I tested for temporal autocorrelation in movement directions using a modified version of Pearson's correlation coefficient (Zar 1998 p 649-651, Fisher 1993, p 151, see Appendix A). The correlation coefficient

was,

$$r_{aa} = \frac{\sum_{j=1}^{n-1}\sum_{k=i+1}^{n}\sin(a_j - a_k)\sin(b_j - b_k)}{\sqrt{\sum_{j=1}^{n-1}\sum_{k=i+1}^{n}\sin^2(a_j - a_k)\sum_{j=1}^{n-1}\sum_{k=i+1}^{n}\sin(b_j - b_k)}} \tag{A.80}$$

(Fisher and Lee, 1983), where $a_j = \theta_t$, $b_j = \theta_{t+i}$ and n is the total number of (θ_t, θ_{t+i}) pairs extracted from the GPS data. Here, the quantity $a_j - a_k$ is the difference between each element of a and all other elements where $j < k$. I tested for the temporal autocorrelation in movement angles for each wolf and each subsampling regime using the computational version of Eq. (A.80),

$$r_{aa} = \frac{4\left(\left(\sum_{t=1}^{n} c_1 c_1\right)\left(\sum_{t=1}^{n} s_1 s_2\right) - \left(\sum_{t=1}^{n} c_1 s_2\right)\left(\sum_{t=1}^{n} s_1 c_2\right)\right)}{\sqrt{\left(n^2 - \left(\sum_{t=1}^{n} c_{21}\right)^2 - \left(\sum_{t=1}^{n} s_{21}\right)^2\right)\left(n^2 - \left(\sum_{t=1}^{n} c_{22}\right)^2 - \left(\sum_{t=1}^{n} s_{22}\right)^2\right)}} \tag{A.81}$$

(Zar 1998 p 649-651, Fisher 1993, p151) where $c_1 = \cos(\theta_t), c_2 = \cos(\theta_{t+i}), s_1 = \sin(\theta_t), s_2 = \sin(\theta_{t+i}), c_{21} = \cos(2\theta_t), c_{22} = \cos(2\theta_{t+i}), s_{21} = \sin(2\theta_t), s_{22} = \sin(2\theta_{t+i})$. For values of r_{aa} close to zero, θ_t and θ_{t+i} are uncorrelated. I tested whether r_{aa} is significantly different from zero for $\alpha = 0.05$. For all wolves and all subsampling regimes, $n >> 25$; therefore, the appropriate test for $H_0 : r_{aa} = 0$ was performed as in Fisher (1993, p 152 - for $n < 25$ a different test for significance is suggested). If $p < 0.05$, r_{aa} is significantly different from zero and θ_t and θ_{t+i} are correlated.

Appendix B

Supplemental Data

Data sources are Phillips and Smith (1997), Smith (1998), Smith et al. (1999), Smith et al. (2000), Smith et al. (2001), Smith and Guernsey (2002) and Smith et al. (2003) all of which are available online at, http://www.nps.gov/yell/nature/animals/wolf/wolfup.html.

Table B.1: Number of wolves in YNP 1996-2002.

Year	Number of wolves
1996	20
1997	38
1998	80
1999	83
2000	90
2001	122
2002	138

Table B.2: Year of formation for GYE wolf packs.

Pack name	Date formed	Formed naturally	Year 1
Rose Creek	March 29, 1995	No	n/a
Mollie's Pack (Crystal Ck)	March 31, 1995	No	n/a
Yellowstone Delta (Soda Butte)	March 31, 1995	No	n/a
Leopold Pack	Jan, 1996	Yes	1996
Druid Peak	Apr, 1996	No	n/a
Chief Joseph	Apr, 1996	No	n/a
Nez Perce	Apr, 1996	No	n/a
Lone Star	Apr, 1996	No	n/a
Thorofare	Apr, 1996	Yes	n/a
Washakie	1996	Yes	1997
Sheep Mtn (Cf Joseph II)	early 1996*	Yes	1996
Teton	1998	Yes	1999
Sunlight	March, 1998**	Yes	1998
Gros Ventre (Jackson Trio)	1998	Yes	1999
Swan Lake	2000***	Yes	2001
Absaroka	2000***	Yes	2001
Beartooth	2000***	Yes	2001
Taylor	2000***	Yes	2001
Gravelly	2000***	Yes	2001
Mill Creek	2000***	Yes	2001
Tower	early 2001$^{\triangle}$	Yes	2001
Cougar Creek	2001	Yes	2002
Freezeout	2001	Yes	2002
Pinedale	2001	Yes	2002
Meeteetse	2001	Yes	2002
Big Piney	2001	Yes	2002
Red Lodge	2001	Yes	2002
Buffalo Fk	2002	Yes	2003
Geode	2002	Yes	2003
Agate	2002	Yes	2003
Greybull R	2002	Yes	2003
Green R	2002	Yes	2003
Bechler	2002	Yes	2003

Year 1 is the year of the first April after pack formation
* Formed due to a split of Chief Joseph Pack. Date of first disassociation with main pack
** Paired too late to reproduce
*** Evidence that this date is the correct data of pair formation is in the 2001 YNPWP annual report
$^{\triangle}$ Formed due to a split of the Rose Creek Pack. Date of split reported in 2001 annual report.

Table B.3: Disperser production and pack size of GYE wolves

Pack size at yr start	Number of dispersers produced during yr	Pack name and year	Method of Estimation
2	0	Crystal Ck, 1997	inferred
5	0	Soda Butte, 1997	inferred
5	2	Druid, 1997	documented
10	1	Rose Ck, 1997	documented
2	0	Thorofare, 1997	inferred
2	0	Washakie, 1997	inferred
8	0	Crystal Ck, 1998	inferred
8	1	Soda Butte, 1998	documented
8	0	Cf. Joseph I, 1998	inferred
3	0	Cf. Joseph II, 1998	inferred
7	1	Druid, 1999,	documented
22	4	Rose Ck, 1999	documented
13	0	Leopold, 1999	documented
16	1	Crystal Ck, 1999	documented
11	2	Cf. Joseph, 1999	documented
3	0	Gros Ventre, 1999	inferred
7	2	Soda Butte, 1999	documented
6	1	Sheep Mt, 1999	documented
2	0	Sunlight, 1999	inferred
2	0	Teton, 1999	inferred
11	2	Leopold, 2000	documented
13	1	Crystal Ck, 2000	documented
8	1	Cf. Joseph, 2000	documented
13	1	Nez Perce, 2000	documented
5	0	Grox Ventre, 2000	inferred
13	2	Leopold, 2001	documented
22	1	Nez Perce, 2001	inferred
4	0	Mollie's, 2001	inferred
5	0	Absaroka, 2001	inferred
3	0	Beartooth, 2001	interred
18	5	Rose Ck, 2001	documented*
37	9	Druid, 2002	documented*
2	1	Tower, 2002	documented
14	4	Leopold, 2002	documented
6	2	Mollies's, 2002	documented
11	4	Cf. Joseph, 2002	documented
18	3	Nez Perce, 2002	documented
16	1	Yellowstone Delta, 2002	documented
12	5	Teton, 2002	documented

* Pack split. Documented means that progress reports specify the number of dispersers produced in the text. Inferred applies to observations of zero dispersers only and means that this years pack size is equal to last years pack size plus pup production and known usurptions and minus known mortalities. Therefore as the fate of all pack members is known, no members of the pack have dispersed.

Table B.4: Reason for pack size disperser observation non-inclusion in Table B.3

1. **Pack was released from an acclimation pen less than 1 year ago**
   Rose Creek, Crystal Creek, and Soda Butte (1995), Druid, Chief Joseph, Nez Perce, and Lonestar (1996).
2. **USFWS intervention**
   Nez Perce (1998 – recaptured), Chief Joseph II (1997 – supplemental feeding)
3. **Fate of all previous years pack members unknown**
   Leopold and Rose Creek (1998), Nez Perce (1999), Druid, Soda Butte, Sheep Mountain, Chief Joseph, Washakie, Sunlight and Rose Creek (2000), Druid, Swan Lake, Chief Joseph, Yellowstone Delta, Teton, Taylor, Gravelly and Sheep Mountain (2001), Rose Creek, Swan Lake, Cougar Creek, Sunlight, Beartooth and Grey Bull River (2002).
4. **Last years pack size + known reproduction + usurption - known mortality exceeds this reported years pack size**
   Teton, Sheep Mountain, Soda Butte and Druid (2000)
5. **Exact number of pack members in previous year unknown**
   Sunlight and Gros Ventre (2002)
6. **Pack was first formed less than a year ago**
   Freezeout (2001), Green River, Slough Creek, Geode, Bechler and Agate (2002)

Table B.5: Pack sizes in the first 3 years for naturally formed packs

Pack name	Pack size after		
	1 year	2 years	3 years
Leopold	5	9	13
Washakie	6	0	0
Sheep Mountain	3	9	7
Teton	6	4	12
Sunlight Basin	2	9	10
Swan Lake	8	8	16
Absaroka	8	9	4
Taylor Peaks	3	4	4
Gravelly Range	3	0	0
Tower	2	2	0

This data represents all the naturally formed packs where pack size is known exactly for the first three years.

Appendix C

This appendix contains figures of the GPS data used for the analysis in Chapter 4. All of the data shown was collected at a 15 minute sampling frequency. Further details of the collar success rate can be found in Tab. (4.1)

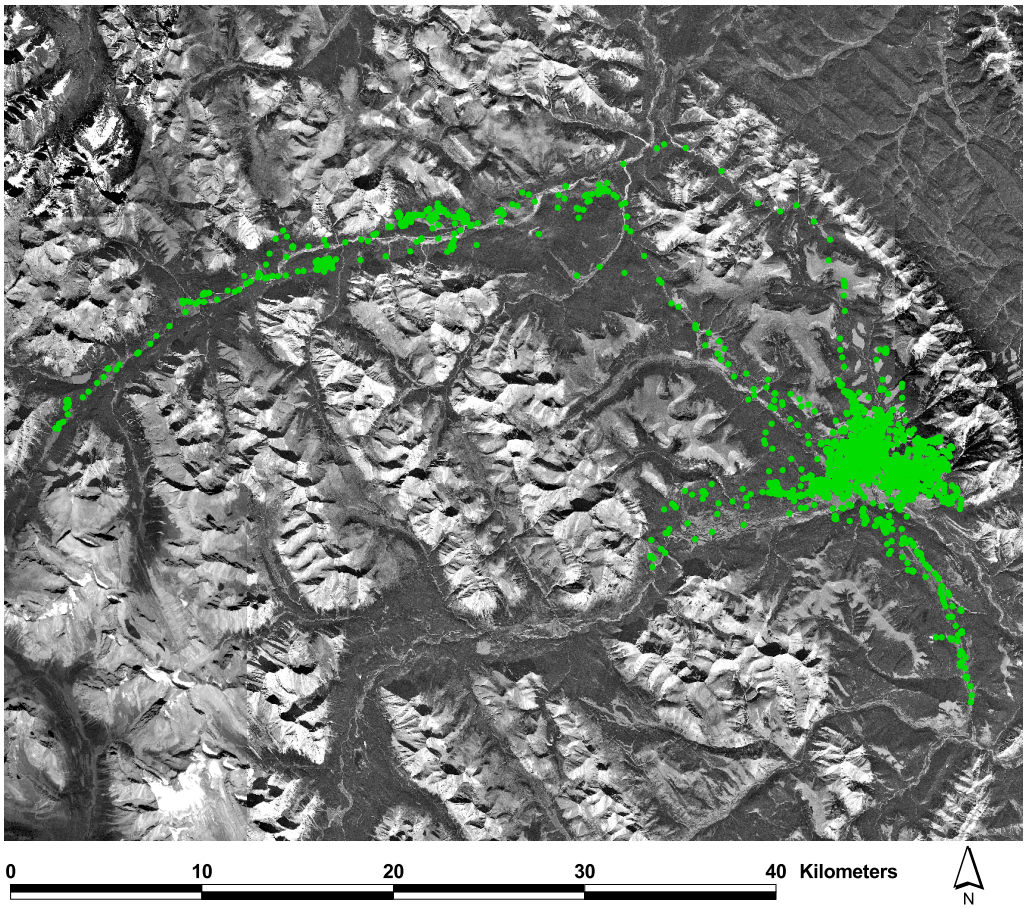

Figure C.1: The GPS data for wolf 77. Projection: UTM (Universal Trans Mercator), Datum: NAD 1983, zone 11. UTMs for the bottom left corner are 555963 Easting, 5716158 Northing, and for the top right corner, 608462 Easting and 5756294 Northing

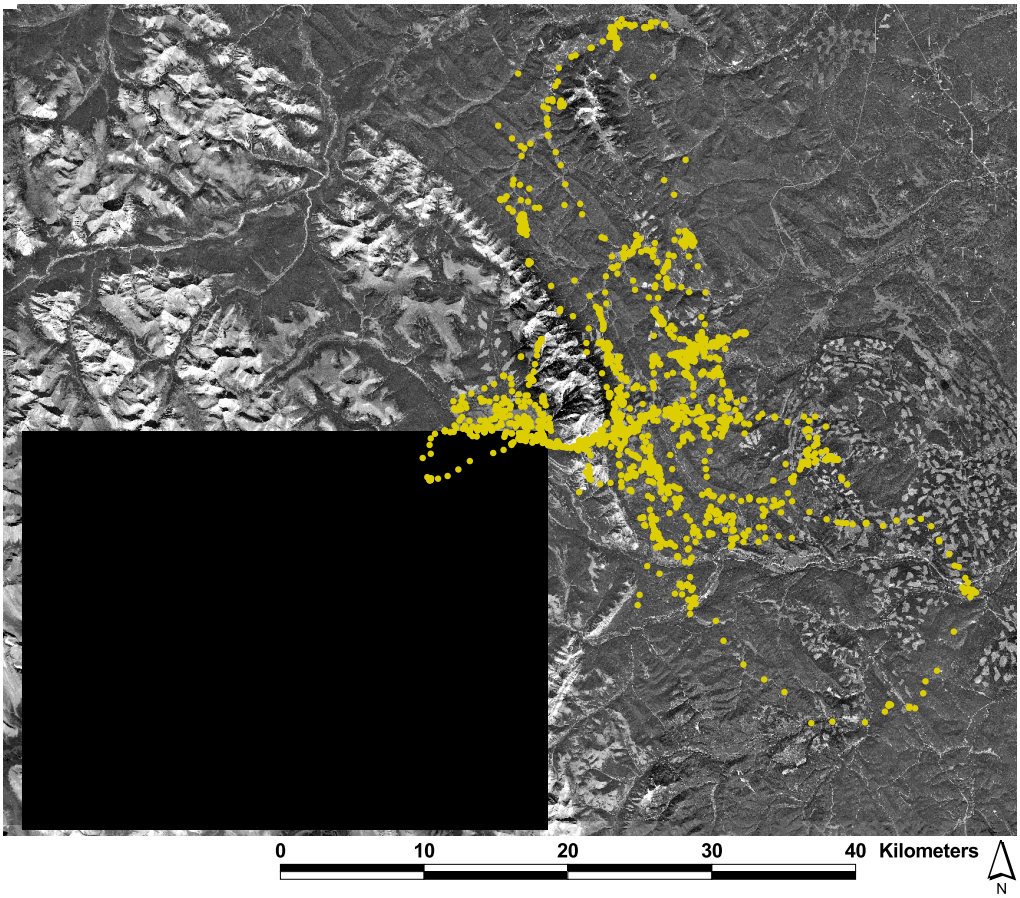

Figure C.2: The GPS data for wolf 78. Projection: UTM (Universal Trans Mercator), Datum: NAD 1983, zone 11. UTMs for the bottom left corner are 568668 Easting, 5709044 Northing, and for the top right corner, 638224 Easting and 5762157 Northing

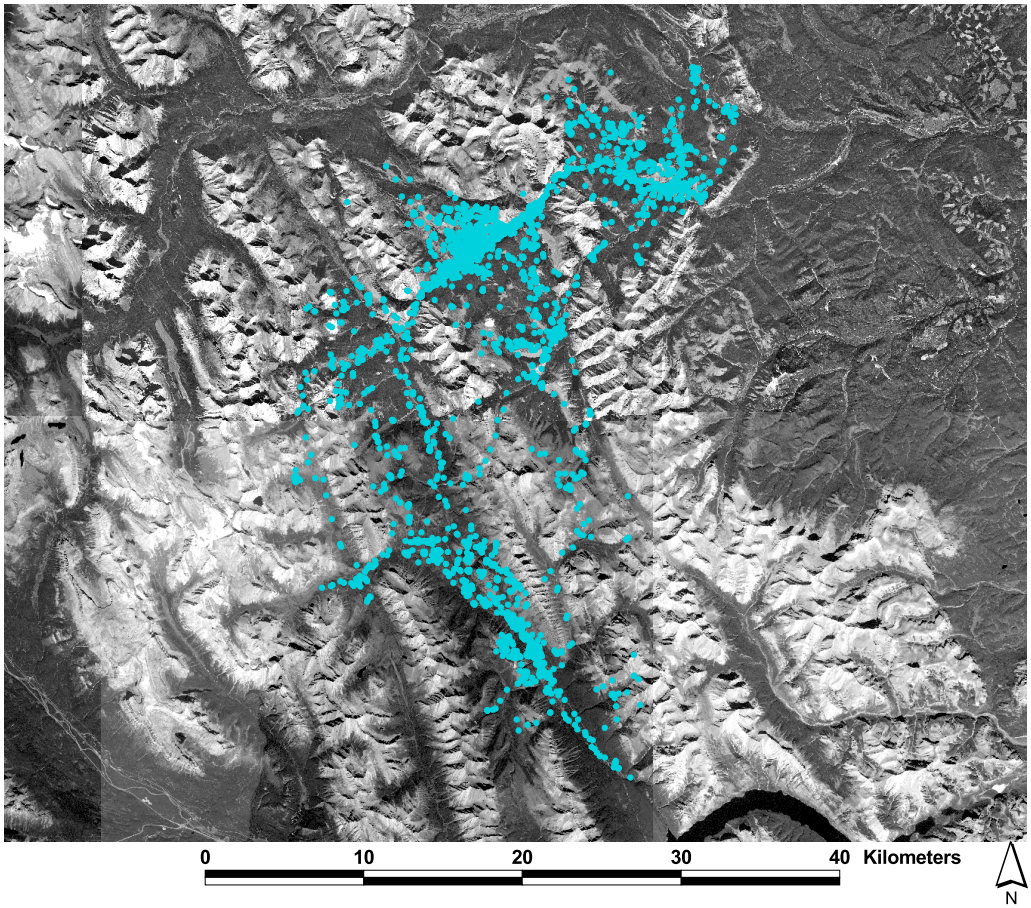

Figure C.3: The GPS data for wolf 85. Projection: UTM (Universal Trans Mercator), Datum: NAD 1983, zone 11. UTMs for the bottom left corner are 563696 Easting, 5680970 Northing, and for the top right corner, 627381 Easting and 5729570 Northing

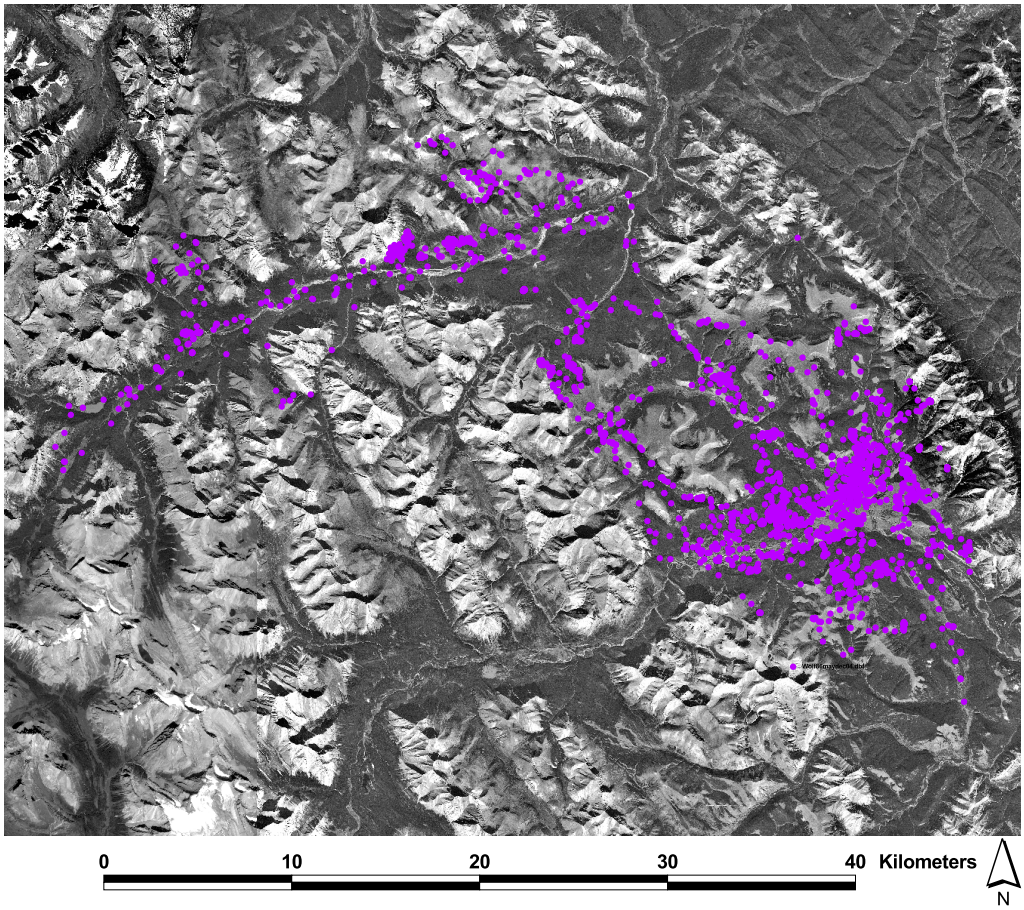

Figure C.4: The GPS data for wolf 86. Projection: UTM (Universal Trans Mercator), Datum: NAD 1983, zone 11. UTMs for the bottom left corner are 555276 Easting, 5717506 Northing, and for the top right corner, 608516 Easting and 5758364 Northing